The Relationship between Astrocytes, Inflammation and Epileptogenesis

Dissertation
zur
Erlangung des Doktorgrades (Dr. rer. nat.)
der
Mathematisch-Naturwissenschaftlichen Fakultät
der
Rheinischen Friedrich-Wilhelms-Universität Bonn

vorgelegt von
Dilaware Khan
aus
Dera Ghazi Khan, Pakistan

Bonn 2017

Angefertigt mit Genehmigung der Mathematisch-Naturwissenschaftlichen Fakultät
der Rheinischen Friedrich-Wilhelms-Universität Bonn

1. **Gutachter** **Prof. Dr. Christian Steinhäuser**
Institut für Zelluläre Neurowissenschaften
Universität Bonn

2. **Gutachter** **Prof. Dr. Horst Bleckmann**
Institut für Zoologie
Universität Bonn

Tag der Promotion: 26.06.2017
Erscheinungsjahr: 2017

"The brain is wider than the sky"
Emily Dickinson (1830-1886)

Acknowledgments

First, I would like to thank my supervisor Prof. Dr. Christian Steinhäuser for giving me the opportunity to work on this interesting project and for his support. He has always encouraged me to pursue my own ideas and enlightened me with his valuable academic advice.

I also would like to thank Prof. Dr. Horst Bleckmann for his willingness to act as a second supervisor. Likewise, my thanks go to Prof. Dr. Benjamin Odermatt and Prof. Dr. Klaus Mohr, who agreed to review my PhD thesis and be part of the defense committee.

My special thanks go to Dr. Peter Bedner for fruitful input on gap junctions, analysis of Western blot and staining data. I also want to thank him for introducing me kainate mouse model of epilepsy, and for his experimental support to obtain EEG data.

I also would like to thank PD Dr. Gerald Seifert for genotyping Cx3cr1^{CreER}:Tak1$^{fl/fl}$ and guiding tamoxifen administration.

My sincere thanks go to Stephanie Griemsmann, Julia Müller and Camille Philippot for endless hours of cell counting.

I also would like to thank my all lab colleagues for great time and friendly working atmosphere: Alex, Aline, Annika, Daniel, Ines, Ivana, Johannes, Julia, Kerstin, Kirsten, Magda, Michel, Ronald, Semi, Stefan, Steffi A., Susan, Tushar and Verena. My special thanks for excellent technical support, ordering and administration go to Ina Fiedler, Anja Matijevic, Dr. Ines Heuer, Dr. Silke Künzel and Thomas Erdmann.

I would like to thank my siblings and parents especially my father for supporting me emotionally, morally and financially. Last but not least, I want to thank my family and especially my wife Bushra for her support and encouragement in all these years. I want to thank my cute son Hamza and daughter Raeha for their effort to keep me awake at nights and for their smiles.

Table of Contents

Abbreviations

ACSF	artificial cerebrospinal fluid
AEDs	anti-epileptic drugs
AMPA	α-amino-3-hydroxy-5-methyl-4-isoxazolepropionic acid
ANOVA	analysis of variance
AQP4	aquaporin 4
APS	ammoniumpersulfat
ATP	adenosine triphosphate
a.u.	arbitrary unit
BBB	blood brain barrier
BCA	bicinchoninic acid assay
bp	base pair
CA	cornu ammonis
Ca^{2+}	calcium ion
cAMP	cyclic adenosine monophosphate
CCD	charge-coupled device
CNS	central nervous system
Contr.	control
CSF	cerebrospinal fluid
Cx	connexin
Cx30	connexin 30
Cx43	connexin 43
DAMPs	damage associated molecular patterns
DG	dentate gyrus
DH	double hit
DIC	differential interference contrast
DNA	deoxyribonucleic acid
EAAT	excitatory amino acid transporter
eGFP	enhanced green fluorescent protein
EFSs	experimental febrile seizures
ERK	extracellular signal-regulated kinase
FSs	febrile seizures
GABA	γ-Aminobutyric acid
GFAP	glial fibrillary acidic protein
GΩ	gig ohm
GS	glutamine synthetase
HET	house for Experimental Therapy of Universitätsklinikums
HS	hippocampal sclerosis
HT	hyperthermia
IB	immunoblot
IF	immunofluorescence
IGJC	interastrocytic gap junctional coupling
IHC	immunohistochemistry
IKK	IκB kinase
IL-1β	interleukin 1β
IL-6	interleukin 6

ILAE	International League Against Epilepsy
$[Ca^{2+}]_i$	intracellular calcium concentration
ip	intraperitoneal
IP3	inositol trisphosphate
IRAK-4	interleukin-1 receptor-associated kinase-4
JNK	c-jun N-terminal kinase
K^+	potassiumion
kDa	kilo Dalton
kHz	kilohertz
Kir	inwardly rectifying potassium channels
lm	lacunosum moleculare
LPS	lipopolysaccharide
MAPKs	mitogen activated protein kinases
MTS	mesial temporal sclerosis
MyD88	myeloid differentiation primary response 88
Na^+	sodium ion
NAD^+	nicotinamide adenine dinucleotide
NF-κB	nuclear factor-κB
NG2	neural / glialantigen 2
NGS	normal goatserum
NMDA	N-methyl-D-aspartate
OPCs	oligodendrocytes precursor cells
ori.	oriens
PBS	phosphate buffered saline
PAMPs	pathogen associated molecular patterns
PFA	paraformaldehyde
PVDF	polyvinylidene difluoride
pyr.	pyramidale
rad.	radiatum
rcf	relative centrifugal force
SD	standard deviation
SDS	sodiumdodecylsulfate
SGZ	subgranular zone
SPF	specific pathogen free
St.	stratum
TAB	TAK1-binding protein
TAK1	TGF-β activated kinase 1
TAM	tamoxifen
TIR	TLR / IL-1 receptor
TLE	temporal lobe epilepsy
TLRs	Toll like receptors
TBST	Tris-buffered saline with Tween
TNF-α	tumor necrosis factor α
TRAF6	TNF receptor-associated factor 6
UC	untreated control
VEGF	vascular endothelial growth factor
WB	Western blot
WT	wild type

1 Introduction

1.1 Nervous system

In vertebrates the nervous system consists of two parts: central nervous system (CNS) which is composed of brain and spinal cord; and peripheral nervous system that comprises the neuronal network outside of the brain and spinal cord. The brain is located in the head, where it is protected by the meninges and skull. It is composed of five parts: telencephalon, diencephalon, mesencephalon, metencephalon and myelencephalon. It also contains cavities, which are called ventricles, and these ventricles are filled with cerebrospinal fluid (CSF). These ventricles are connected with each other and also with the spinal cord.

The brain tissue is composed of different cell-types, e.g. neurons, glial cells, endothelial cells, etc. In murine brain around $7.1x10^7$ neurons are present, these neurons form around 10^{11} synapses with each other in a complex network (Herculano-Houzel et al., 2006). Almost 65 % of the mouse brain is composed of glial cells (Allen and Barres, 2009). In the brain two different types of nervous tissues can be distinguished optically: highly myelinated white matter and less myelinated grey matter which also contains unmyelinated neurons.

The different brain regions can be subdivided into discrete parts which have specific functions. This study is focused on the hippocampus, which will be explained in detail below.

1.2 Hippocampus

The hippocampus is located in the medial temporal lobe and is part of the limbic system. Its name ‘Hippocampus’ has been derived from the Greek word for seahorse, because of its structural resemblance to seahorse. It is a paired structure with a hippocampus in each hemisphere. It is subdivided into several regions: Cornu Ammonis (CA) 1 to CA3 and the dentate gyrus (DG). The CA region consists of several layers: stratum (st.) pyramidale (pyr.), st. oriens (ori.), st. radiatum (rad.) and

st. lacunosum moleculare (lm.). The st. pyr. contains the somata of excitatory pyramidal neurons, these neurons stretch their axons into the st.ori. The dendrites of these neurons extend into the st. rad. The other layers contain inhibitory interneurons and several types of glial cells. The dentate gyrus has a typical V-shape. It contains the neuronal granular cell layer. The inside of this layer is called hilus and the outer layer is called st. moleculare (Amaral and Witter, 1989). The subgranular zone (SGZ) is the innermost granule cell layer, it is one of the neurogenic niches in the adult brain, and it contains neural stem cells which can differentiate into new neurons (Seri et al., 2001).

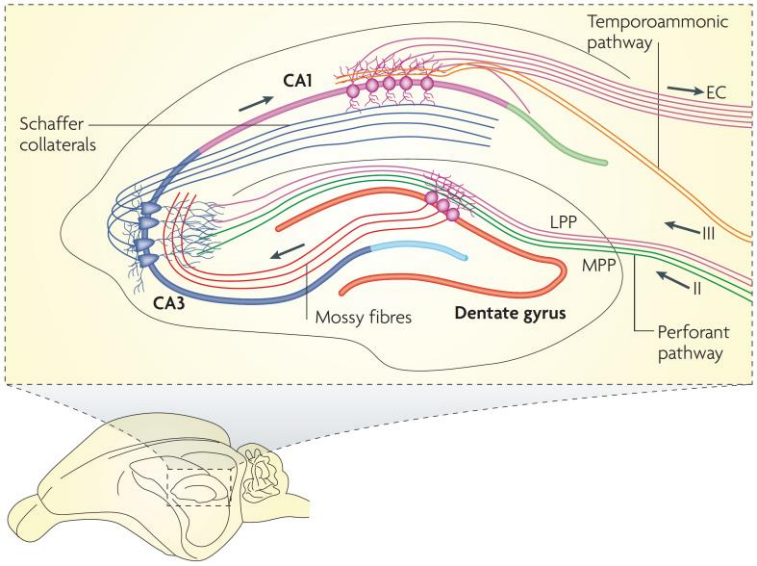

Figure 1.1 Anatomy and neuronal circuit of the hippocampus. In the small inset the localization of the hippocampus in the murine brain has been illustrated. The synaptic input from the entorhinal cortex reaches at DG; from DG it is sent via mossy fibers to the CA3 pyramidal neurons, from CA3 it is transferred by Schaffer collaterals to the CA1 neurons, CA1 neurons signal back to the entorhinal cortex. LPP, lateral perforant pathway; MPP, medial perforant pathway. From Deng et al., 2010.

In the hippocampus the neuronal circuit is a trisynaptic excitatory pathway as shown in figure 1.1. From the entorhinal cortex the synaptic input arrives in the DG and from DG it is propagated by mossy fibers to the CA3 pyramidal neurons. From CA3 neurons Schaffer collaterals project to the dendrites of CA1 pyramidal neurons in the

st. rad. From the CA1 neurons the signal is sent back to the entorhinal cortex (Deng et al., 2010).

The hippocampus plays a vital role in learning and memory. Long lasting changes in synaptic transmission on the cellular level are called synaptic plasticity, and these changes have been found to be correlated with memory formation. Long lasting changes in synaptic strength have been observed in rodents which were exposed to hippocampus related learning tasks (Martin and Morris, 2002). Furthermore, the hippocampus has been found to be involved in emotional behavior, and the emotional status has been shown to influence adult neurogenesis in the SGZ (Deng et al., 2010). In addition, reduced adult neurogenesis impairs learning, therefore, the integration of newly formed neurons is essential for memory formation (Martin and Morris, 2002).

1.3 Glial cells

In the central nervous system neurons are responsible for the fast and accurate transmission of signals and stimuli. However, these cells cannot perform their function without the support of glial cells. The term "glia" was introduced by Rudolf Virchow (1821-1902) in the mid-19th century and is translated from the Greek as "glue". This idea was based on the conviction that these cells are exclusively responsible for supporting and holding the neurons. Today, we know that the glial cells contribute much more to the neuronal physiology than first thought. For example, a rapid information transmission without the oligodendrocytes would be unthinkable, because they form the myelin sheath and thus insulate the axons electrically. Microglia combined with astrocytes form the innate immune system of the brain and both of these cell types are responsible for the protection against infection. Thus, each cell type has an important function in the brain and is therefore essential for homeostasis.

Basically, the glial cells are divided into two groups: microglia and macroglia. Macroglia are further subdivided into different cell subtypes: NG2 cells, oligodendrocytes and astrocytes.

1.3.1 NG2 cells

The term NG2 is derived from nerve / glial antigen 2, a proteoglycan expressed on the surface of these cells. Originally, NG2- positive cells were viewed as precursors of oligodendrocytes (oligodendrocytes precursor cells, OPCs) (Polito and Reynolds, 2005). However, increasing evidences support that these cells represent an independent glial cell type (Nishiyama et al., 2009) and it has been widely accepted as a fourth major glial cell type comprising 2-8 % of the cells in adult CNS, distinct from oligodendrocytes, astrocytes and microglia (Nishiyama et al., 2009). Also, it has been shown that NG2 can differentiate into astrocytes (Zhu et al., 2011), which suggests that the fate of NG2 cells is not determined toward oligodendrocytes lineage. In 2000, Bergles and colleagues provided evidence for the existence of functional synapses between neurons and glial cells in the hippocampus (Bergles et al., 2000). The postsynaptic glial cells were identified as NG2-positive OPCs. Additional properties of these cells included the expression of α-amino-3-hydroxy-5-methyl-4-isoxazolepropionic acid (AMPA) and γ-aminobutyric acid (GABA) receptors (Bergles et al., 2000; Bergles et al., 2010), lack of gap junction-mediated coupling, and the absence of glutamate transporters (Matthias et al., 2003).

1.3.2 Oligodendrocyte

As already mentioned before, the oligodendrocytes form an insulating layer around the axons of the neurons in vertebrates. This insulating layer is called myelin sheath and consists of the complex and lipid-rich myelin. This insulation is interrupted at nodes of Ranvier and primarily accelerates the signal transduction, because the action potentials can only arise at the nodes of Ranvier, called "saltatory conduction" (Huxley and Stampfli, 1949). The myelin sheath is probably not only the electrical insulation, but has also neuroprotective and neurotrophic effects (Nave, 2010; Wilkins et al., 2003). Demyelination and thus an impaired signal transduction takes place during some neurodegenerative diseases such as multiple sclerosis or acute disseminated encephalomyelitis (Love, 2006). In this case, the immune system and the overproduction of cytokines such as tumor necrosis factor α (TNF-α) and interferon play a central role (Ledeen and Chakraborty, 1998). Oligodendrocytes also

express AMPA, kainate and N-methyl-D-aspartate (NMDA) receptors in addition to ATP-gated P2X7 receptors (Bradl and Lassmann, 2010).

1.3.3 Microglia

Microglia represent the immune system of the brain (Kreutzberg, 1996). It is the only cell type in the brain that is not derived from the neuroectoderm. These are phagocytic descendants of the mesoderm, which migrate into the brain during embryonic development (Vilhardt, 2005). Microglia promote neuronal survival, regulate generation of neurons and oligodendrocytes, play a vital role in the processes involved in learning and memory, in addition to supporting synaptic plasticity and cognitive function (Eyo et al., 2016). Interestingly, the morphology and density of microglia varies as a function of their localization in the brain (Lawson et al., 1990). Microglia density in the healthy brain is highest in the hippocampus especially in the CA1 and DG (Jinno et al., 2007).

In the resting state, microglial cells have a ramified morphology, a small cell soma with fine extensions. By using these active motile appendages they continuously monitor their surroundings without disturbing the neural integrity (Davalos et al., 2005; Dibaj et al., 2010; Nimmerjahn et al., 2005). The surface of these appendages is decorated with numerous receptors for chemokines, cytokines, and also receptors from the complement family (Kettenmann et al., 2011). A characteristic feature of microglia is its activation at a very early stage after an injury or infection (Cherry et al., 2014; Rock et al., 2004). The cells respond not only to gross violations of the structural integrity, but also to more subtle changes in the environment, such as variations in the ion balance (Kreutzberg, 1996). Microglia detect pathological changes in the tissue, and become activated. Microglia activation is characterized by increased proliferation, morphological transformation, the release of various types of pro-inflammatory cytokines such as Interleukin 1β (IL-1β), Interleukin 6 (IL-6), TNF-α and / or chemokines (Banati et al., 1993; Smith et al., 2012; Vezzani et al., 2008). In addition to the neutralization and removal of the invaders, toxic substances, cellular debris and apoptotic neurons (Ahlers et al., 2015) by phagocytosis (Sierra et al., 2013), microglia can act as antigen presenting cells (O'Keefe et al., 2001). They are

also responsible for the elimination of synapses, for example during postnatal development (Tremblay et al., 2011).

Besides their inflammatory response to damage associated molecular patterns (DAMPs) and pathogen associated molecular patterns (PAMPs) (Heneka et al., 2014; Town et al., 2005), it has been revealed that microglia also exchange information with neurons. Microglia physically interact with neurons, modulate neurotransmission (Eyo et al., 2016), regulate synaptic activity (Ji et al., 2013), and actively participate in remodeling synaptic architecture (Tremblay et al., 2010). It has been suggested that microglia modulate neuronal activities (Bechade et al., 2013; Eyo and Wu, 2013). On one hand, receptors for cytokines such as IL-1β can be found on the surface of nerve cells, these receptors exert an influence on neuronal activity (Viviani et al., 2003), while on the other hand, the microglia express the receptors for different neurotransmitters, which may cause inflammatory or neuroprotective outcomes depending on the situation (Pocock and Kettenmann, 2007).

During neuro-pathophysiological conditions microglia can play both neuroprotective as well as neurotoxic roles depending on the situation (Ransohoff and Perry, 2009). Activated microglia have been observed in animal models of epilepsy (Avignone et al., 2008; Eyo et al., 2014) as well as in the brain tissue obtained from temporal lobe epilepsy (TLE) patients (Beach et al., 1995). Activated microglia release inflammatory cytokines such as IL-1β (Smith et al., 2012; Vezzani et al., 2008) and it has been shown that IL-1β promotes febrile seizures (FSs) (Dube et al., 2005; Heida et al., 2009; Yu et al., 2012). Furthermore, in humans polymorphism in the IL-1β gene has been found to increase the susceptibility for FSs (Kira et al., 2010; Virta et al., 2002a).

1.3.4 Astrocytes

The name ‘astrocyte’ is derived from their typical star-like morphology. These cells have a ramified structure with fine processes. The main component of intermediate filaments of all astrocytes is the glial fibrillary acidic protein (GFAP), which is

expressed in adult astrocytes (Brenner et al., 1994). A distinction is made between the protoplasmic astrocytes, especially in the gray matter and the fibrous astrocytes, which are found mainly in the white matter. The fibrous astrocytes have an elongated shape and are often aligned parallel to the axons. However, the protoplasmic astrocytes are characterized by a more compact form, which is caused by a very dense network of lateral branches that arises from the thicker primary projections. With the help of different staining methods, it has been found that protoplasmic astrocytes are organized into domains (Bushong et al., 2002; Ogata and Kosaka, 2002). In this case, a cell occupies a polyhedral shaped space, so that all synapses and blood vessels in this area are in contact with one astrocyte. Therefore, an astrocyte can contact several thousand synapses (Clarke and Barres, 2013; Halassa et al., 2007). The domains of adjacent cells slightly overlap only at the outer borders. This phenomenon was observed in both murine and human astrocytes in the cortex and hippocampus (Oberheim et al., 2006). However, there is also evidence that the size of astrocytes and their degree of overlap are not constant, but can change during the course of life (Grosche et al., 2013). Studies have shown that protoplasmic astrocytes are approximately 2.5 times larger in diameter and have a 10 times denser network of main extensions in humans than those in rodents (Oberheim et al., 2009). Also, the ratio of astrocytes per neuron increases with increasing brain complexity (Allaman et al., 2011; Nedergaard et al., 2003). In the human brain astrocytes are the most common cell type, they make up around 80 % of all the cells in the brain (Kettenmann and Ransom, 1995). The fact that the ratio between glial cells and neurons, called ‘Glia index’ increases with the degree of development of the living organism (Nedergaard et al., 2003) can be the first evidence that supports the involvement of astrocytes in information processing.

The astrocytes form end feet at the extensions that have contact with the blood vessels. This structure can be regarded as a special compartment, with an increased expression of certain proteins such as aquaporin 4 (AQP4), inwardly rectifying potassium channel (Kir) 4.1, glucose transporter and connexin43 (Cx43) (Crunelli et al., 2015; Wang and Bordey, 2008). Through their end feet enwrapping blood vessels, astrocytes take up water and metabolites from the blood and release

excess water, ions and toxins into the blood (Nedergaard et al., 2003; Strohschein et al., 2011). Astrocytes provide a link between the capillaries and neurons (Nagelhus et al., 2004; Simard and Nedergaard, 2004), and thus play a central role in the neuro-metabolic coupling. Increased neuronal activity triggers Ca^{2+} release in astrocytes. This leads to the release of vasoactive substances from astrocytes that regulate local blood flow (Attwell et al., 2010; Takano et al., 2006). This enables the supply to the neurons to be adjusted according to the actual neural activity. Of course, an increased neuronal activity requires more energy and thus reshapes astroglial metabolic networks (Escartin and Rouach, 2013).

The processes of astrocytes often surround and envelop synaptic connections and form the so called tripartite synapse (Nedergaard and Verkhratsky, 2012; Pannasch and Rouach, 2013). The astrocytes not only take up K^+ ions and neurotransmitters such as glutamate (Coulter and Eid, 2012) and GABA but are actively involved in the processing of information. They can receive signals from neurons and react to it (Clarke and Barres, 2013) by releasing so-called “gliotransmitters”, including glutamate, D-serine and ATP (Harada et al., 2015), and thus can influence neuronal activity (Bazargani and Attwell, 2016; Haydon, 2001; Volterra and Meldolesi, 2005). In fact, on astrocytes similar receptors can be found as on neurons; depending on the brain region, the receptors can be for glutamate, purine, GABA, noradrenaline, histamine and others (Agulhon et al., 2008; Dani and Smith, 1995; Martin, 1992). Thus, astrocytes are capable of receiving signals from the neurons. Most of these are metabotropic receptors that have a connection to second messenger systems, including phospholipase C, inositol trisphosphate (IP3), Ca^{2+} and cyclic adenosine monophosphate (cAMP) (Verkhratsky et al., 1998; Volterra and Meldolesi, 2005). It has been shown that in acute hippocampal slices neural activity at the mossy fiber CA3 synapses increases the intracellular Ca^{2+} concentration ($[Ca^{2+}]_i$) and triggers interastrocytic Ca^{2+}-waves (Dani et al., 1992). This applies not only to glutamate, but also similar Ca^{2+} signals in the hippocampus can be triggered by the release of acetylcholine (Araque, 2008). Further analysis showed that these signals can be divided into two groups: 1) Ca^{2+} oscillations, defined as recurrent increases in $[Ca^{2+}]_i$ within a cell and 2) Ca^{2+} -waves, defined as radially propagating increases of $[Ca^{2+}]_i$

emanating from a cell and then spreading to neighboring cells (Berridge et al., 1998). In addition to glutamate, GABA and ATP can trigger Ca^{2+} oscillations (Dani and Smith, 1995). The astrocytes are not only able to receive signals from the neurons but also Ca^{2+} signals in astrocytes may in turn cause the release of neuroactive substances in the extracellular space. These include transmitters, eicosanoids, steroids, neuropeptides and growth factors (Araque, 2008; Araque and Navarrete, 2010; Haydon and Carmignoto, 2006; Martin, 1992). One possible function of this ability of astrocytes to influence neuronal activity is the synchronization of large neuron clusters. If one considers that the processes of a single astrocyte contact thousands of synapses and that the astrocytes form the largest network in the brain, the potential of this cell type is evident.

Since astrocytes are coupled to each other via gap junction channels that are composed of connexins (Cxs) (Dermietzel et al., 2000; Giaume and McCarthy, 1996; Gosejacob et al., 2011; Kielian, 2008), they make up the largest network in the brain. In the hippocampus this network is formed during early postnatal development (Schools et al., 2006). The astrocytes are responsible for the supply of nutrients to neurons, removal and recycling of glutamate from the synapses (Coulter and Eid, 2012), and the buffering of extracellular K^+ ions (Kofuji and Newman, 2004; Steinhäuser et al., 2012; Steinhäuser et al., 2016). The functional interastrocytic gap junctional coupling (IGJC) plays a key role in these processes. The gap junction channels are permeable to substances smaller than 1.2 kDa and are regulated by a number of factors including pH, Ca^{2+} concentration, intracellular voltage differences and inflammatory mediators like IL1-β (Meme et al., 2004; Meme et al., 2006; Rouach et al., 2002a).

Studies performed on sclerotic hippocampi from epilepsy patients and experimental animal models have shown that astrocytes are uncoupled in the last chronic stage of the disease (Bedner et al., 2015). During neuronal activity K^+ ions are released. These ions must be removed quickly, otherwise they lead to a sustained depolarization of the membrane and thus can affect the activity of ion channels, receptors and transporters (Steinhäuser and Seifert, 2012). During a pathologically

increased neuronal activity, the extracellular concentration of K^+ ions can increase from 3 mM to 10-12 mM (Heinemann and Lux, 1977; Steinhäuser et al., 2012). The activity of Na^+ / K^+ pumps present in the cells is not sufficient to rapidly transport as much K^+ ions into the cells. Two additional mechanisms for K^+ buffering have been described, the Na^+ / K^+ / 2Cl cotransporter and the "spatial buffering" (Kofuji and Newman, 2004; Steinhäuser et al., 2016). The former is likely to play a minor role. Besides, intracellular K^+ accumulation results in water influx and cell swelling. The concept of spatial buffering, however, states that astrocytes take up the excess K^+ ions in regions of high neuronal activity, and carry it away by the astrocytic network to regions of lower K^+ ions concentrations, where it is then released into the extracellular space (Kofuji and Newman, 2004; Steinhäuser et al., 2012; Steinhäuser et al., 2016). Uptake and release of K^+ ions takes place here by Kir4.1. The effectiveness of the K^+ buffering depends on the proper function and distribution of K^+ channels, water channels AQP4 and IGJC (Hibino et al., 2010; Reimann and Ashcroft, 1999; Steinhäuser et al., 2012; Steinhäuser et al., 2016).

Transporting the metabolic substrates such as glucose, lactate and amino acids to the neuron is needed not only for the energy supply, but also for the synthesis of neurotransmitters such as GABA and glutamate. After the neurons have released neurotransmitters at synapses, these are taken up by astrocytes from the extracellular space (Coulter and Eid, 2012). Here a special role is played by the glutamate transporters expressed in astrocytes, because glutamate is potentially neurotoxic and is mainly taken up by astrocytes (Coulter and Eid, 2012). These transporters are very effective and keep the extracellular glutamate concentration in the nM range (Danbolt, 2001). A down-regulation of astrocytic glutamate transporter leads to an accumulation of the neurotransmitter in the extracellular space and thus creates a continuous excitation of neurons, which can ultimately lead to their death (Herman and Jahr, 2007; Jabaudon et al., 1999; Sah et al., 1989). Indeed, dysfunction of glutamate transporters, named excitatory amino acid transporter (EAAT) 1 and EAAT2, were observed in pathological conditions, including epilepsy (Seifert et al., 2006). Another mechanism that leads to the accumulation of glutamate in the extracellular space and is likely to contribute to the development of epilepsy is

the loss of activity of the enzyme glutamine synthetase (GS) in astrocytes (Coulter and Eid, 2012; Eid et al., 2008; Nedergaard et al., 2003; Norenberg, 1979; van der Hel et al., 2005). This enzyme converts glutamate to glutamine in astrocytes, which is released into the extracellular space and is subsequently taken up by the neurons (Coulter and Eid, 2012). GS deficiency slows down glutamate uptake, leading to increased glutamate levels in the ECS. The glutamate-glutamine cycle is essential for replenishing the neurotransmitter pool and maintenance of synaptic activity. Interruption of the cycle rapidly depletes inhibitory (GABAergic) transmission, while excitatory synaptic function is sustained (at least transitionally) due to the higher reserve pools of cytoplasmic glutamate (Liang et al., 2006; Robel and Sontheimer, 2016; Steinhäuser et al., 2016).

It has been suggested that under neuro-pathological conditions, astrocytes can play pro-inflammatory as well as anti-inflammatory roles depending on the plethora of molecular, cellular and physiological conditions (Sofroniew, 2015). In response to traumatic CNS insults, astrocytes undergo biochemical, physiological and morphological changes (Wilhelmsson et al., 2006), collectively termed as “reactive astrogliosis” (Sofroniew and Vinters, 2010). Reactive astrogliosis has been classified into three categories: mild to moderate reactive astrogliosis, severe diffuse reactive astrogliosis and severe reactive astrogliosis with compact glial scar formation (Sofroniew and Vinters, 2010). Astrocytes interact with other cell types, especially fibromeningeal and other glial cells to form complex glial scars in the CNS (Sofroniew, 2009). It has been shown that the scars formed by reactive astrocytes can have positive affect including repairing blood brain barrier (BBB), limiting leukocyte infiltration and act as a neuroprotective barrier (Bush et al., 1999; Faulkner et al., 2004; Herrmann et al., 2008). Reactive astrocytes can have both pro- and anti-inflammatory effect on microglia (Davalos et al., 2005; Min et al., 2006). In response to IL-1β astrocytes generate and release vasoactive substances like VEGF, which increases BBB permeability and promotes leukocytes infiltration (Argaw et al., 2009; Argaw et al., 2012). It has been suggested that brief disruption in the BBB is enough to induce focal epilepsy in rats (Seiffert et al., 2004). Under inflammatory conditions, astrocytes release inflammatory cytokines such as TNF-α and IL-1β (Dube et al.,

2010). The inflammatory cytokines depolarize astrocyte which as a result decreases K^+ and glutamate uptake (Kielian, 2008) resulting in hyperexcitability which can promote epileptogenesis.

1.4 Connexins

For intercellular communication cells are connected via gap junctions. Gap junctions allow the transfer of ions and small molecules between the cytoplasm of cells bypassing the extracellular space. Gap junctions are composed of Cxs. In human 21 genes and in mice 20 genes have been identified to encode for Cxs (Sohl and Willecke, 2004). In the rodent brain 11 Cxs have been detected. Cxs are named based on their molecular mass. Cx43, for instance, has a molecular weight of 43 kDa (Sohl and Willecke, 2004).

After and / or during translation Cxs integrate into the endoplasmic reticulum. Oligomerization of six Cxs to form a hexameric hemichannel called ‘connexon’ has been suggested to take place in a progressive fashion, it starts in the endoplasmic reticulum and completes in the Golgi apparatus (Laird, 2006; Musil and Goodenough, 1993). Connexons are transported in vesicles via microtubules to the plasma membrane. Each Cx protein has two extracellular loops, four transmembrane domains, one cytoplasmic loop, one cytoplasmic C- and one cytoplasmic N- terminus (see Fig. 1.2b). The transmembrane domains form the wall and pore of the channel. The extracellular loops are involved in cell-cell recognition and docking processes. Each extracellular loop contains three cysteine residues which form disulfide bonds between the connexons of opposite plasma membranes. When two hemichannels from opposing cells come in contact a functional gap junction is formed.

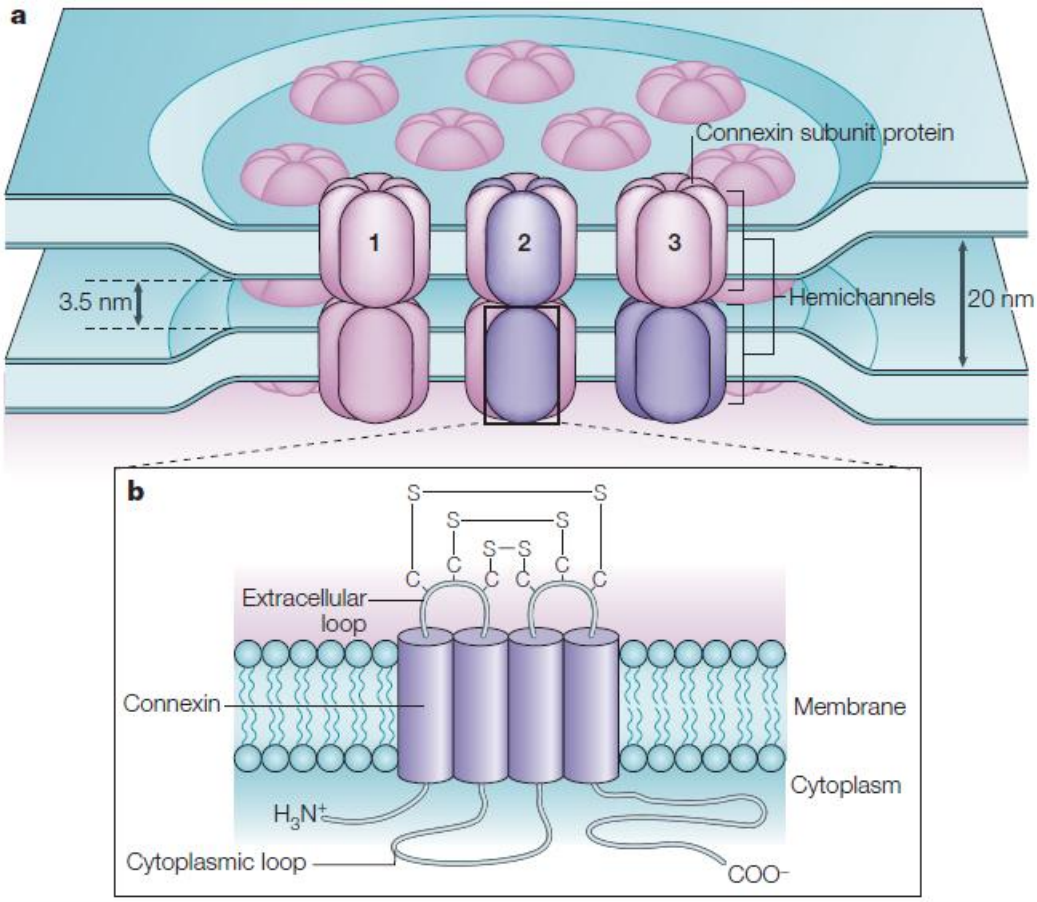

Figure 1.2 Gap junction plaque configuration and connexin structure. a) A gap junction plaque consists of several hemichannels formed of hexameric connexons. Gap junctions are comprised of two connexons connected together from two plasma membranes. Gap junctions composed of one Cx isoform are called homotypic or homomeric (1), gap junctions formed of connexons where each connexon consists of different Cx isoforms are termed as heteromeric (2), gap junctions made of two different homomeric connexons are called heterotypic gap junctions (3). (b) Each Cx consists of two extracellular loops, four transmembrane domains, one cytoplasmic loop, one cytoplasmic C- and one cytoplasmic N- terminus. From Sohl et al., 2005.

Gap junctions formed between cells can be homotypic, heterotypic and / or heteromeric intercellular channels. Homotypic or homomeric intercellular channels are formed by identical connexons, heterotypic channels are composed of two connexons of different Cx composition (Dedek et al., 2006) and gap junctions formed from connexons composed of different Cx isoforms (He et al., 1999) are named heteromeric gap junctions (see Fig. 1.2a). It has been shown that the combination of

the same and / or different Cxs and connexons to form functional gap junctions increases the diversity of intercellular gap junctions with a variety of functions and adds different physiological properties including permeability, single and multiple channel conductance's states (Goodenough and Paul, 2009). Originally it was suggested that small molecules up to 1.2 kDa can freely move through gap junctions (Simpson et al., 1977), but later studies suggested selective permeability of gap junctions depending on their composition (Kielian, 2008; Mese et al., 2007). The gap junctions formed of different Cxs showed similar permeability for ions but displayed differences in permeability for larger metabolites and second messengers (Mese et al., 2007). Membrane-spanning hemichannels which cannot form gap junctions and / or before forming gap junctions can also be functional under different conditions and open into the extracellular space resulting in the release of ATP, glutamate, nicotinamide adenine dinucleotide (NAD^+) and prostaglandin E2, which act as paracrine messengers (Evans et al., 2006). Gap junction channels cluster into microdomains in the plasma membrane, called gap junction plaques (Gaietta et al., 2002). A gap junction plaque is a highly dynamic structure which is in a continuous process of formation and degradation, where newly formed gap junction channels are added to the periphery of the plaque and old channels are removed from the center of the plaques (Gaietta et al., 2002) and internalized into pleomorphic vesicles called 'annular junction' (Jordan et al., 2001). Gap junctions in annular junction are then subject to lysosomal or proteasomal pathways for degradation (Falk et al., 2014).

Cxs are expressed in almost all cell types in the brain, except in NG2 cells. In brain, astrocytes display the highest level of two Cxs, i.e. Cx30 and Cx43 which are the major Cxs co-expressed in hippocampal astrocytes (Giaume and McCarthy, 1996; Gosejacob et al., 2011). In addition to Cx30 and Cx43, the expression of other Cxs namely Cx26, Cx32, Cx40, Cx45 and Cx46 have been detected in astrocytes (Blomstrand et al., 2004; Dermietzel et al., 2000) which have been reported to play compensatory roles (Dermietzel et al., 2000; Scemes et al., 1998). Nevertheless, the two Cx proteins Cx30 and Cx43 provide the structural basis for the formation of astroglial networks through which intercellular transfer of energy metabolites

(Rouach et al., 2008), gliotransmitters, signaling molecules (Harris, 2007), and spatial buffering of K^+ takes place (Wallraff et al., 2006).

Gap junction communication can be regulated at several levels including transcription, translation, post-translational processing like phosphorylation, insertion and / or removal from plasma membrane (Kielian, 2008). Furthermore, the permeability of gap junctions is regulated by a number of factors including pH, Ca^{2+} concentration, intercellular voltage differences, etc (Rouach et al., 2002a). In many studies, inflammation, inflammatory cytokines and mediators have been suggested to play a critical role in the regulation of gap junctional communication (Kielian, 2008). Though astrocytes express both Cx30 and Cx43, the former is more important in the thalamus while the latter has been suggested to play the major part in gap junctional coupling in the hippocampus (Dermietzel et al., 2000; Gosejacob et al., 2011; Griemsmann et al., 2015; Kielian, 2008). It has been shown that IL-1β inhibits gap junctional communication in primary human fetal astrocytes which was suggested to be caused by the reduction in Cx43 mRNA and protein expression (Duffy et al., 2000; John et al., 1999). In similar studies reduction in IGJC under the influence of IL-1β and TNF-α has been reported (Meme et al., 2004; Meme et al., 2006). TNF-α has also been shown to reduce Cx43 promoter activity (Fernandez-Cobo et al., 1999). Furthermore, TNF-α was found to reduce gap junction coupling via Cx43 phosphorylation (Haghikia et al., 2008b). Moreover, the presence of activated microglia has been found to reduce gap junctional coupling and Cx43 expression (Faustmann et al., 2003; Rouach et al., 2002b). Also, lipopolysaccharide (LPS), which induces inflammatory responses, has been shown to reduce IGJC and Cx43 protein level (Bedner et al., 2015; Meme et al., 2006; Retamal et al., 2007).

Malfunction and / or dysregulation of gap junctional communication between astrocytes especially in the hippocampus has been associated with diseases and pathological conditions like epilepsy (Steinhäuser et al., 2012; Steinhäuser et al., 2016). Loss of IGJC has been shown in sclerotic hippocampal tissue resected from mTLE patients while IGJC was present in non-sclerotic specimens (Bedner et al., 2015). In the same study a mouse model of epilepsy was used which mimics

characteristics of human mTLE. In this model reduced IGJC preceded apoptotic neuronal death and the onset of chronic seizures and caused impaired K^+ clearance (Bedner et al., 2015). As a result of pathologically increased neuronal activity, the extracellular concentration of K^+ ions may increase from 3 mM to 10-12 mM (Heinemann and Lux, 1977; Steinhäuser et al., 2012). The extracellular K^+ ion concentration is mainly balanced and / or controlled by spatial buffering via IGJC (Kofuji and Newman, 2004; Steinhäuser et al., 2016). Impaired or reduced IGJC results in decreased or no spatial buffering of K^+, which can consequently lead to a sustained depolarization of the membrane and hyperexcitability that can trigger epileptiform activity (Steinhäuser et al., 2016).

In addition to the gap junction mediated communication, Cx43 is also involved in a number of other processes. The C-terminal domain of Cx43 contains binding sites for different proteins and appears to interact with the cell cycle, transcription control and the cytoskeleton (Giepmans, 2004). Beside astrocytic gap junctional communication, at least two channel-independent functions of Cx43 are known to date. These are the regulation of neurogenesis, neuronal migration and differentiation (Elias et al., 2007; Kunze et al., 2009; Prochnow and Dermietzel, 2008; Wiencken-Barger et al., 2007), and the regulation of the expression of P2Y1 receptors (Scemes, 2008). Moreover, it was shown that Cx43 regulates the transcription of a number of genes in the brains of mice (Iacobas et al., 2007; Spray and Iacobas, 2007).

1.5 Temporal lobe epilepsy

Coordinated activity of neurons is the basis for normal neuronal functioning. However, abnormal firing of neurons such as hypersynchronization and hyperactivity can result in seizures. Recurrent spontaneous seizures are the typical characteristics of epilepsy. Epilepsy has been regarded as a neuronal disorder or a family of neuronal disorders, but in 2014 the International League against Epilepsy (ILAE) characterized epilepsy as a disease and redefined epilepsy by any of the following conditions: "*1) At least two seizures occurring more than 24 h apart, 2) one unprovoked (or reflex) seizure and a probability of further seizures similar to the*

general recurrence risk (at least 60%) after two unprovoked seizures, occurring over the next 10 years, 3) diagnosis of an epilepsy syndrome" (Fisher et al., 2014). It affects about 2 % of the population worldwide (Hesdorffer et al., 2011). Most of the focal epileptic seizures in adults originate from the temporal lobe. Hippocampal sclerosis (HS) has been observed in most of the cases of TLE (Blumcke, 2009). The occurrence of TLE can be sporadic as well as familial (Kobayashi et al., 2001). One third of the epileptic patients suffer from intractable epilepsy and do not respond to anti-epileptic drugs (AEDs) (Jacobs et al., 2001; Wahab et al., 2010) and TLE represent almost even two thirds of cases of intractable epilepsy managed surgically (Blair, 2012).

1.6 Febrile seizures

Retrospective studies have revealed that more than 60 % of TLE patients with intractable epilepsy experienced FSs during childhood (Bender et al., 2004; French et al., 1993). In follow-up studies it was observed that 2-10 % of children with complex FSs developed subsequently epilepsy (Shinnar, 2003). FSs are the most common form of seizures in children. The frequency of the incidences in America and Europe is 2-5 %, Japan 8 % and the Marianas Islands around 14 % (Heida and Pittman, 2005; Stanhope et al., 1972; Tsuboi and Okada, 1984). The occurrence may be sporadic, but familial cases have also been reported. It is likely that both genetic and environmental factors might play a role in the development of FSs (Berg et al., 1999). FSs occur in infants and young children between the ages of 6 months to 5 years, with peak incidence at around 18 months (Hauser, 1994). Simple FSs last less than 15 min, do not recur and are generalized without a focal origin. Around 30 % of FSs are complex, i.e. they have a focal origin, last longer than 15 min and recur in 15-20 % of the cases within 24 h (Nelson and Ellenberg, 1976).

However, the role of the FSs in the onset of epilepsy is controversial because both prospective and retrospective studies revealed that the simple FSs seem to have no measurable effect on the development of epilepsy or other cognitive deficits (Berg and Shinnar, 1996; Verity et al., 1985; Verity et al., 1998). However, complex FSs can increase 10 times the risk for developing TLE (Pavlidou and Panteliadis, 2013).

Also, using magnetic resonance imaging studies it has been revealed that TLE patients with a history of FSs have greater probability to develop HS than patients without FSs (Sagar and Oxbury, 1987). It was suggested that either FSs cause mesial temporal sclerosis (MTS) and MTS subsequently leads to TLE or FSs cause TLE and later MTS results from epileptic seizures (McClelland et al., 2011). But in either case FSs seem to be the trigger that initiates a cascade of events which subsequently lead to epilepsy (see Fig. 1.3). Experimental FSs (EFSs) generated in rats revealed that complex seizures originate in the hippocampus or amygdala (Dube et al., 2009). After EFSs interictal activity has been observed in almost 90 % of the rats and 35-45 % of the rats became epileptic (Dube et al., 2006; Dube et al., 2010).

There are some genetic factors that might favor the generation of FSs (Berg et al., 1999). Both in humans and rodents mutations in Na^+ channels and GABA receptors as well as polymorphism of IL-1β have been associated with FSs and epilepsy (Escayg et al., 2000; Harkin et al., 2002; Virta et al., 2002a; Wallace et al., 1998).

1.7 Inflammation

Inflammation is a response of the body to noxious stimuli. The typical symptoms of inflammation are redness, warmth, swelling and pain. Inflammation can be acute and / or chronic. Acute inflammation returns the tissue to its normal state and is then resolved. But if the cause of inflammation is persistent than inflammation is increased and becomes chronic. Chronic inflammation has been found to be associated with many neurodegenerative diseases and epilepsy (Vezzani, 2014).

In the CNS an inflammatory response is elicited by two glial cell types: astrocytes and microglia. In response to DAMPs and / or PAMs these cell types are activated (Heneka et al., 2014; Town et al., 2005) and respond to maintain homeostasis of the tissue (Kreutzberg, 1996). Activated microglia and astrocytes have been observed in tissue resected from patients with intractable epilepsy (Beach et al., 1995; Najjar et al., 2011) and also have been shown in animal models of epilepsy (Avignone et al., 2008; Dube et al., 2010; Eyo et al., 2014; Patterson et al., 2015). Both cells types undergo pathophysiological, morphological, biochemical changes and release

inflammatory cytokines such as IL-1β and TNF-α (Dube et al., 2010; Smith et al., 2012; Vezzani et al., 2008). These cytokines have been found to be associated with epilepsy (Vezzani, 2014; Vezzani and Viviani, 2015). Significantly increased levels of the inflammatory cytokines IL-1β and TNF-α haven been observed in the serum (Choi et al., 2011), plasma (Tutuncuoglu et al., 2001; Virta et al., 2002b) and CSF (Haspolat et al., 2002; Tutuncuoglu et al., 2001) of FSs patients but not in control patients with fever without seizures. Similarly, in rats increased protein expression of IL-1β has been observed only in animals which developed epilepsy after EFSs (Dube et al., 2010).

It has been reported that IL-1β and TNF-α inhibit glutamate reuptake (Hu et al., 2000; Zou and Crews, 2005) and increase glial glutamate release (Bezzi et al., 2001), which consequently increases neuronal excitability (Vezzani and Granata, 2005), reduces seizure threshold and contributes to the generation of EFSs (Dube et al., 2005) and promotes epileptogenesis. Inflammatory cytokines have also been reported to increase hyperexcitability by their direct effects on neurons. IL1-β modulates NMDA receptor activity (Viviani et al., 2003; Yang et al., 2005) which results in hyperexcitability (Zhang et al., 2008; Zhang et al., 2010) and promotes seizure generation (Balosso et al., 2008). TNF-α increases hyperexcitability by enhancing exocytosis of AMPA receptors (Beattie et al., 2002; Stellwagen et al., 2005) and reducing inhibitory transmission through endocytosis of GABA-A receptors (Stellwagen et al., 2005). In addition, as a result of inflammation the BBB is disrupted and this compromises the capability of astrocytes to reuptake glutamate and buffer K^+, ultimately leading to hyperexcitability (Vezzani, 2014). Moreover, a positive correlation between BBB leakage and the frequency of spontaneous seizures was reported (van Vliet et al., 2007). The suggested cascade of inflammatory events leading to epilepsy has been summarized in figure 1.3.

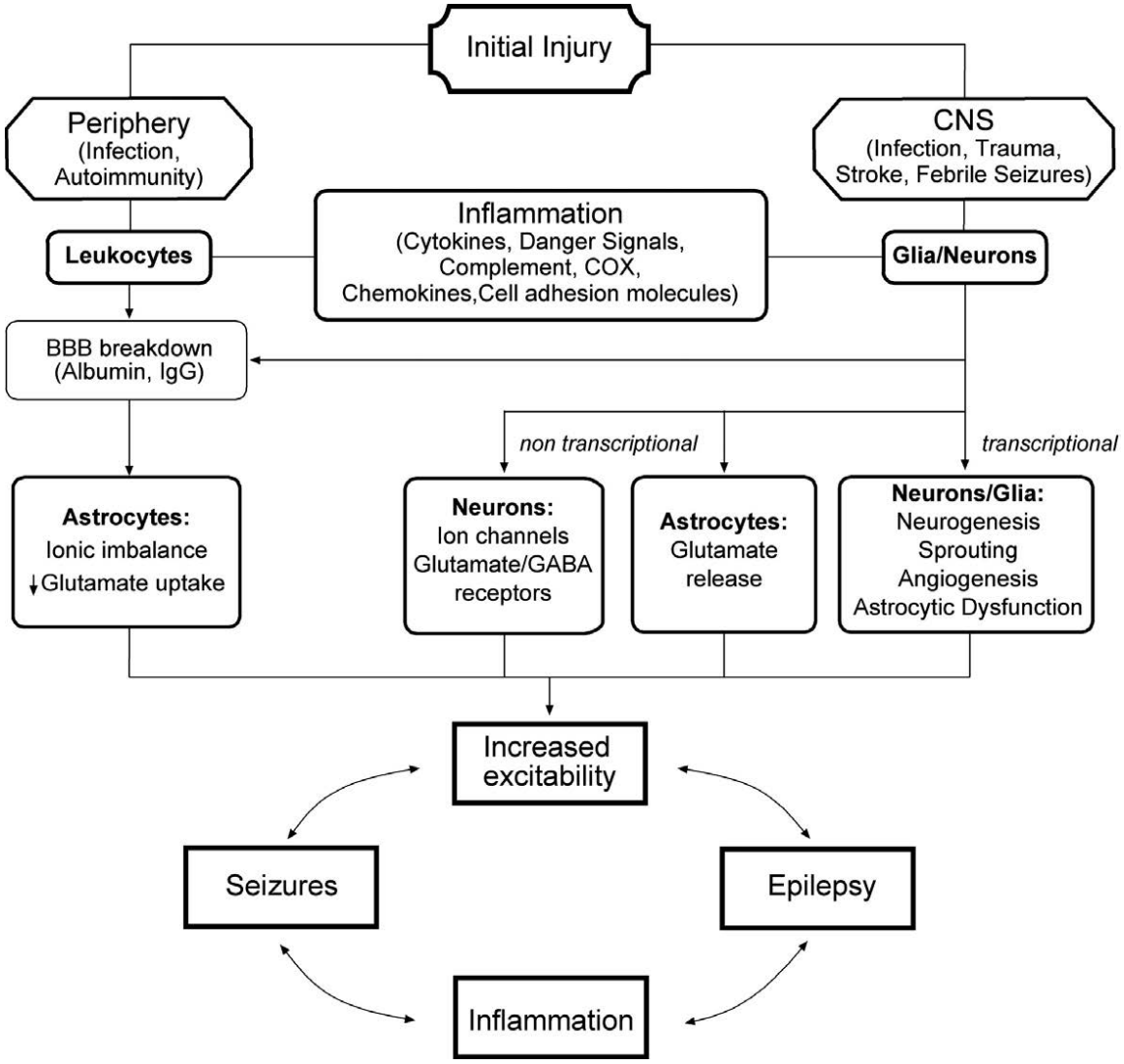

Figure 1.3 Pathophysiological cascade of events leading from inflammation to epilepsy (Vezzani, 2014).

1.8 TGF-β activated kinase 1 (TAK1) pathway

TAK1 is a member of the mitogen activated protein kinases (MAPKs) family (Yamaguchi et al., 1995). Toll like receptors (TLRs) upon recognition of PAMPs and / or DAMPs dimerize and activate downstream signaling pathways. It results in the recruitment of myeloid differentiation primary response 88 (MyD88) to the receptor via the TLR / IL-1 receptor (TIR) domain. As a consequence MyD88 recruits and activates IL-1R-associated kinase-4 (IRAK-4), which in turn phosphorylates and activates TNF receptor-associated factor 6 (TRAF6). Upon phosphorylation and

activation TRAF6 activates a complex containing TAK1, TAK1-binding protein (TAB) -1, and TAB-2/3 (Wang et al., 2001). This activated TAK1 complex mediates the activation of a nuclear factor-κB (NF-κB) pathway and the MAPK pathway (Sato et al., 2005; Shim et al., 2005; Wang et al., 2001).

The TAK1 complex phosphorylates and activates the IκB kinase (IKK) complex, which consists of IKKα, IKKβ, and NEMO (Wang et al., 2001). Upon activation, the IKK complex phosporylates IKβ, which than dissociates from NF-κB and is degraded via a proteasomal pathway. When NF-κB is released from IKβ, it is activated and translocated to the nucleus and results in the activation of gene transcription. In addition to NF-κB, TAK1 activates MAPKs including p38, c-jun N-terminal kinase (JNK), and extracellular signal-regulated kinase (ERK) that further activates the transcription factor AP-1 (Newton and Dixit, 2012). NF-κB and AP-1 promote the transcription of pro-inflammatory cytokines like TNFα, IL-6, and IL-1β and chemokines (Hayden et al., 2006; Zenz et al., 2008). The activation of TAK1 and its downstream signaling molecules is summarized in figure 1.4 (modified from Pathak et al., 2012).

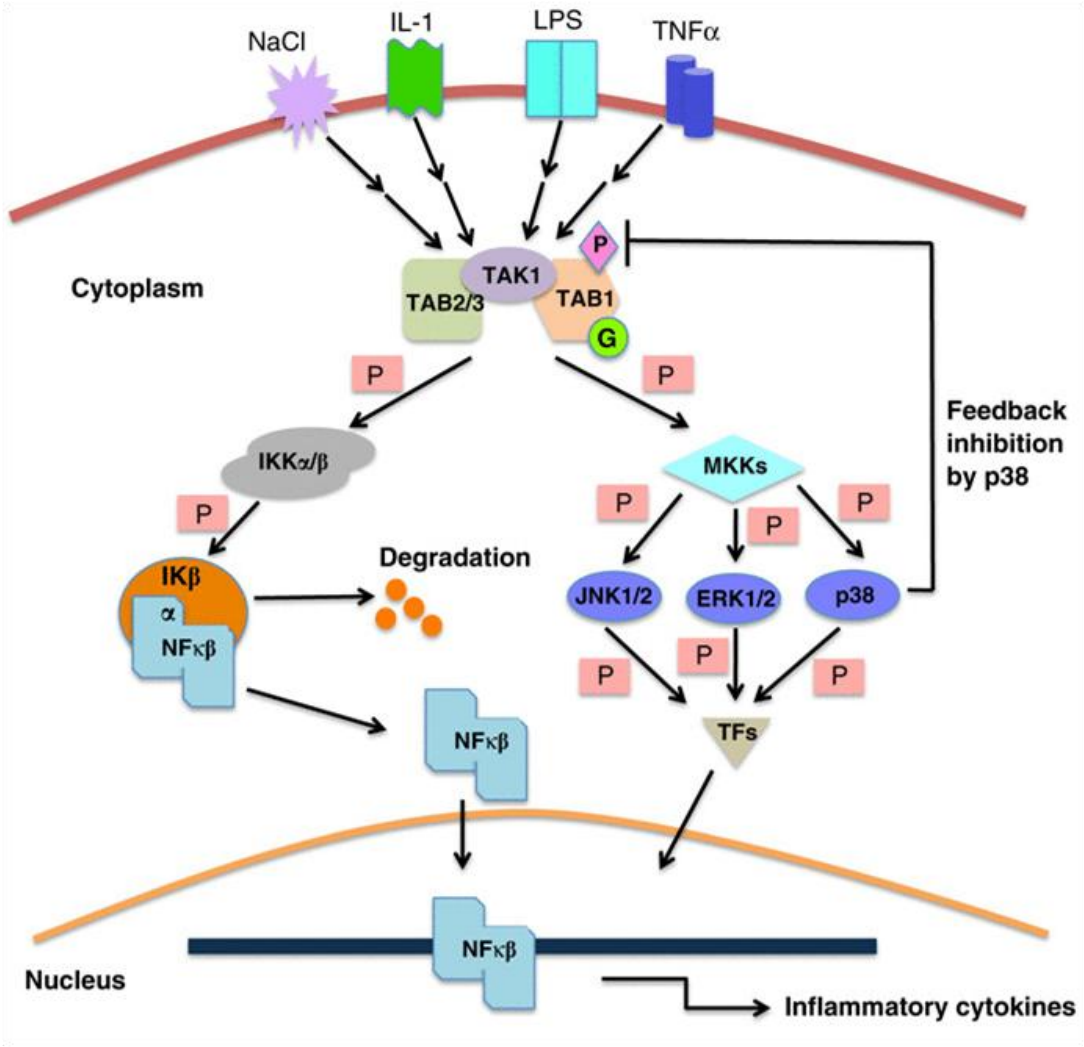

Figure 1.4 A brief overview of the TAK1 pathway. TAK1 is activated via TLRs in response to noxious stimuli, LPS and inflammatory mediators. Upon activation, TAK1 can activate MAPKs and NF-κB, which are involved in the transcription and / or activation of vital inflammatory, anti-apoptotic and cell signaling molecules. Modified from Pathak et al., 2012.

1.9 Lipopolysaccharide

The most important pro-inflammatory component of gram-negative bacteria is LPS (Rietschel et al., 1996). This molecule has an activating effect on cells of the immune system including microglia and astrocytes in the brain (Bourdiol et al., 1991; Kitchens, 2000). As a result, the activated cells release different inflammatory mediators such as IL-1β and TNF-α (Chung and Benveniste, 1990; Szczepanik et

al., 1996). TLR4 is responsible for the activation of the signaling cascade by LPS. It belongs to the group of TLR receptors that play a central role in innate immunity. These receptors recognize in the absence of pathogens also DAMPs (Miller et al., 2005), that are mostly cytosolic or nuclear proteins that are released as a result of the destruction of and / or damage to cells. The TLR family and IL-1 receptors belong to the same superfamily of transmembrane receptors that share TIR, a common intracellular domain and thus trigger the same signaling cascades (O'Neill and Bowie, 2007).

Escherichia coli (*E. coli*.) containing LPS is among the most important gram-negative pathogens. This bacterium is responsible for most of the meningitis diseases in infancy. Despite potent antibiotic therapies meningitis caused by gram-negative and gram-positive bacteria is correlated with higher complication and mortality rates. Up to 70 % of patients with septic meningitis develop septic encephalopathy (Schumann et al., 1998). It has been reported that seizures occur in 40 % of patients with bacterial meningitis (Anderson, 1993). Experimental results corroborate these observations. In animal models it has been demonstrated that LPS reduces the threshold for triggering seizures (Galic et al., 2008; Sayyah et al., 2003).

2 Aim of the study

In both retrospective and prospective studies, FSs in children have been suggested to increase the risk of developing epilepsy. Also, in animal models it has been shown that EFSs increase seizure susceptibility. In previous studies microgliosis, astrogliosis and IGJC have been linked with epileptogenesis. The aim of the first part of the present study was to investigate EFSs in mice as a consequence of glial dysfunction and to explore the probability for epilepsy development in EFS-induced animals.

There is increasing evidence, suggesting that inflammation promotes epileptogenesis and exacerbates tissue damage. TAK1 has been shown to affect inflammation and influence release of inflammatory cytokines. The objective of the second part of the present study was to employ cell type-specific TAK1KO mice to examine CNS inflammatory responses via microglia activation after *status epilepticus* and to investigate chronic seizure generation in cell type-specific TAK1KO mice.

3 Materials

3.1 Chemicals

In this work, chemicals and solutions from the following manufacturers have been used: Applied Biosystems (California, USA), Applichem (Darmstadt, Germany), Biostatus (Shepshed, UK), B. Braun (Melsungen, Germany), Carl Roth (Karlsruhe, Germany) , Dianova (Hamburg, Germany), Cell Signaling (Danvers, USA), Invitrogen (Darmstadt, Germany), Merck (Darmstadt, Germany), Millipore (Darmstadt, Germany), Polysciences (Warrington, USA), Promega (Madison, USA) Qiagen (Hilden, Germany), Roche (Manheim, Germany), R & D Systems (Germany), Sakura Finetek Europe (Zoeterwoude, The Netherlands), Sarstedt (Nümbrecht, Germany), Sigma Aldrich (Munich, Germany), Thermo Scientific (Waltham , MA, USA), Vector Laboratories (Burlingame, USA), Xencor (Monrovia, USA).

Kits

GoTaq DNA polymerase (Promega)
Pierce BCA protein assay Kit (Thermo Fisher Scientific)
SuperSignal West Dura extended duration substrate (Thermo Fisher Scientific)

3.2 General material

Borosilicate Glass	Science Products, Hofheim, Germany
Coverslips, Object slides	Engelbrecht, Edermünde, Germany
Disposable pipettes	Roth, Karlsruhe, Germany
Glass pipettes	Brand, Wertheim, Germany
Gloves	Ansell, Staffordshire, UK
Instant adhesive	Uhu, Bühl, Germany
Kimtech	Kimberley Clark
Needles and Syringes	BD, Franklin Lakes, USA
Parafilm	Pechiney Plastic Packaging, Chicago, USA
Plastic Pasteur pipettes	Roth, Karlsruhe, Germany
Pipetman	Gilson, Middleton, USA

PVDF membrane	Millipore, Schwalbach, Germany
Razor blade	Wilkinson, Bucks, UK
Reaction tubes, Well plates	Sarstedt, Nümbrecht, Germany
Surgical instruments	Fine Science Tools, Heidelberg, Germany
Syringe filters 4 mm	Thermo Fisher Scientific, Waltham, USA
Tape	Leukoplast, Hamburg, Germany
Tips, Tubes	Greiner Bio-One, Frickenhausen, Germany
Venofix	Braun, Melsungen, Germany
Whatman paper	Whatman International, Maidstone, UK

3.3 Software

Dataquest A.R.T. 4.00	DataSciences International, St. Paul, USA
Gold / Platinum	
GeneTools	Synoptics, Cambridge, UK
Igor Pro	Wave Metrics, Lake Oswego, USA, with Macros programmed by Dr. R. Jabs
ImageJ	NIH, Maryland, USA
Inkscape	TheInkscape Team
LAS AF	Leica Microsystems, Wetzlar, Germany
MC Stimulus II	Multi Channel Systems, Reutlingen, Germany
MetaVue	Molecular Devices, Sunnyvale, USA
SoftAmx	Pro Molecular Devices, Sunnyvale, USA
Tida	Heka, Lambrecht, Germany
SeeTec Office 5	Philippsburg, Germany

3.4 Equipment

Anti-Vibration Table	Newport Corporation, Irvine, USA
Bath chamber	Luigs & Neumann, Ratingen, Germany
Cryostat	Cryostat Microm HM560, Thermoscientific, Waltham, MA, USA

Chemiluminescence chamber	Gene Gnome 5 inkl. GeneSys Software Syngene, Cambridge, UK
EEG-Transmitter (telemetric)	TA10EA-F20, DataSciences International, St. Paul, USA
Glass pipett	Borosilikatglas GB150F-10, Hilgenberg, Malsfeld, Germany
Hair Dryer (6 steps)	Magic, SD-28, 1800 Watt, Germany
Infra red camera	Optronis VX45, Optronis GmbH, Germany
Micromanipulator	Micromanipulator 5171, Eppendorf, Germany
Microscope (immunofluorescence)	Axiophot Carl Zeiss GmbH, Göttingen, Germany With software Metaview, Universal Imaging, West Chester, USA
Microscope (Patch-Clamp)	AxioskopFS1 Zeiss, Oberkochen, Germany
Patch-Clamp amplifier	EPC 9 and Software Tida 5.x HEKA Electronic, Lambrecht / Pfalz Germany
Peristaltic pump	ISM 930C Ismatec / Idex, Wertheim / Mondfeld, Germany
Photometer	Molecular Devices, OptiMAX Sunnyvale, USA
Puller (Pipette puller)	P-87 und P-2000 (Sutter Instruments, Novato, USA)
Receiver plate for EEG transmitter	RPC-1 DataSciences International, St. Paul, USA
SDS-Page-Systen	Mini-PROTEAN® 3 Cell # 165-3301 Bio-Rad, Hemel Hempstead, UK
Support for stereotactic injection	TSE Systems GmbH, Bad Homburg, Germany
Transponder for measuring body temperature	IPTT-300 BioMedic Data Systems, Seaford, USA

Temperature transponder reader	DAS-7007s BioMedic Data Systems, Seaford, USA
Vibratome	VT1000S Leica Microsystems, Wetzlar, Germany
Video monitoring system with Infra red cameras	SeeTec Axis 221 Indoor Vario
Voltage source for SDS-PAGE and WB	PowerPac™ HC Power Supply Bio-Rad, Hemel Hempstead, UK
Water bath	WB-10 PD-Industriegesellschaft mbH, Germany
Water immersion objective	LUMPlanFL/IR 60 x Olympus, Japan
WB-System	Mini Trans-Blot® # 170-3930 Bio-Rad, Hemel Hempstead, UK

3.5 Solutions and buffers

3.5.1 Solutions for the patch clamp experiment

Sucrose-preparation solution

NaCl	87	mM
KCl	2.5	mM
NaH_2PO_4	1.25	mM
$MgCl_2$	7	mM
$CaCl_2$	0.5	mM
$NaHCO_3$	25	mM
Glucose	25	mM
Sucrose	75	mM

pH 7.4 adjusted with carbogen (95 % O_2 and 5 % CO_2)

ACSF

NaCl	126	mM
KCl	3	mM
$MgSO_4$	2	mM
$CaCl_2$	2	mM
Glucose	10	mM
NaH_2PO_4	1.25	mM
$NaHCO_3$	26	mM
and pH 7.4 adjusted with carbogen (95 % O_2 and 5 % CO_2)		

Pipette solution (with biocytin)

K-Gluconate	130	mM
$MgCl_2$	1	mM
Na_2-ATP	3	mM
HEPES	20	mM
EGTA	10	mM
Biocytin	0.5 %	w / v
(N-biotinyl-L-lysin)		
pH 7.2		

3.5.2 Solutions and buffers for immunohistochemistry

Phosphate buffered saline (PBS) 10x

NaCl	1.5	mM
Na_2HPO_4	83	mM
NaH_2PO_4	17	mM
pH 7.4 adjusted with HCl		

Fixative solution (4% PFA)

A. dest	800	ml
Paraformaldehyde	40	g
- dissolve and add NaOH until the solution is clear		
PBS (10x)	100	ml
- fill with A. dest to 1000 ml		
pH 7.4 adjusted with NaOH or NaCl		

PBS with sodium azide

NaN_3 dissolved in 1x PBS	0.01%	w / v

Blocking solution

NGS	10 %	v / v
Triton X-100	2 %	v / v
diluted in 1x PBS, pH 7.4		

Streptavidin Cy3 solution

Streptavidin	1:300	
NGS	2 %	v / v
Triton-X	0.1 %	v / v
diluted in 1x PBS, pH 7.4		

Primary antibody solution

NGS	5 %	v / v
Triton-X	0.1 %	v / v
diluted in 1x PBS, pH 7.4		

Secondary antibody solution

NGS	2 %	v / v
diluted in 1x PBS, pH 7.4		

Nuclear staining solutions

Hoechst	1 %	v / v

Or

Draq5	0.1 %	v / v
diluted in dH_2O		

3.5.3 Solutions for the protein analysis (SDS and WB)

Lysis buffer

Tris	50	mM
NaCl	150	mM
NP-40	0.5 %	v / v
Na-deoxycholate (10 %)	0.5 %	v / v
Triton X-100	1 %	v / v
Fill up to 500 ml with dH_2O, pH 7.5		

10 x SDS-Page running buffer

Tris	25	mM
Glycin	192	mM
SDS	1 %	w / v
pH 8.3 (not adjusted, only measured)		

10 x Transfer buffer (WB)

Tris	25	mM
Glycin	192	mM
pH 8.3 (not adjusted, only measured)		

10 x TBST (Wash buffer)

Tris	25	mM
NaCl	150	mM
Tween 20	0.05 %	v / v
pH 7.4 (adjusted with HCl or NaOH)		

Blocking solution (WB)

Milk powder	5 %	w / v
Dissolve in wash buffer		

Ammoniumpersulfat (APS) (10%)

APS	0.1	g
in 1 ml of deionized water		

Stacking gel buffer

Tris	0.5	M
SDS	0.4 %	w / v
pH 6.3		

Resolving gel buffer

Tris	1.5	M
SDS	0.4 %	w / v
pH 8.8		

3.6 Antibodies

Primary antibodies

Table 3.1: Overview of the primary antibodies used.

Antigen	Species/Isotype	Reaktivity	Dilution	Source
α-Tubulin	M /IgG1	Y, H, Ch, R, A, F, B, M	IB 1:10.000	Sigma, Cat#T9026
Cx30	Rb/IgG	R, M, C, H	IB 1:250	Invitrogen, Cat#71-2200
Cx43	Rb/IgG	M	IB 1:5000	Custom made
GFAP	Rb/IgG	H, M, R, C, D, S	IF 1:400	Dako, Cat# Z0334
Iba1	Rb/IgG	H, M, R	IF 1:400	WAKO, Cat# 019-19741
Iba1	M/IgG	H, M, R	IF 1:300	Millipore, Cat# MABN92
NeuN	M /IgG1	Av, Ch, Ft, H, M, Po, Sal	IF 1:200	Millipore,Cat# MAB377

abbreviations: H=human, B=bovine, R=rat, M=mouse, Mk=monkey, Ch=chicken, GP=guniea pig, Rb=rabbit, Y=yeast, F=fungi, A=amphibian, IF: Immunofluorescence; IB: Immunoblot.

Secondary antibodies

Table 3.2: Overview of the secondary antibodies used.

Antigen	Species	Dilution in WB	Source
Anti-mouse HRP	sheep anti-mouse	IB 1:10.000	GEHealthcare
Anti-rabbit HRP	donkey anti-rabbit	IB 1:10.000	GEHealthcare
Streptavidin Cy3	anti-biocytin	IF: 1: 300	Sigma Aldrich
Alexa fluor 594	goat anti-rabbit	IF: 1: 500	Molecular probes
Alexa fluor 488	goat anti-mouse	IF: 1: 500	Molecular probes

abbreviations: IF: Immunofluorescence; IB: Immunoblot.

3.7 PCR primers

TAK1$^{fl/fl}$

A: 5‘- GGC TTT CAT TGT GGA GGT AAG CTG AGA -3’
B: 5’- GGA ACC CGT GGA TAA GTG CAC TTG AAT -3’

Cx3CR1^{creER}

Cx3CR1^{cre} Mainz fw: 5’- CCT CTA AGA CTC ACG TGG ACC TG -3’
Cx3CR1^{cre} Mainz rvwt: 5’- GAC TTC CGA GTT GCG GAG CAC -3’
Cx3CR1^{cre} Mainz spec 1: 5’- GCC GCC CAC GAC CGG CAA AC -3’

3.8 Experimental animals

All the animals were kept in the House for Experimental Therapy (HET) of the University of Bonn. Maintenance and handling of all animals used in this study was according to the guidelines of European and German animal protection laws. All mice were bred and maintained under specific pathogen-free (SPF) conditions. Mice were kept under standard housing conditions (12 h / 12 h dark-light cycle, food and water ad libitum). All measures were taken to minimize the number of animals used.

3.8.1 Animals used in EFSs experiments

For hyperthermia (HT) and double hit (DH) experiments C57Bl6J and hGFAP-eGFP mice were used. For all experiments only male animals have been used. In all HT

experiments only hGFAP-eGFP mice were used from the FVB strain. In these animals, the gene for green fluorescent protein (enhanced green fluorescent protein, eGFP) is expressed under the control of the human GFAP (hGFAP) promoter (Nolte et al., 2001). Thus, two populations of fluorescent cells are visible in the hippocampus: NG2 glial cells usually displayed very faint fluorescence and have shorter, less branched processes. In contrast, astrocytes show bright fluorescence, are usually larger and show highly branched processes (Matthias et al., 2003).

The astrocytes in which all the electrophysiological experiments have been carried out were identified in the following way: first I searched for highly fluorescent cells with finely branched processes. These cells were then examined electrophysiologically. The cells that showed fluorescence, voltage- and time-independent current patterns, were used for further experiments. HT and DH experiments were carried out with animals aged from 9 to 15 d (p9-p15). All tests were performed in the CA1 region of the hippocampus. The focus was on the stratum radiatum of the CA1 region. In this region both all staining and coupling analysis have been performed.

3.8.2 Animals used in TAK1 experiments

$Cx3cr1^{CreER}$:$Tak1^{fl/fl}$

To investigate the role of inflammation in epileptogenesis $Cx3cr1^{CreER}$:$Tak1^{fl/fl}$ and $Tak1^{fl/fl}$ animals were used. In these mice TAK1 is conditionally knocked out by Cre-recombinase fused to a mutant estrogen ligand-binding domain ($Cx3cr1^{CreER}$) (Yona et al., 2013). For the activation of Cre-recombinase and subsequent deletion of TAK1 the presence of tamoxifen (TAM) is required. The receptor Cx3cr1 is also expressed in peripheral immune cells. But due to the longevity and self-renewal of microglia and replacement of peripheral immune cells within short time, TAK1 remains knocked out only in CNS microglia after TAM administration (Goldmann et al., 2013). In these animals TAM (1 mg / mouse) was injected two times a day for 5 d consecutively 6 or 7 weeks after birth, and three weeks after TAM injection the animals were used for experiments.

4 Methods

4.1 Intraperitoneal injections

4.1.1 Intraperitoneal injection of LPS

The concentration of solutions was so adjusted that the final injectable volume of 50 µl was attained. The substances were dissolved in sterile 0.9 % NaCl solution. The dose of LPS administered was 5 mg / kg body weight.

4.1.2 Intraperitoneal injection of TAM

For intraperitoneal injection TAM was dissolved in sunflower oil in combination with ethanol. For making a homogenous solution, the mixture (TAM = 1 mg; sunflower = 45 µl; ethanol = 5 µl) was subject two times to sonication for 15 min. The dose of TAM administered was 1 mg / mice.

4.2 Experimental febrile seizure generation

4.2.1 Body temperature measurement

For the measurements of the body temperature disinfected temperature sensitive transponders (IPTT-300 BioMedic Data Systems, Seaford, USA) were implanted 1-2 days before the measurement. These transponders were about 2 x 10 mm in size and could easily be introduced under the skin using a special disinfected syringe. Thereafter, the animals were observed. The wound healed well and no signs of inflammation were evident. In the absence of inflammation, the animals were used for further experiments. The use of the transponders allowed the measurement of body temperature without taking the animals out of the cage. This has advantages over the usual rectal measurements, as the animals can stay at the same ambient temperature in the cage. The handling of the animals for rectal measurements can also be a source of possible variations, because the animals can be highly stressed especially when measurements need to be taken over a longer period, which would lead to a rise in the temperature.

4.2.2 Hyperthermia induction

The day the pups were born was considered as P0 (postnatal day 0). Before HT-treatment, the weight of the animals was at least 5 g, to increase the chances of survival and to ensure comparability between test series. The litter size was reduced to 5-6 animals for this purpose. Only male animals were used. All experiments were performed between 10 am and 4 pm. Due to the young age of the animals, they were placed before and after the experiments with their mother and siblings in a cage. Before and after HT-treatment the mice were weighed. For HT-treatment, the animals were placed at the bottom of a 3 l beaker. The floor of the beaker was covered with a two-layer towel cloth. The beaker was placed in a water bath which was preheated to 39 °C, to avoid cooling of the animals. In addition, it could also derive the surplus heat.

Table 4.1 Behavioral scoring used to characterize EFSs (van Gassen et al., 2008).

Stage	Behavior	Description
0	Normal	Normal explorative behavior
1	Hyperactivity	Hyperactive behavior, jumping and rearing
2	Immobility	Sudden total immobility (duration 3-10 seconds)
	Ataxia	Unsteady, jerk gait
3	Circling	Running in tight circles
	Shaking	Whole body shaking
	Clonic seizures	Contractions of fore and / or hind limb with reduced consciousness
4	Tonic-clonic convulsions	Continuous tonic–clonic convulsions with loss of consciousness

The animals were warmed by using a temperature regulated stream of warm air (41 – 48 °C) coming from a hair dryer. The distance between the hair dryer and the animals was approximately 50 cm. With the help of a transformer the heat and speed of the air jet could be controlled. The animals were warmed slowly to avoid rapid heating and burning of the animals. HT was induced for 36 and 60 min. The duration of HT was measured from the time at which the animals showed the behavior "sudden immobility". At this stage the first spikes arise in the EEGs (Dube et al., 2000; Dube et al., 2005). The temperature of the mice was raised to 41.5 °C and

kept at 41.5 ± 0.3 °C for 36 or 60 min. The desired temperature of 41.5 °C was reached within a few min. The body temperature of the pups was controlled every two min. From a measured body temperature of 41.7 °C, the strength and temperature of the air jet was reduced until the body temperature had reached the value of 41.3 °C. The temperature of 42 °C was not exceeded at any time. During the entire duration of HT-treatment behavioral scoring was performed (see Table 4.1). After 36 or 60 min the protocol was immediately stopped and the body temperature of the pups was brought to normal by using water at room temperature. The pups were placed back with their mother. For control experiments, untreated littermates were used.

4.2.3 Double hit treatment

In the first experiment, the transponders for temperature measurement were inserted in the mice at P11. Either at P13 or P14, LPS (5 mg / kg) was injected intraperitoneally (ip). One day after LPS injection (P14 or P15), HT (36 min) was induced in the mice using warm air (see section 4.2.2).

In the next experiment, the transponders for temperature measurement were inserted in the pups at P11. At P12 LPS (5 mg / kg) was injected ip. HT (36 min) was induced on two consecutive days on P14 and P15. From P12 to P16, the cage containing pups and mother was kept in water bath to keep them in a warm environment, so that they did not lose heat to the environment. The temperature of the water bath was maintained at 37 °C.

In the next experiments, the transponders for temperature measurement were inserted in the pups at P8. At P9 LPS 5 mg / kg was injected ip. At P11 and P12 HT was induced either for 36 min (both days) or 60 min (both days). For these experiments two strains of mice, hGFAP-eGFP and C57Bl6J were used. From P9 to P13, the cage containing pups and mother was kept in a water bath to keep them in a warm environment so that they did not lose heat to the environment. The temperature of the water bath was set at 37 °C.

4.3 Electrophysiology

4.3.1 Preparation of acute brain slices

For the preparation of acute brain slices, mice were anaesthetized by a mixture of gases containing 50 % CO_2 / 50 % O_2 and killed by decapitation. The brain was rapidly removed and transferred to ice-cold preparation solution. The cerebellum and the frontal third of the brain were cut off. The brain was then glued frontally onto a specimen holder with superglue. Subsequently, the specimen holder with the brain was fixed in the buffer tray of the vibratome containing ice-cold preparation solution constantly gassed with 5 % CO_2 / 95 % O_2. The brain was cut into 200 µm thin slices in coronal orientation. The space around the cutting chamber was filled with a water-ice mixture. After cutting, the sections were incubated for 20 min in preparation solution at 35 °C. The slices were then transferred to gassed (5 % CO_2 / 95% O_2) artificial cerebrospinal fluid (ACSF) (preheated to 35 °C), cooled down to and stored at room temperature until further use.

4.3.2 Electrophysiological setup and recording conditions

The electrophysiological setup used in the present study was composed of the following components: An upright microscope (AxioskopFS1 Zeiss, Oberkochen, Germany) was mounted on a vibration isolation platform (Newport Corporation, Irvine, USA) to ensure stable measurements and placed in a Faraday cage to reduce electrical noise. The microscope was equipped with a motorized focus. The microscope was further equipped with differential interference contrast (DIC) optics to enhance the contrast and improve the recognition of cellular structures in the brain slices. To visualize fluorescent proteins expressed by living cells of transgenic mice, the setup was equipped with a fluorescence system. The optical signals were detected by a CCD-camera and displayed on a monitor. A recording chamber was fixed under the objectives of the microscope. The recording chamber was mounted on a holder that could be manually moved in x- and y-directions. An electrically-driven micromanipulator (Micromanipulator 5171, Eppendorf, Germany) was available to move the recording pipette. Glass pipettes for patch-clamp recordings were pulled with a horizontal puller (P-87 and P-2000, Sutter Instruments, Novato,

USA) and had a resistance of 3-4.5 MΩ when filled with pipette solution. Electrical signals were recorded by a teflon-coated silver electrode with an uninsulated chlorinated tip connected via the preamplifier (head stage) to the patch-clamp amplifier (EPC 9, HEKA Electronic, Lambrecht / Pfalz Germany). The reference electrode in the recording chamber similarly consisted of a silver/silver chloride pellet.

The patch-clamp amplifier operates in two different modes, the voltage-clamp mode and the current-clamp mode. In the voltage-clamp mode, the amplifier compares the resting potential of a patched cell with the selected holding potential. Whenever a difference occurs, current is injected via the pipette electrode to compensate for this difference and to keep the cell at the desired holding potential. Consequently, this current represents the current flowing over the membrane of the cell and is recorded by the amplifier. In the current-clamp mode, the patched cell is at its physiological resting potential and no current is injected. Therefore, in this mode physiological activity patterns may be recorded as changes in the resting potential.

Signals were filtered at 3 and 10 kHz and sampled at 10 and 30 kHz. The appropriate technical devices and software used in the present study are listed in section 3.4.

4.3.3 Patch-clamp technique

Electrophysiological measurements were obtained by applying the patch-clamp technique developed by Erwin Neher and Bert Sackmann (Neher and Sakmann, 1976). Experiments were performed in the conventional whole-cell configuration (Edwards et al., 1989; Neher and Sakmann, 1976).

To do so, a brain section was transferred to the recording chamber of the electro-physiological setup and fixed in place with a u-shaped platinum wire stringed with nylon threads. The chamber was constantly perfused (1-2 ml / min) with gassed ACSF at room temperature. The recording pipette was filled with pipette solution and a constant overpressure was applied via a tubing system. This caused a permanent

outflow of pipette solution that prevented plugging of the pipette tip by tissue fragments. In the voltage-clamp mode, a depolarizing 10 mV step was applied via the pipette electrode to monitor changes in resistance. The pipette was then moved under optical control close to the cell membrane. Subsequently, the overpressure was released and mild negative pressure applied. This resulted in the formation of the cell-attached configuration characterized by a tight connection between cell membrane and pipette tip causing a strong increase in resistance ideally reaching more than 1 GΩ. During this process the cell was clamped to the holding potential of -70 mV (ACSF). Capacitive artifacts caused by the glass pipette were compensated at this point. By applying brief pulses of negative pressure the small membrane patch under the pipette tip was ruptured resulting in a sudden drop in resistance. In this so called whole-cell configuration, currents over the entire cell membrane were measured in the voltage-clamp mode. By switching to the current-clamp mode, the resting membrane potential was determined. Whole-cell current patterns in response to de- and hyperpolarizing voltage steps were offline compensated for capacitive artefacts by using IGOR Pro macros custom-written by Dr. Ronald Jabs.

4.3.4 Biocytin visualization

Functional coupling was analyzed with the biocytin-diffusion method. The biocytin molecule is small enough (372.48 Da) to diffuse through gap junctions and its spread in the network provides information about the coupling status of the cells. To fill the initial cell with biocytin, it was added to the pipette solution in a concentration of 0.5 % (m / v). The test cells were maintained for 20 min in whole-cell recording to allow diffusion of biocytin into the cytosol. During the whole measurement the connection between the cell cytosol and the pipette was controlled by recording membrane potential, membrane resistance and series resistance every 10 min. Immediately after completion of the 20 min, the sections were transferred into a 4 % paraformaldehyde (PFA) solution, and incubated at 4 °C overnight to fix biocytin in the cells and to prevent further spreading. From this step, until the mounting of the tissue to the slide, the slices were kept in 24-well plates with each well containing 250 µl PBS.

The next day, the sections were washed three times with PBS (pH 7.4). The washing steps were carried out on a shaker at room temperature and lasted 10 min. This was followed by an incubation with blocking solution containing 10 % NGS and 1 % Triton X-100 in PBS (pH 7.4) for 2 h at room temperature on a shaker. Thereafter, the blocking solution was replaced with the antibody solution (Cy3-streptavidin) and incubated at 4 °C overnight. The sections were then washed three times and incubated for 10 min with Hoechst. After the last washing step, the sections were mounted on slides. Attention was paid to the orientation of the slices, so that the tissue side stained with biocytin was facing upwards. In general, four slices were mounted on a microscope slide. Excess wash solution was removed using filter paper. In the middle of the slightly dried sections a drop of mounting medium was applied and then covered with a coverslip. After at least 30 min, the sections were photographed under the microscope. The program MetaVue was used. Since biocytin propagates in all three dimensions in the brain section, several layers were taken at a thickness of 1 µm, so that the entire coupling could be detected. For counting biocytin-positive cells, the software program ImageJ was used.

4.4 Temporal lobe epilepsy model

Dr. P. Bedner and Dr. K. Huttmann from our Institute established a new model for TLE (Bedner et al., 2015). In this model kainate was injected into the cortex above the hippocampus, avoiding mechanical damage to the hippocampus. The new model has several advantages compared to the intrahippocampal injection model (Heinrich et al., 2006). For instance, mice subjected to intrahippocampal injections do not always show spontaneous generalized seizures. Moreover, due to mechanical damage produced by the procedure, seizure-induced morphological changes in the hippocampus can hardly be investigated. Briefly, animals were anaesthetized with a ketamine / cepetor mixture and injected stereotactically into the right parietal cortex (coordinates from bregma point: AP:-1.9 mm and ML:-1.5 mm, DV: 1.8 mm) with 70 nl kainate (20 mM) using a Hamilton microsyringe. Mice were removed from the stereotactic frame and the skin was sutured over the skull. Anesthesia was stopped by an ip injection of Antisedan (5 mg / ml Atipamezol hydrochloride) and Ringer in a 1:4 ratio. Mice were transferred to a clean cage.

4.5 Implantation of the EEG electrodes and video monitoring

These experiments were carried out in collaboration with Dr. Peter Bedner and Julia Müller. Mice were anesthetized by ip injection of Cepetor (1 mg / ml) and Ketamine (10 %) in a ratio of 3:2. To protect the eyes from drying, eye ointment (Bepanthen) was applied. Body hair was removed from the scalp and the right abdominal region. The shaved areas were disinfected by scrubbing with Cutasept. The mice were fixed in a flat skull position in the stereotactic frame holder for stereotactic injection (TSE Systems GmbH, Bad Homburg, Germany). A midline skin incision of about 10 mm was made in the bregma region and the periosteum was removed to expose the skull. On the stereotactic frame a high speed dental drill was mounted. The tip of the drill was gently placed on bregma and the stereotactic coordinates were determined. The drill was moved 1.9 mm posterior to bregma. Two holes of 0.7 mm diameter were drilled bilaterally 1.5 mm from sagittal suture into the skull. In both holes stainless steel screws (length 2 mm; thread diameter 0.8 mm; Hummer & Rieß, Nürnberg) were inserted. The mouse was removed from the stereotactic frame. For implantation of the telemetric transmitter (TA10EA-F20, Data Sciences International, St. Paul, USA), a 15 mm long skin incision was made in the right abdominal region, and a subcutaneous skin pouch was created by blunt dissection underneath the skin. A tunnel for the leads was made in the same manner by moving cranially until reaching the mid-sagittal incision. The disinfected telemetric transmitter was placed into the previously prepared skin pouch and the skin was closed with wound clips. The two monopolar leads were subcutaneously pulled cranially and connected to the screws. The connected leads were then covered with dental cement (Paladur, Heraeus Kulzer GmbH) and the skin was sutured. Anesthesia was stopped by ip injection of Antisedan (5 mg / ml Atipamezol hydrochloride) and Ringer in a 1:4 ratio. Mice were injected with Carprofen (4 mg / kg, ip.) for 3 d to reduce pain and 0.25 % Enrofloxacin was administrated via drinking water to reduce the risk of infection. Mice were transferred to a clean cage and placed on a receiver plate (RPC-1; Data Sciences International). The plates received the signals from the telemetric transmitter and sent it to a computer with Dataquest ART 4:00 Gold / Platinum

software (DataSciences International). At the same time, the behavior of the animals was recorded using a Video Surveillance System (SeeTec, Phillipsburg, Germany) equipped with two infrared cameras (Axis 221 Indoor Vario).

4.6 Immunohistochemistry

4.6.1 Cardiac perfusion and fixation

To obtain well preserved brain sections for immunohistochemistry (IHC) transcardial perfusion was carried out. First, mice were anesthetized with ip injection of Cepetor-KH (1 mg / ml) and Ketamine (10 %) in a ratio of 3:2. With fine scissors the chest was opened and the pericardium exposed. Subsequently, a 25-G cannula was inserted into the left ventricle. The right atrium was cut open with scissors so that the blood can flow out. During the whole perfusion process, 30 ml PBS (pH 7.4) was slowly injected to remove blood, followed by further pumping of 30 ml 4 % PFA for fixation. Successful perfusion was indicated by the animal becoming rigid. Later, the skull was opened and the brain isolated, then fixed again in 4 % PFA overnight at 4 °C. The next day the brain was transferred to 30 % sucrose solution in PBS and was kept at 4 °C for at least 3 days.

4.6.2 Cryosection preparation

After 3 days in sucrose solution the brain was embedded in Tissue-Tek (Sakura Finetek, Europe) and frozen at -80 °C. The sections for IHC were cut on a cryostat (Microm HM560, Thermoscientific, Waltham, MA, USA) and were 40 µm thick. Storing of the sections was carried out in PBS (pH 7.4) in 24-well plates and 0.01 % sodium azide as a preservative in order to ensure a longer life.

4.6.3 Immunofluorescence staining

All stainings were performed on 40 µm thick cryosections. The sections were washed 3 times in PBS (pH 7.4) at room temperature. Subsequently, they were incubated for permeabilization in blocking solution for 1 h at room temperature. The blocking solution contained 10 % NGS and 1 % Triton X-100 in PBS (pH 7.4). Thereafter, the sections were incubated with respective primary antibodies (see

Table 3.1) in PBS containing 5 % NGS and 0.1 % Triton X-100 overnight at 4 °C. Later, the sections were washed three times with PBS at room temperature. The sections were incubated with respective secondary antibody (see Table 3.2) in PBS containing 2 % NGS and then washed three times with PBS at room temperature. Next, nuclear staining was performed with Hoechst 1:100 in PBS. Again, the sections were washed three times in PBS. Thereafter, the sections were mounted on slides and observed under the microscope.

For p-TAK1 x Iba1 staining, mouse monoclonal anti-Iba1 antibody (see Table 3.1) was used and the sections were incubated with L. A. B. medium for 15 min at room temperature. After this, the sections were washed three times in PBS (pH 7.4) at room temperature followed by incubation for permeabilization. For nuclear staining Draq5 was used. Furthermore, the sections were incubated with primary antibodies for three days. The rest of the protocol was similar as already described.

4.6.4 Fluoro-Jade C staining

For fluoro-jade C / DAPI double staining, Biosensis Ready-to-Dilute (RTD) TM kit (Cat# TR-100-FJ, Biosensis, Thebarton, Australia) was used following the manufacturer instructions. First, 40 µm thick brain sections were mounted on superfrost Ultraplus slides (Thermo Scientific, Braunschweig, Germany) and dried at 50 °C for 30 min on a slide warmer. For 5 min, slides were incubated in a coplin jar containing one part sodium hydroxide mixed with 9 parts of 70 % ethanol at room temperature. After this the slides were washed with 70 % ethanol for two min at room temperature. Then the slides were rinsed with distilled water for two min at room temperature. The slides were transferred into a new coplin jar containing a mixture of one part $KMNO_4$ in 9 part water and incubated for 10 min. After this the slides were rinsed in distilled water for two min. The slides were transferred into a new coplin jar containing one part Fluoro-Jade C, one part DAPI and 8 parts water, and incubated for 10 min at room temperature. The slides were rinsed three times in distilled water for one min at room temperature. The slides were air dried on a slide warmer at 50 °C for 5 min. For clearing, the slides were immersed in xylene for two min at room

temperature. The slides were coverslipped using DPX mountant (Sigma) and images were taken using a confocal microscope (Leica SP8).

Slices from mice intracortically injected with kainate (see section 4.4) were used as positive controls.

4.6.5 Micrographs

Immunofluorescence stainings were analyzed by microscopy. Images were acquired at 1 µm intervals using either a fluorescence microscope (Axiophot employing MetaVue software) or a confocal (LSMs Leica SP8). Fluorescence image resolution was 2084 x 2084 pixels and LSM images were acquired at 1024 x 1024 pixels. Tracer filled networks were imaged employing a 20 x objective. For co-localization studies confocal images were acquired. Cell type analysis in different brain areas was performed on image stacks of 290.62 x 290.62 x 15-20 μm^3 volumes if not stated otherwise. The images obtained were analyzed using Fiji software and figures were edited using ImageJ.

4.7 Protein chemistry

4.7.1 Total protein extraction from tissue

Hippocampi of mice were used for protein extraction. All steps were performed on ice. An inverted petri dish covered with filter paper was used as a base. Mice were sacrificed by cervical dislocation. The brain was immediately isolated and it was dissected out. It was washed with ice-cold PBS to remove residual blood. The cerebellum was removed and the brain was separated into two hemispheres. Then, the olfactory bulbs were cut off with part of frontal cortex and the rest of the brain was put on a coronal plane. Using two small spatula the cortex was then carefully removed. With the aid of the blunt side of the spatula, hippocampi were carefully isolated from the midbrain, collected in an Eppendorf tube and immediately frozen in liquid nitrogen. The tissue was stored at -80 °C or subsequently prepared in a modified RNA Immuno- Precipitation Assay (RIPA) lysis buffer (50 mM Tris, 150 mM NaCl, 0.5 % Nonidet P40, 0.5 % Na-DOC, 1 % Triton X-100, 0.5 % SDS)

supplemented with halt protease and a phosphatase inhibitor cocktail (Thermo Scientific). Then, the tissue was homogenized with a plastic pestle in a 1.5 ml tube in about 300 µl lysis buffer and disrupted with a pre-chilled 27 gauge needle (Braun, Melsungen; Germany) and supersonic salt (until homogeneous). After incubation on ice for ~ 30 min, supernatants were collected by centrifugation for 30 min at 13,000 x rcf at 4 °C. Total protein content was assayed with the BCA (Pierce, Bonn, Germany) method using 5 µl supernatant of each sample. To avoid frequent frosting and defrosting of the samples, aliquots were prepared with 70 µl volume. The samples were stored at -80 °C.

4.7.2 SDS-page and Western blot

For immunoblotting studies, 40 µg total protein per sample was analyzed in each sample. The lysates were treated with the "Laemmli" sample buffer (Rotiload 4x) and denatured by heating for 10 min at 65 °C. After that samples were spin briefly and separated with 12 % SDS resolving gel for 60 - 90 min at 80-180 V in denaturing conditions. To estimate protein size, pre-stained protein ladder (PageRuler, Thermo Scientific) was loaded along with the samples. Since the markers used were conjugated with a dye to directly observe movement of the proteins in the gel, there was small run imprecision in individual bands. Polyvinylidene fluoride (PVDF) membranes (Millipore, Darmstadt, Deutschland) were used for electroblotting of separated proteins for 2 h at 500 mA running condition. Subsequently, the membranes were blocked with 5 % milk powder in TBST (pH 7.4) containing 0.05 % Tween-20 and incubated overnight at 4 °C on a rotator with primary antibodies: rabbit polyclonal anti-Cx43 (1:5000, custom made), rabbit polyclonal anti-Cx30 (1: 250, Invitrogen, Darmstadt, Germany), mouse monoclonal anti-α-tubulin (1:10,000, Sigma, Steinheim, Germany). Visualization was performed with HRP-conjugated secondary antibodies. The membranes were first washed three times for 10 min with TBST to remove unbound primary antibody. This was followed by incubation with the secondary antibodies for 1 h at room temperature. Secondary antibodies used: goat-anti-mouse HRP conjugate (1:10,000, GE Healthcare, Little Chalfont Buckinghamshire, UK) goat-anti-rabbit HRP conjugate (1:10,000, GE Healthcare). All antibodies, including secondary antibodies, were diluted in 5 % milk powder in TBST

(pH 7.4) containing 0.05 % Tween-20. For visualization of HRP, the Super signal West Dura substrate (Pierce) was used and chemiluminescence was detected with the Gene Gnome digital documentation system (Synoptics, Cambridge, UK). Equal loading of the lanes was confirmed by α-tubulin staining of the same membrane. For inactivation of secondary antibodies, membranes were incubated in 100 mM sodium azide in 5 % milk overnight at 4 °C. Quantification was performed using the program ImageJ software. Quantification and analysis of phosphorylation states of Cx43 were performed by PhD student Tushar Deshpande. The chemiluminescent intensity of each band was measured and normalized against the corresponding α-tubulin band. Because all samples were exposed to identical conditions (substrate and time), a relative comparison of protein expression between different samples was possible.

4.8 Data analysis

All error bars in the bar graphs represent standard deviation (SD). For statistical analysis the following methods have been applied: when comparing two groups Student's T-test was used; when comparing more than two groups, two-sided variance analysis (ANOVA) followed by Tukey's test has been used. In all cases, a significance level of 5 % was applied ($p < 0.05$). Exception to this rule is explicitly stated in the text and in figure captions.

4.9 Genotyping

4.9.1 DNA extraction

Genomic DNA was obtained from small tail tips of 3 weeks old mice. Samples were incubated in 300 µl Laird buffer supplemented with Proteinase K (20 U / ml) at 55 °C overnight in a water bath. The next day lysates were vortexed and centrifuged at 13,000 rcf for 10 min at room temperature. The supernatant was transferred to a new tube and the DNA was precipitated by adding 300 µl isopropanol and gently mixing the solutions. After another centrifugation step at 13,000 rcf for 10 min at room temperature the supernatant was discarded. The DNA pellet was washed in 70 % ethanol (500 µl) and centrifuged again at 13,000 rcf for 10 min at room temperature. The supernatant was discarded and the DNA pellet was air dried for 1 h and

dissolved in 50 µl of ddH_2O. Genomic DNA was subsequently used for routine genotype analysis with different primers.

4.9.2 Polymerase chain reaction

DNA samples were amplified by polymerase chain reaction (PCR). The method relies on several thermal cycling reactions for melting, primer annealing and subsequent replication of the target DNA. Primers were designed to bind at the 3'-end of the sense and antisense strands of the DNA sequence to be amplified. Employing a heat-stable Taq polymerase the DNA strands were amplified by elongation of the primers in 5'-3' direction. This enzyme was originally isolated from the bacterium *Thermus aquaticus*. The following Tables 4.2, 4.3, 4.4 and 4.5 show the PCR mix and the applied PCR protocols for genotyping animals of the $TAK1^{fl/fl}$:$Cx3cr1^{CreER}$ mouse line; the presence of a floxed TAK1 and the presence of a cre-recombinase allele was detected by PCR. After the completetion of the PCR, the samples were kept at 8 °C (step 6 in table 4.3 and table 4.5) untill taken out from the PCR machine. The total volume of the PCR mix was 24 µl and 1-2 µl DNA were added.

Table 4.2 $TAK1^{fl/fl}$ PCR protocol

PCR mix	**Volume [µl]**
ddH2O	14.3
PCR buffer 5x	5
$MgCl_2$ (25 mM)	1
Primer A (10 pmol/µl)	1.25
Primer B (10 pmol/µl)	1.25
dNTP (each 10 mM)	1
Taq polymerase	0.2

Table 4.3 TAK1$^{fl/fl}$ PCR program

Step	Temp. [°C]	Time [min]	Cycles
1	94	5	1
2	94	0:45	2-4 35x
3	67	0:45	
4	72	0:45	
5	72	7	1
6	8	∞	1

Table 4.4 Cx3cr1^{CreER} PCR protocol

PCR mix	Volume [µl]
ddH2O	13.05
PCR buffer 5x	5
$MgCl_2$ (25 mM)	1
Primer Cx3CR1^{cre} Mainz fw (10 pmol/µl)	1.25
Primer Cx3CR1^{cre} Mainz rvwt (10 pmol/µl)	1.25
Primer Cx3CR1^{cre} Mainz spec 1 (10 pmol/µl)	1.25
dNTP (each 10 mM)	1
Taq polymerase	0.2

Table 4.5 Cx3cr1^{CreER} PCR program

Step	Temp. [°C]	Time [min]	Cycles
1	94	5	1
2	94	0:45	2-4 35x
3	62	0:45	
4	72	0:45	
5	72	7	1
6	8	∞	1

4.9.3 Agarose gel electrophoresis

The PCR products were separated by agarose gel electrophoresis. The DNA samples were separated by their size and charge, therefore a 1.5 % agarose gel containing 0.8 µg / ml ethidium bromide was prepared. Due to the negatively charged phosphate groups, DNA moved to the anode and the migration velocity was

proportional to their molecular mass. Ethidium bromide was added to visualize the DNA under ultraviolet light; it intercalates double stranded DNA. Gel electrophoresis was performed at 110 V for 45 – 60 min. At the same time, a 100 bp DNA ladder was run along with the samples to estimate the molecular size of the amplified DNA fragments. All genotyping experiments were performed by PD Dr. Gerald Seifert.

5 Results

5.1 Consequences of EFSs on the hippocampal astrocytic network

5.1.1 EFSs generation

Retrospective studies have shown that 20-60 % of the patients suffering from intractable TLE had a childhood experience of FSs (French et al., 1993; Hamati-Haddad and bou-Khalil, 1998). Also, in some follow up studies it has been observed that FSs during early childhood increase the risk of developing TLE in later life (Annegers et al., 1987; Nelson and Ellenberg, 1976). It has been shown that this risk varies among individuals and can be dependent on various factors like the duration of FSs, its reoccurrence and age of the patient at the time of the first FS (McClelland et al., 2011). It has been revealed that the risk of developing TLE is lower for simple FSs and higher for complex FSs. Between 2 and 6 % of children suffer from FSs during early childhood (Nelson and Ellenberg, 1976; Shinnar and Glauser, 2002).

To investigate the effects of FSs in infants, EFSs were induced in hGFAP-eGFP and C57Bl6J mice under different conditions (Table 5.1). The decrease in body weight was less than 5 % in all EFS experiments (Table 5.1). The duration of EFS generation was measured from the time point when the animals showed the first sudden immobility phase (Table 5.1). It has been shown that the first sudden immobility phase indicates the onset of seizure (see section 4.2.2) (Dube et al., 2000; Dube et al., 2005). After completion of the protocol for EFSs generation the mice were partly submerged in water of room temperature to quickly normalize their body temperature and were subsequently returned to their mother. The summary of important parameters recorded during the EFS experiments is given in table 5.1. During HT-treatment for EFSs generation the behavior was recorded and scaled (see Table 4.1) as previously described by van Gassen et al. (2008).

Table 5.1 Summary of different parameters used for EFSs generation

	LPS day	Episode	HT day	Body weight loss (%)	Interval till first sudden immobility	Average body temperature		duration of HT	n
						at first sudden immobility	during HT treatment		
FVB-hGFAP-eGFP									
HT			P14 or P15	3.3 ± 1	6 ± 2 min	39.4 ± 0.2	41.2 ± 0.6	36 min	21
DH-I	P13 or P14		P14 or P15	3.7 ± 0.7	5 ± 2 min	40.7 ± 0.4	41.5 ± 0.3	36 min	21
DH-II	P12	1st	P14	3.2 ± 0.7	7 ± 4 min	39.7 ± 0.8	41.3 ± 0.6	36 min	10
		2nd	P15	3.6 ± 0.8	7 ± 2 min	40.2 ± 0.6	41.4 ± 0.4		
DH-III	P09	1st	P11	3 .3 ± 1	5 ± 1 min	39.7 ± 0.2	41.3 ± 0.4	36 min	9
		2nd	P12	4.0 ± 1.6	5 ± 2 min	39.9 ± 0.4	41.4 ± 0.4		
DH-IV	P09	1st	P11	3 .0 ± 1	5 ± 2 min	39.4 ± 0.2	41.3 ± 0.4	60 min	18
		2nd	P12	3.7 ± 1	5 ± 1 min	39.5 ± 0.2	41.3 ± 0.4		
C57Bl6J									
DH-V	P09	1st	P11	3.1 ± 1	7 ± 1 min	40.3 ± 0.2	41.4 ± 0.3	36 min	8
		2nd	P12	3.1 ± 1	6 ± 2 min	40.4 ± 0.2	41.5 ± 0.2		
DH-VI	P09	1st	P11	3.4 ± 1	9 ± 1 min	40.1 ± 0.5	41.4 ± 0.3	60 min	6
		2nd	P12	3.7 ± 0.7	7 ± 2 min	40.4 ± 0.3	41.4 ± 0.3		

abbreviations: HT = hyperthermia, DH = double hit experiment

In the HT experiments (Table 5.1), animals showed hyperactivity including jumping, rearing, chewing, swallowing and grooming. Some animals also showed ataxia and falling on side or back. Typical behavior during the last 10 min of the protocol was lying on one side. Seldom clonic contraction of fore and / or hind limbs was observed. Very few pups showed circling or running in tight circles but all showed face automatisms (chewing, swallowing and grooming).

During HT induction, the temperature of the body and brain increases, which causes FSs. As the animals are kept in SPF conditions, it is unlikely that they experience any infection before HT-treatment and FSs onset. However, in most human cases, children first get an infection which leads to an increase in body temperature, and in some cases causes FSs (Chiu et al., 2001). It has been reported that a handsome percentage of TLE patients experienced FSs during early childhood (Cendes et al., 1993). Therefore, to mimic early childhood FSs generation in humans, LPS was injected ip before HT-treatment. Also, it has been shown that administration of LPS

in pups in early age increases seizure susceptibility (Galic et al., 2008). Therefore, in DH experiments a single dose of LPS (5 mg / kg) was injected prior to HT-treatment (see Table 5.1).

In double hit I (DH-I) experiments, LPS was injected one day before HT treatment (Table 5.1). The animals showed hyperactivity including jumping, chewing, swallowing, ataxia, lying on side or back. Running in tight circles, shaking and falling on side or back were also observed in some animals. During the last half of the protocol animals showed clonic contractions of fore and / or hind limbs as well as face automatisms. But when back in the cage with the mother, the animals became immobile within 5 min and their body temperature fell down. Around 25 % of the animals could not increase their body temperature and died of freezing. The rest of the animals became mobile in 15-20 min.

After LPS administration, the animals became much more sensitive to HT-treatment, and almost 25 % of the animals died within one day after HT-treatment. Considering the acute inflammatory response in some animals being responsible for the disability to regulate body temperature, the LPS administration day and the duration between LPS administration and HT-treatment was changed. The cages of the animals were kept in a water bath which had a stable temperature of 37 °C to avoid heat loss from the experimental animals. The cage of the animals was removed from the water bath one day after HT-treatment. This avoided sudden heat loss or freezing of animals after LPS administration and subsequently mortality rate decreased to less than 5 % after HT-treatment. As it has been reported that recurrence of seizures within 24 h (i.e. complex FSs) increases the risk for developing TLE (Pavlidou and Panteliadis, 2013), a second episode of HT-treatment was given within 24 h. In double hit II (DH-II) experiments LPS was injected on P12, and HT was induced on two consecutive days (P14 and P15). These animals showed less hyperactivity (jumping) than the animals in the previous experiment. These animals showed ataxia and lying on side or back. Face automatisms accompanied with clonic contractions were observed but falling on side or back was missing. Very few animals showed running in tight circles but shaking was observed. When placed back with the mother, after 5 min animals

became immobile and remained immobile for about 30-35 min. During this time the animals continued to show face automatisms and clonic contractions. Due to the stable temperature of the water bath which avoided heat loss of the animals, fall in body temperature of the animals after HT-treatment was not observed.

The mammalian brain keeps continue maturation after birth and passes through different stages (Stiles and Jernigan, 2010). Also the inflammatory response can change with age. Therefore, the postnatal day for LPS administration and HT-treatment was changed to investigate the effect of age on the consequences of DH treatment. In the double hit III (DH-III) experiment, LPS (5 mg / kg) was administered on P9 and HT-treatment was performed on P11 and P12 (Table 5.1). The animals showed ataxia and sudden immobility throughout the protocol. Falling on side or back was also observed. Some pups displayed clonic contractions of fore and / or hind limbs combined with face automatisms. When put back with their mother after stopping the protocol, animals continued to show face automatisms and clonic contractions of fore and / or hind limbs for 10-15 min.

As the total duration of FSs can also have effects on epileptogenesis, the duration of HT-treatment was increased to 60 min in the double hit IV (DH-IV) experiment (Table 5.1). During the first 10-15 min after the first sudden immobility phase, these pups showed hyperactivity, but later on hyperactivity was decreased. The pups did not show circling or running in tight circles, but falling on side or back was observed. The pups exhibited whole body shaking, contractions of fore and / or hind limbs and face automatisms. In the last 20-25 min the pups started to show tonic clonic contractions of fore and hind limbs combined with loss of consciousness for short periods of time (10 – 20 s), the duration of which progressively increased to more than 120 s towards the end of the protocol. When back with the mother, the pups continued to have continuous tonic clonic contractions of fore and hind limb with loss of consciousness for 15-20 min.

Using HT-treatment it has been shown that different strains of mice show different seizure susceptibility during EFS generation (van Gassen et al., 2008). To

investigate whether seizure susceptibility changes or remains the same in a different strain of mice during FSs generation caused by HT-treatment in combination with LPS administration, C57Bl6J animals were used.

In the double hit V (DH-V) experiment, LPS (5 mg / kg) was injected on P9 and HT was induced on two consecutive days (P11 and P12) for 36 min (Table 5.1). The animals showed hyperactivity for a short period of time after a first sudden immobility phase. These pups exhibited ataxia and immobility throughout the protocol. They also presented whole body shaking, circling, and clonic contractions of fore and / or hind limbs. When back with the mother, for 10-15 min the pups showed episodes of continuous tonic–clonic convulsions with loss of consciousness.

The duration of HT-treatment was increased to 60 min in the double hit VI (DH-VI) experiment. The pups showed hyperactivity in the first few minutes after a first sudden immobility phase. They displayed sudden immobility and ataxia throughout the protocol. Whole body shaking and running in circles was also present. Clonic contractions were observed 10 min after first sudden immobility until 40 min. After this the animals started to show tonic-clonic convulsions (30-90 s long), which were succeeded by *status epilepticus* in the last 8-10 minutes. When back with the mother the pups continued showing tonic-clonic convulsions for about 45 - 60 min.

5.1.2 Neuronal degeneration and neuronal density

In adult animal models of hippocampal epilepsy, neuronal cell death in the CA1 and CA3 pyramidal cell layers in addition to the hilus have been shown, which is similar to the situation in human TLE (Freund et al., 1992; Nadler, 1981). To investigate whether HT-induced seizures also induce neurodegeneration, Fluoro Jade C stainings were performed 6 h and 5 d after HT-treatment. For positive control sections from mice perfused 5 d after kainate-induced *status epilepticus* were used. Here, massive neuronal degeneration was observed (Fig. 5.1A). However, no neuronal death was found in pups 6 h (see Fig. 5.1B) and 5 d (see Fig. 5.1C) after HT-treatment.

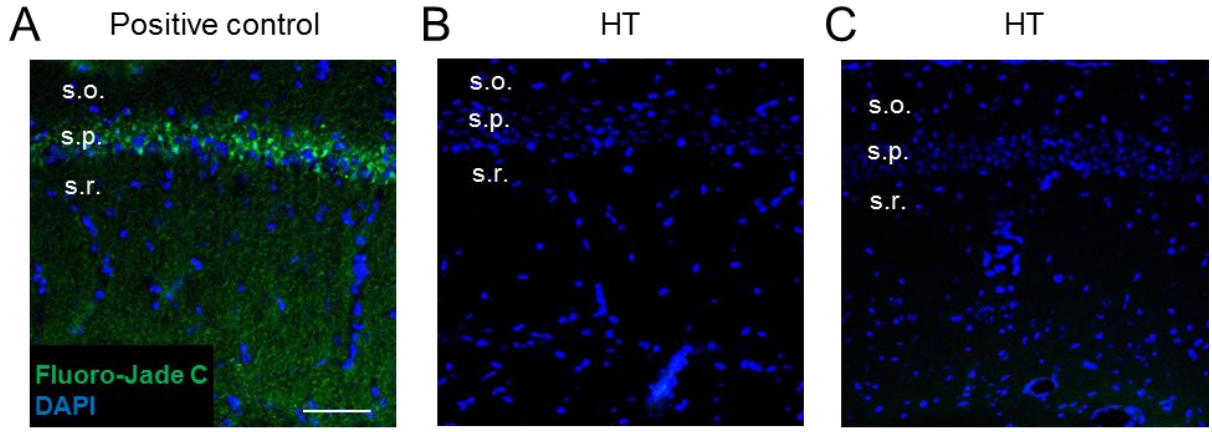

Figure 5.1 Fluoro Jade C staining for neuronal degeneration. Fluoro-Jade C staining did not indicate EFSs-induced neuronal degeneration. (A) Fluoro-Jade C (green) / Dapi (blue) signal in slices from animals intracortically injected with kainate, which served as a positive control. Five days after kainate-induced *status epilepticus*, many pyramidal neurons displayed green fluorescence. (B and C) Representative images showing Fluoro-Jade C / DAPI double staining in the hippocampal CA1 subfield 6 h and 5 d (respectively) after EFSs (HT). Note lack of Fluoro-Jade C immunoreactivity. s.o. = stratum oriens; s.p. = stratum pyramidale; s.r. = stratum radiatum. Scale bar = 50 µm.

The density of pyramidal neurons in CA1 region of hippocampus was investigated by NeuN staining. Neuronal staining for untreated controls and HT-treated pups is shown in figure 5.2A. The number of NeuN positive cells was counted in a volume of 290.62 x 290.62 x 15 μm^3 within the CA1 stratum pyramidale of the hippocampus. There was no difference in the number of NeuN positive cells in hippocampi of EFS (HT) mice and untreated control (UC) littermates (number of Neun positive cells: UC = 277956 ± 34141 vs. HT = 278896 ± 26152, n = 9 slices from 3 animals were used for each condition, p = 0.9, T-test; see Fig. 5.2B).

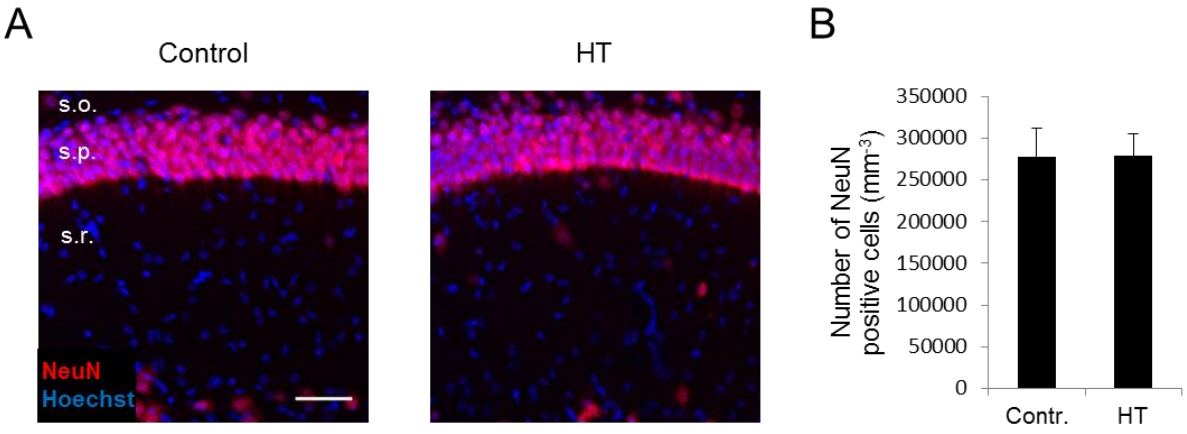

Figure 5.2 Immunohistochemical analysis of neuronal density in hippocampal sections from immature mice subjected to EFSs. Slices were prepared from brains obtained from mice perfused 5 d after EFSs and untreated control littermates. (A) NeuN (red) / Hoechst (blue) double staining revealed no reduction in the numbers of pyramidal neurons (B). s.o. = stratum oriens; s.p. = stratum pyramidale; s.r. = stratum radiatum. Scale bar = 50 µm.

5.1.3 Microglia activation

To investigate whether EFSs cause inflammation, microglia activation was examined 5 d after HT-treatment through Iba1 antibody immunostaining (see Fig. 5.3). Altered microglia morphology (hypertrophic cell bodies and processes) was observed in the hippocampi of HT-treated mice as compared to room temperature-treated and untreated control littermates (Fig. 5.3A). Iba1 immunoreactivity was significantly increased in hippocampi of HT-treated mice compared to hippocampi of room temperature-treated and untreated control littermates (area occupied by Iba1: HT = 2.8 ± 0.2 % vs. room temperature = 0.8 ± 0.5 % and UC = 1.1 ± 0.6 %, n = 9 slices from 3 animals for each condition, $p < 0.05$, post hoc Tukey HSD; Fig. 5.3B). The number of Iba1-positive cells observed in a volume of 290.62 x 290.62 x 15 μm^3 was also significantly higher in HT-treated mice when compared with room temperature-treated and untreated control littermates (number of Iba1-positive cells: HT = 39729 ± 2772 vs. room temperature = 29731 ± 1205 and UC = 27889 ± 3893, n = 9 slices from 3 animals for each condition, $p < 0.05$, post hoc Tukey HSD; Fig. 5.3C).

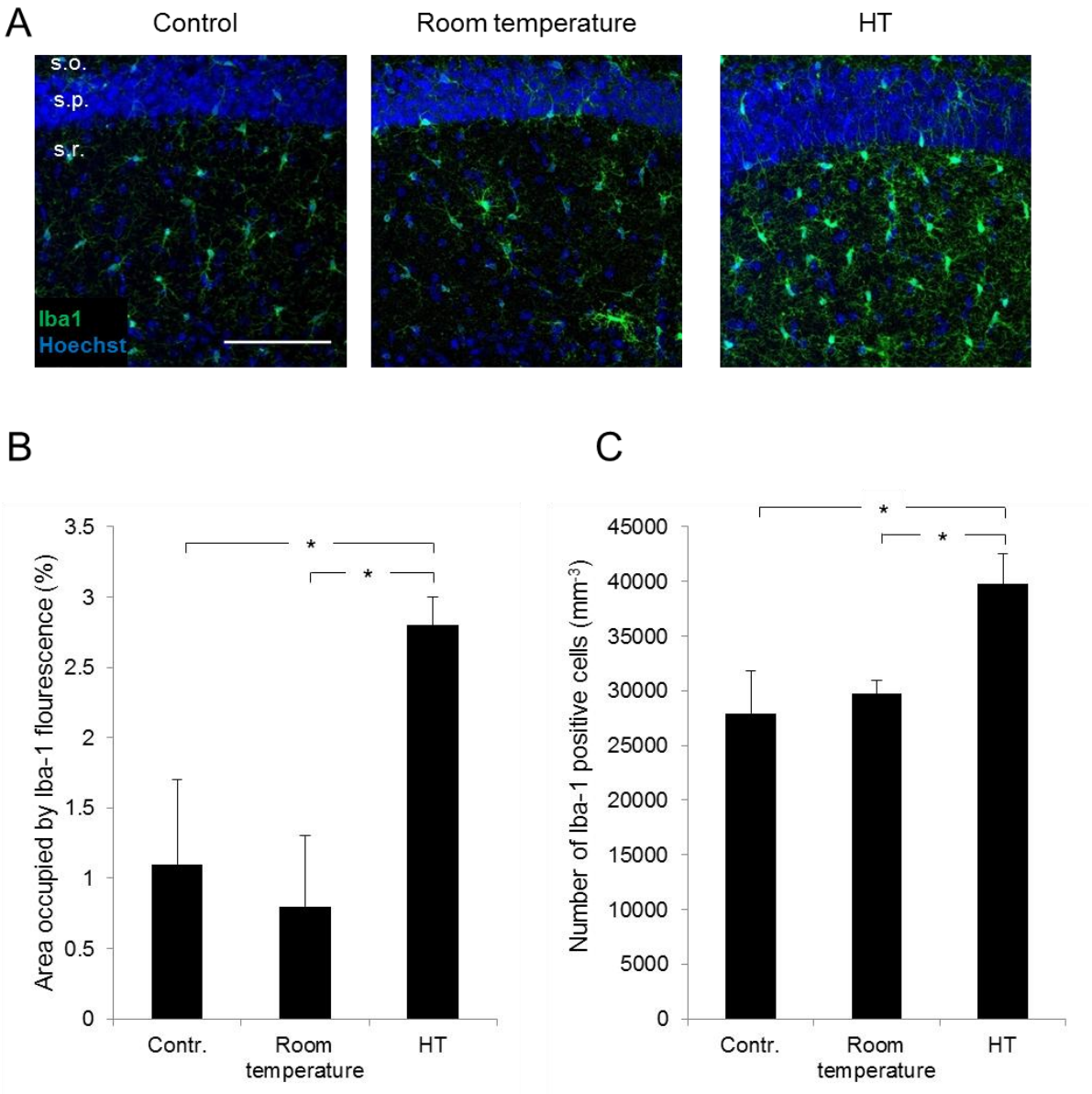

Figure 5.3 Immunohistochemical analysis of Iba1-positive microglia in hippocampal sections from immature mice subjected to EFSs. Slices were prepared from brains of animals perfused 5 d after HT-treatment, room temperature-treatment and untreated control littermates. Microglia activation could be detected by Iba1 (green) / Hoechst (blue) double staining (A). The area occupied by Iba1-positive cells was significantly higher in HT-treated mice than in room temerature-treated and untreated control littermates (B). The number of Iba1-positive cells was significantly higher in HT-treated mice as compared to room temperature-treated and untreated control littermates (C). s.o. = stratum oriens; s.p. = stratum pyramidale; s.r. = stratum radiatum. Scale bar = 50 µm. Asterisk indicates $p < 0.05$ (post hoc Tukey HSD).

5.1.4 Reactive astrogliosis

Astrocytes play an important role in maintaining ion and neurotransmitter homeostasis in the healthy brain (Volterra and Meldolesi, 2005). In addition to their response in the form of potentiating and restricting CNS inflammation (Sofroniew, 2015), astrocytes actively contribute to neural metabolism, synaptic plasticity and neuroprotection (Chung et al., 2015; Colangelo et al., 2014). In response to toxins, traumatic insults or inflammation the morphology, biochemistry and physiology of astrocytes change and their density increases. These changes in response to CNS insults are collectively termed as “reactive astrogliosis” (Sofroniew and Vinters, 2010).

To investigate reactive astrogliosis, 40 µm thick sections obtained from HT-treated and untreated control mice were stained with GFAP antibody. Under both conditions GFAP positive cells displayed similar gross morphology and density (Fig. 5.4A). The area occupied by GFAP in the stratum radiatum of the hippocampal CA1 region was quantified using image J. There was no difference in the area occupied by GFAP between HT-treated mice and untreated control littermates (percent area occupied by GFAP: UC = 0.65 ± 0.09 % vs. HT = 0.61 ± 0.14 %, n = 9 slices from 3 animals were used for each condition, p = 0.7, T- test; Fig. 4B).

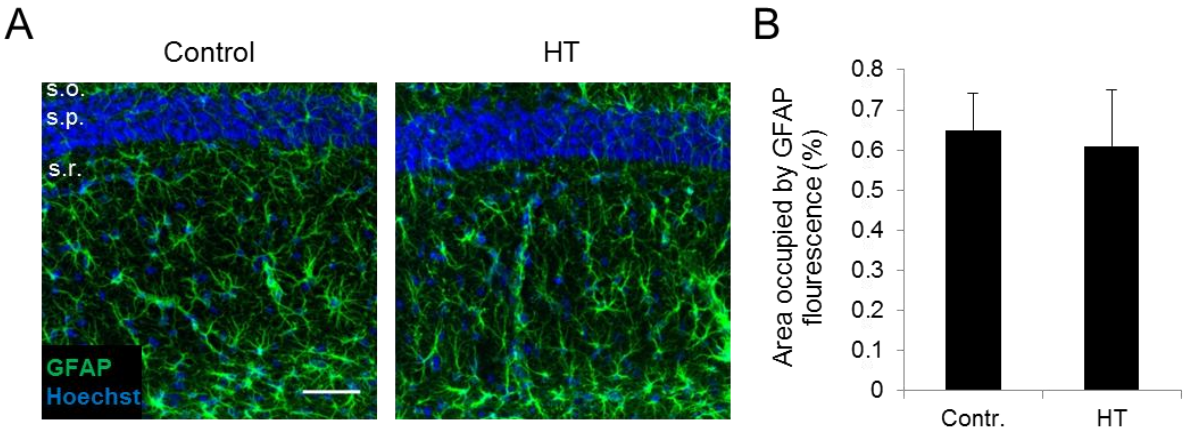

Figure 5.4 Immunohistochemical analysis of GFAP activation in hippocampal sections from immature mice subjected to EFSs. Slices were prepared from brains isolated from animals perfused 5 d after HT-treatment and from untreated

control littermates. (A) GFAP (green) / Hoechst (blue) double staining revealed no astrogliosis (B). s.o. = stratum oriens; s.p. = stratum pyramidale; s.r. = stratum radiatum. Scale bar = 50 µm.

5.1.5 EFSs induce a reduction in IGJC

Previously it has been shown that kainate-induced *status epilepticus* triggers a rapid reduction of astrocyte gap junctional coupling, a glial dysfunction that is considered to be a major event in epileptogenesis (Bedner et al., 2015). To investigate the influence of EFSs on astrocyte coupling, astrocyte gap junctional networks were studied in acute brain slices obtained from hGFAP-eGFP mice 5 d after EFSs generation under different conditions and untreated control littermates (see Table 5.1 and Table 5.2). The extent of astrocyte coupling was estimated by evaluating intercellular diffusion of biocytin to neighboring astrocytes from an individual astrocyte (see Fig. 5.5A2 & B2), filled with the tracer through the patch pipette during 20 min of whole cell recording (Bedner et al., 2015; Wallraff et al., 2004). Astrocytes were identified by the green fluorescence (eGFP) and their typical passive current patterns (see Fig. 5.5A1 and B1). The resting membrane potential of astrocytes from DH-IV animals was significantly lower than that of astrocytes from DH-I and untreated control littermates (UC = -72.5 ± 5.4 mV, n = 20; HT = 74 ± 6.4 mV, n = 35; DH-I = -72.7 ± 5.7 mV, n = 39; DH-IV = -76.8 ± 4.1 mV, n = 44, $p < 0.05$, post hoc Tukey HSD; Table 5.2). The input resistance of astrocytes from HT and DH-IV animals was significantly higher than that of astrocytes in untreated control littermates (UC = 2.2 ± 0.9 MΩ, n = 20; HT = 4.4 ± 2.5 MΩ, n = 35; DH-I = 3.3 ± 1.6 MΩ, n = 39; DH-IV = 3.8± 1.8 MΩ, n = 39, $p < 0.05$, post hoc Tukey HSD; see Table 5.2).

Table 5.2 Summary of electrophysiological recording measurements and IGJC

	Treatment	Membrane potential		Input resistance		Coupled cells	
			n (cells)		n (cells)		n (mice)
Control	Untreated Control	72.5 ± 5.4	20	2.2 ± 0.9	20	186 ± 49	4
HT	HT = 36 min	74 ± 6.4	35	4.4 ± 2.5	35	89 ± 50	8
DH-I	LPS_P13 or P14, HT P14 or P15, HT = 36 min	72.7 ± 5.7	39	3.3 ± 1.6	39	40 ± 18	8
DH-IV	LPS_P9, HT P11 and P12, HT = 60 min	76.8 ± 4.1	44	3.8 ± 1.8	44	68 ± 45	8

Quantification of interastrocytic biocytin spread revealed that in the hippocampus of EFSs mice the number of tracer coupled cells was significantly lower than in the hippocampus of untreated control littermates (UC = 186 ± 49 coupled cells, n = 20 slices from 4 animals; HT = 89 ± 50 coupled cells, n = 35 slices from 8 animals; DH-I = 40 ± 18 cells, n = 39 slices from 8 animals; DH-IV = 68 ± 45 coupled cells, n= 44 slices from 8 animals, $p < 0.05$, post hoc Tukey HSD; Table 5.2 &Fig. 5.5C). Within EFSs treated mice, there was no difference in the number of coupled cells between HT, DH-I and DH-IV animals.

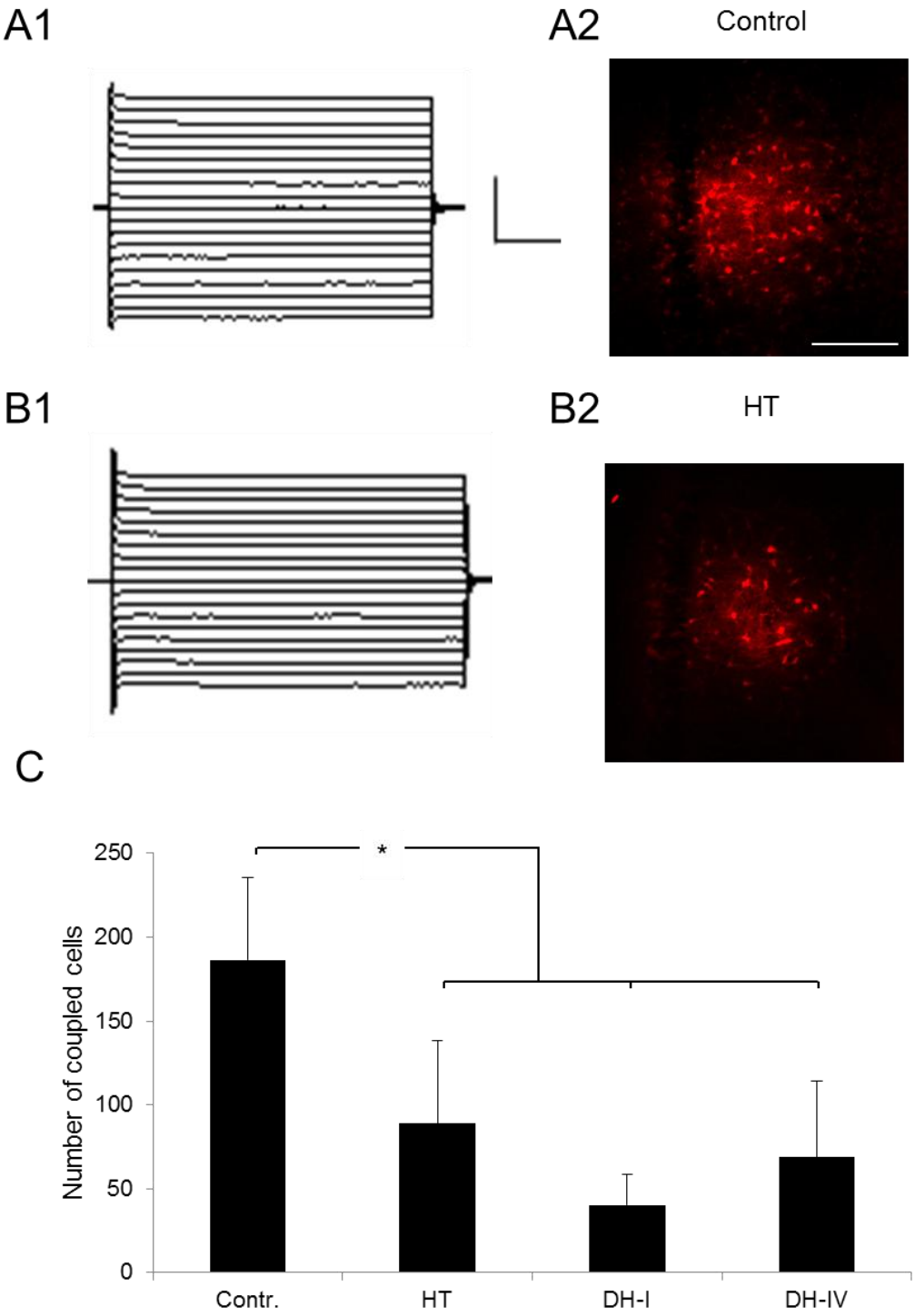

Figure 5.5 Reduced astrocytic tracer coupling in hippocampal slices from mice that experienced EFSs. IGJC in the stratum radiatum of the hippocampal CA1 subfield, assessed by intercellular diffusion of biocytin, was compared between EFSs animals and untreated control littermates. (A1 and B1) Insets represent current responses elicited by 50 ms voltage steps from -160 to +20 mV (V_{hold} = -80 mV). (A2

and B2) Representative images showing the extent of biocytin diffusion through the astroglial network in EFS animals (B2) and control littermates (A2). (C) Graph summarizing the results from the tracer coupling. In EFS mice, IGJC was significantly reduced. Calibration: 10 ms, 5 nA. Scale bar = 50 µm. Asterisk indicates $p < 0.05$ (post hoc Tukey HSD) (Khan et al., 2016).

5.1.6 Protein expression of Cx43 and Cx30 after EFSs

For astrocytes coupling in the hippocampus two Cx proteins, Cx43 and Cx30 have been reported to be responsible (Dermietzel et al., 2000). Reduced astrocyte coupling can be caused by reduced protein expression of Cxs as well as by modification in their phosphorylation state (John et al., 1999; Pahujaa et al., 2007; Solan and Lampe, 2009). To examine protein expression and phosphorylation states of Cxs, Western blot analysis was performed using hippocampal protein lysate obtained from HT-treated mice 5 d after HT-treatment and untreated control littermates. For loading control, membranes were also probed for α-tubulin.

The anti-Cx43 antibody recognized 3 bands within a range of 42-46 kDa (P0, P1 and P2), reflecting different phosphorylation states of Cx43 protein (see Fig. 5.6A). Total amount of Cx43 protein was significantly reduced in the hippocampus of HT-treated mice as compared to untreated control littermates (Cx43 / α-tubulin ratio: UC = 0.54 ± 0.08 vs. HT = 0.35 ± 0.07, n= 3 animals each, $p < 0.05$, T- test; Fig. 5.6B).

Separate quantification of Cx43 P0, P1 and P2 bands revealed that there was no difference in the fractional contribution of P0 band to the total protein (fractional contribution of P0: UC = 79.8 ± 2.3 % vs. HT = 66.8 ± 8.2 %, $p = 0.057$, T- test; Fig. 5.6C). The fractional contribution of the P1 and P2 bands to the total protein was significantly higher in HT-treated mice than in control littermates (fractional contribution of P1 and P2: UC = 14.9 ± 3.9 % vs. HT = 31 ± 1.3 %, $p < 0.05$, T- test; Fig. 5.6D). This observation indicates that HT-treatment induced not only a reduction of Cx43 expression but also alterations in the Cx43 phosphorylation status.

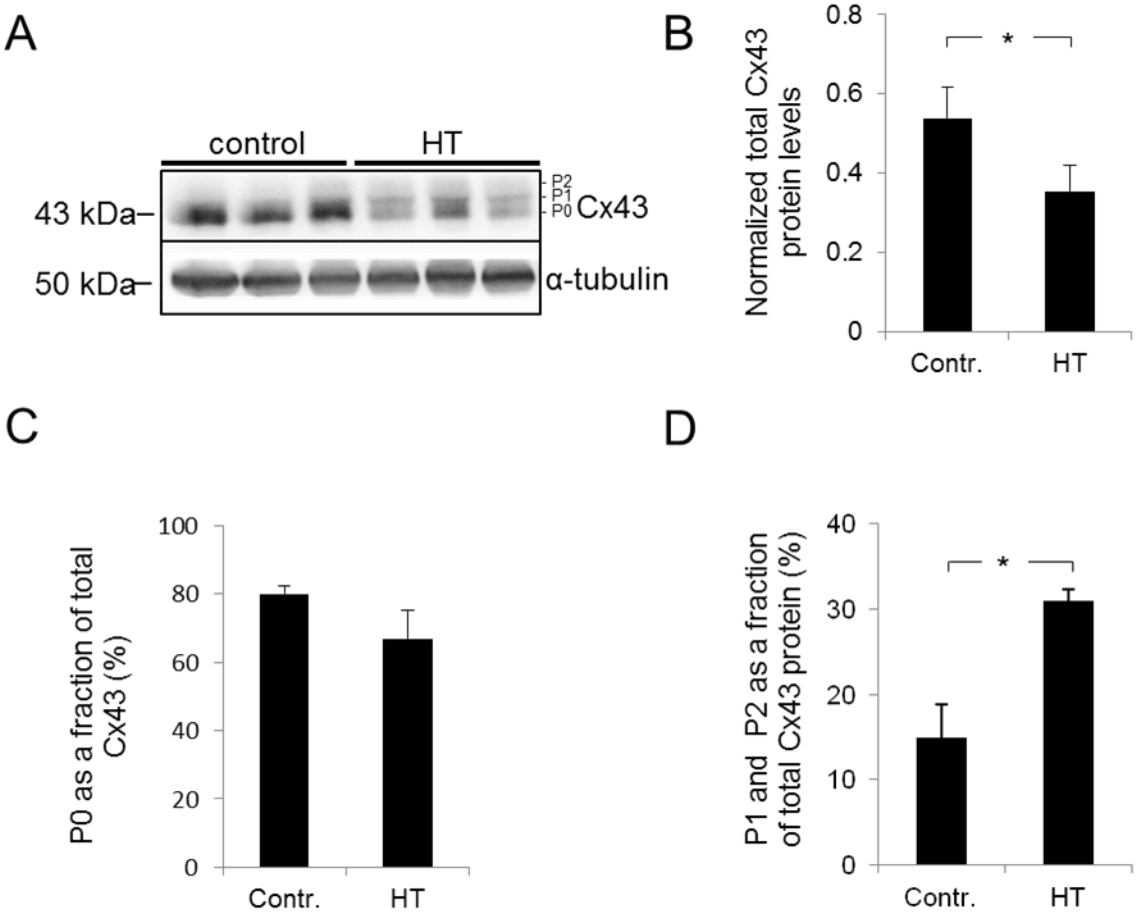

Figure 5.6 Cx43 protein levels in the hippocampus of mice that experienced EFSs. (A) Cx43 levels in hippocampal lysates prepared from immature mice 5 d after HT-treatment and untreated control littermates. α-tubulin was used as a loading control. (B) Quantification of the Western blots revealed that Cx43 protein levels were significantly reduced in HT-treated mice compared to untreated control littermates (n = 3 animals). (C) There was no difference in the P0 fraction of total Cx43 protein between HT treated and untreated control animals. (D) The fractional contribution of the P1 and P2 bands to the total protein was significantly higher in HT mice than in controls. Asterisks indicate $p < 0.05$ (T-test).

The anti-Cx30 antibody recognized a band at 30 kDa (Fig. 5.7A), and there was no significant difference in the amount of total Cx30 protein between HT-treated and untreated control littermates (Cx30 / α-tubulin ratio: UC = 0.28 ± 0.11 vs. HT = 0.33 ± 0.11, n = 3 animals each, $p = 0.6$, T-test; Fig. 5.7B).

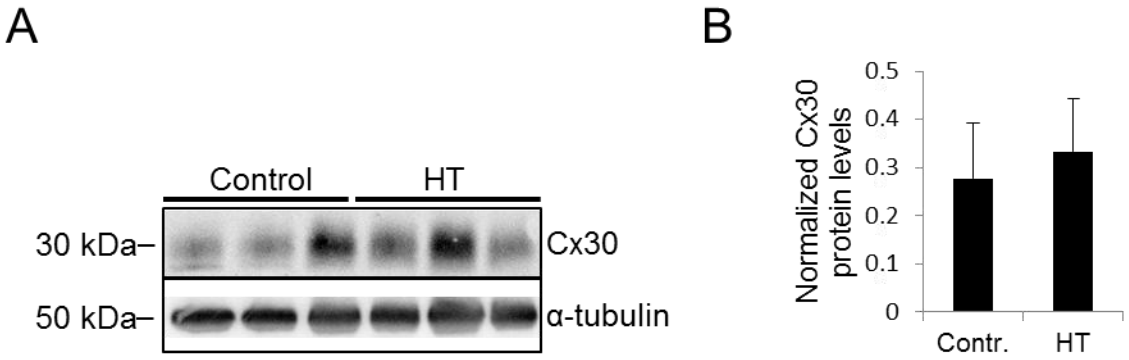

Figure 5.7 Cx30 protein levels in the hippocampus of mice that experienced EFSs. (A) Cx30 levels in hippocampal lysates prepared from immature mice 5 d after HT-treatment and from untreated controls. α-tubulin was used as a loading control. (B) Quantification of the Western blots revealed that Cx30 protein levels were not different between HT-treated and control mice (n = 3 animals).

Together, these data suggest that reduced expression of Cx43 protein and / or changes in its phosphorylation pattern account for the decreased astrocyte gap junctional communication in HT-treated mice.

5.1.7 Generation of unprovoked spontaneous generalized seizures after EFSs

It has been reported that FSs in early childhood in human can lead to epilepsy in later life (MacDonald et al., 1999; Vestergaard et al., 2007). In animal models it has been shown that EFSs during early age increase the susceptibility for seizure generation (Dube et al., 2000). A former PhD student from our laboratory has already shown that HT-treatment (36 min) of immature hGFAP-eGFP mice at P14 or P15 caused unprovoked spontaneous generalized seizure in a proportion of animals (Dupper, 2014). To assess the development of spontaneous generalized seizure after DH-treatment, telemetric EEG transmitters were implanted into animals two months after DH-treatment and the occurrence of generalized seizures was investigated via continuous telemetric EEG recording and video monitoring over a period of two weeks. One out of 19 hGFAP-eGFP animals (including all conditions for EFSs) showed generalized seizure (Fig. 5.8 and Fig. 5.9). Among C57Bl6J mice

one out of 9 animals (including both condition for DH-treatment) displayed generalized seizures with a frequency of 6 seizures / day.

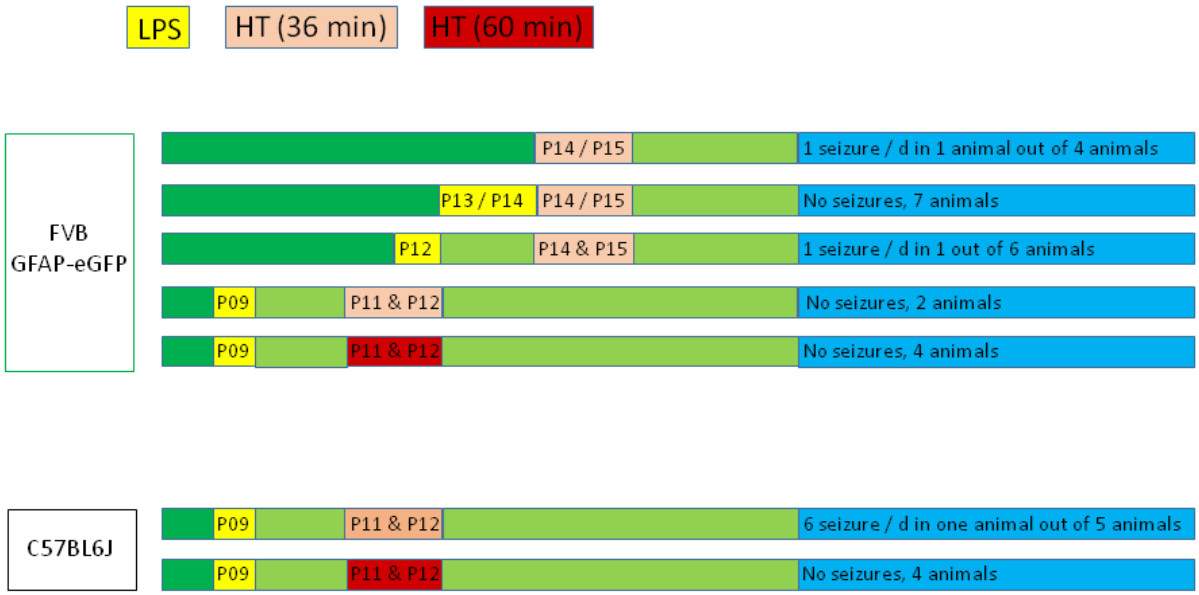

Figure 5.8 Summary of treatment and seizure activity. Mice from two genetic back-grounds were used in the experiments. EFSs were generated in these mice under different conditions regarding age, LPS treatment and duration of HT-treatment. Two months after EFSs generation, the animals were investigated for unprovoked spontaneous seizure activity. HT-treatment (36 min) and EEG recordings of immature hGFAP-eGFP mice at P14 or P15 were performed by (Dupper, 2014).

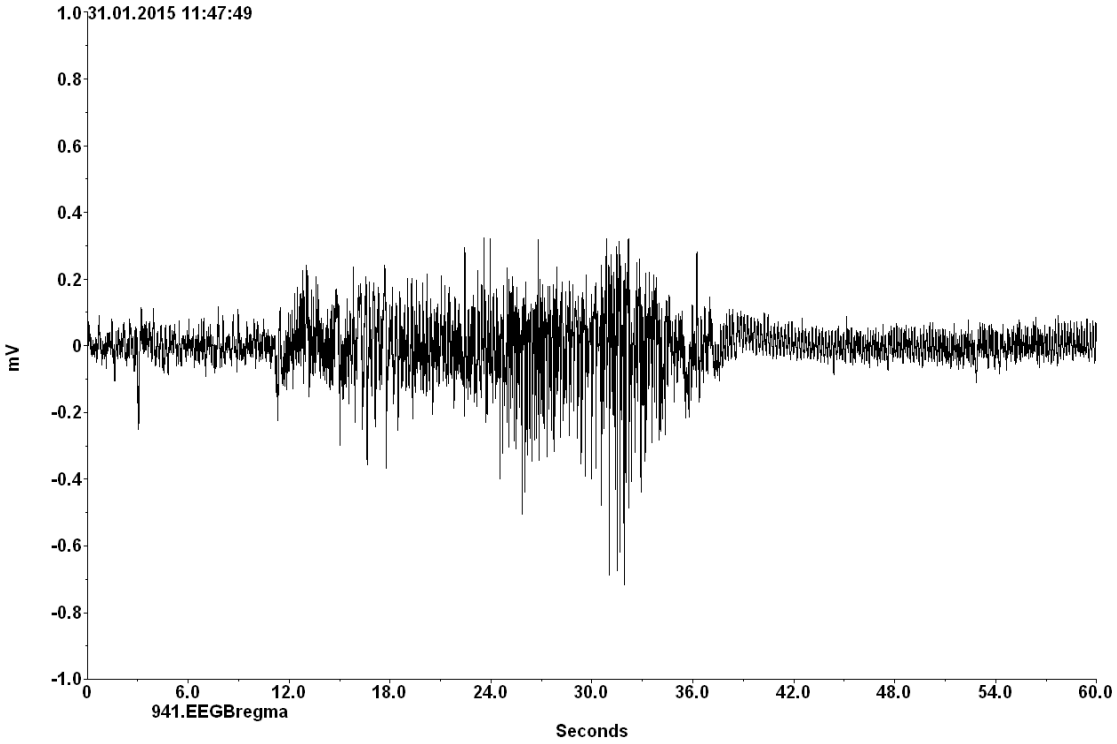

Figure 5.9 Example of an EEG trace during a spontaneous generalized seizure in a DH-treated hGFAP-eGFP mouse. In one out of 19 EFSs treated animals spontaneous generalized seizures were observed. The EEG recordings were performed 2 months after EFSs generation.

5.2 The role of TAK1 in epilepsy

5.2.1 TAK1 activation in astrocytes

In previous studies it has been observed that astrocytes are activated in response to noxious stimuli and can elicit pro- as well as anti-inflammatory response (Sofroniew and Vinters, 2010). During inflammatory response, inflammatory mediators like NF-κB are activated which in turn initiate transcription of inflammatory cytokines (Hayden et al., 2006). TAK1 is activated by phosphorylation and is an upstream modulator of NF-κB activation (Sato et al., 2005; Shim et al., 2005).

To investigate the seizure-induced activation of TAK1 in astrocytes, *status epilepticus* was induced by unilateral intracortical kainate injection and immunofluorescence staining was performed at different time points (4 hpi, 1 dpi and

5 dpi). Activated TAK1 (p-TAK1) could not be detected in astrocytes at none of the investigated time points (Fig. 5.10; data for 4 hpi and 1 dpi not shown).

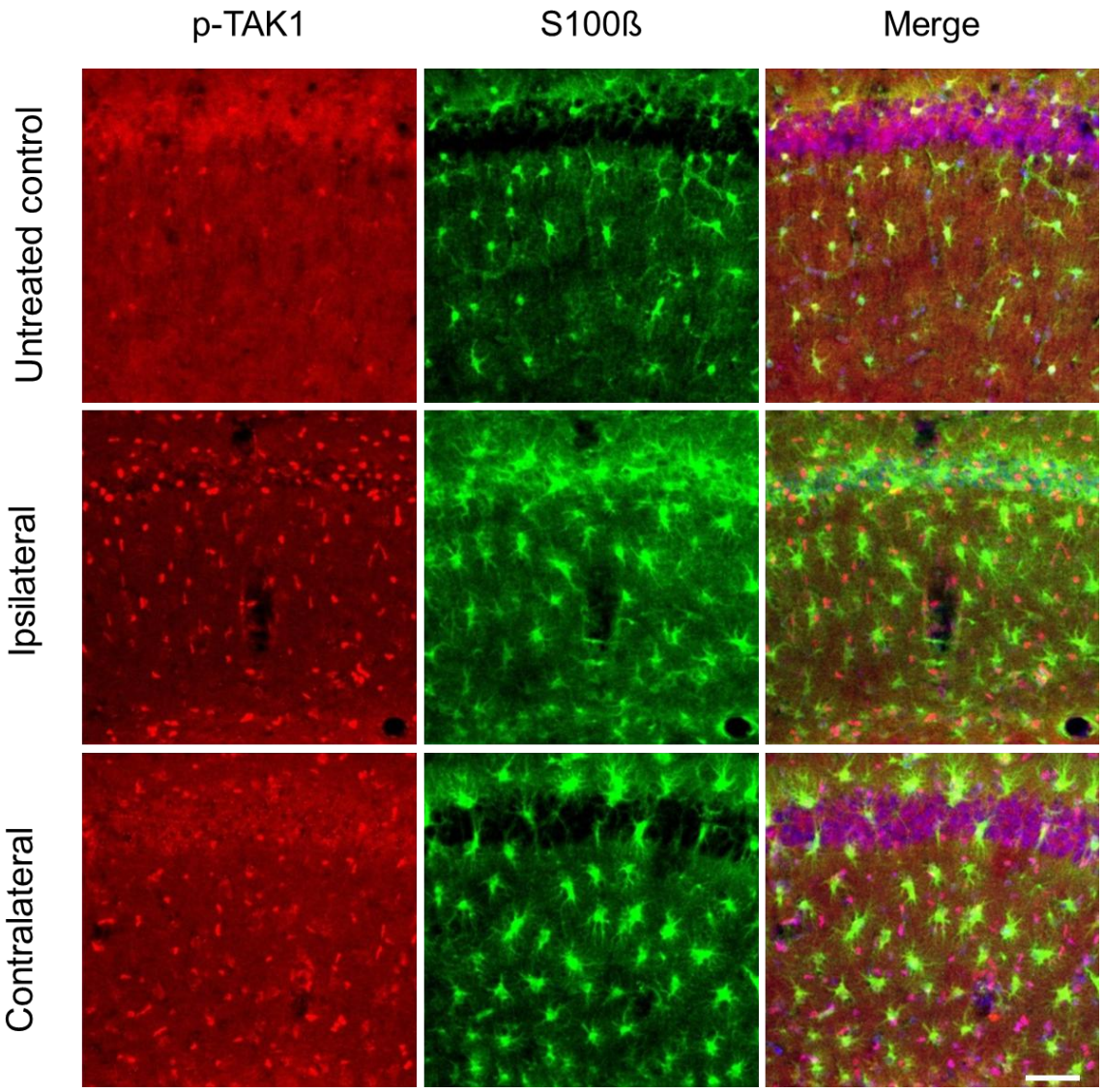

Figure 5.10 p-TAK1 / S100ß / DRAQ5 triple-staining in the mouse hippocampus. Slices were prepared from brains of animals perfused at 5 d after kainate-induced *status epilepticus*. The occurrence of activated TAK1 in astrocytes was assessed by S100β (green) / p-TAK1 (red) / DRAQ5 (blue) triple staining. P-Tak1 was not found to be present in astrocytes at this time point. Scale bar = 50 µm.

5.2.2 TAK1 activation in microglia

Microglia are the major innate immune cells in the CNS (Kreutzberg, 1996). These cells quickly activate in response to DAMPs and PAMPs (Heneka et al., 2014; Town et al., 2005), migrate to and accumulate in regions of injury and / or degeneration (Domercq et al., 2013). Activated microglia produce and release inflammatory cytokines like IL-1β, TNF-α, IFN-γ and chemokines (Banati et al., 1993; Smith et al., 2012). These inflammatory cytokines are produced and released as a consequence of NF-κB activation (Hayden et al., 2006). NF-κB activation has been suggested to be modulated by activation of TAK1 (Sato et al., 2005; Shim et al., 2005). It has been shown that TAK1 deletion and / or inhibition can result in reduced inflammatory response (Goldmann et al., 2013; Zhang et al., 2015).

Therefore, to investigate TAK1 activation in microglia, *status epilepticus* was induced by unilateral intracortical kainate injection. Immunofluorescence staining was performed at different time points (4 hpi, 1 dpi and 5 dpi). TAK1 activation was observed in microglia (Fig. 5.11; data for 4 hpi and 1 dpi not shown). Fluorescence intensity of p-TAK1 increased significantly on ipsilateral side 5 dpi when compared to untreated control and to the ipsi- and contralateral sides of mice 4 hpi and 1 dpi (fluorescence intensity of p-TAK1: UC = 80 ± 23 a.u.; 4 hpi contra = 48 ± 6 a.u.; 4 hpi ipsi = 52 ± 4 a.u.; 1 dpi contra = 69 ± 17 a.u.; 1 dpi ipsi = 80 ± 9 a.u.; 5 dpi contra = 113 ± 34 a.u.; 5 dpi ipsi = 151 ± 30 a.u.; 9 sections from 3 animals for each condition, $p < 0.05$, post hoc Tukey HSD; Fig. 5.12A). The number of microglia cells showing TAK1 activity was significantly higher on the ipsi- as well as contralateral side 5 dpi when compared to the untreated control and to the ipsi- and contralateral sides of mice 4 hpi and 1 dpi (number of microglia cells / mm^3 showing TAK1 activity: UC = 18298 ± 2565; 4 hpi contra = 9773 ± 8543; 4 hpi ipsi = 9618 ± 8381; 1 dpi contra = 13496 ± 465 ; 1 dpi ipsi = 14428 ± 1231; 5 dpi contra = 66709 ± 8394; 5 dpi ipsi = 90755 ± 25908; 9 sections from 3 animals for each condition, $p < 0.05$, post hoc Tukey HSD; Fig. 5.12B).

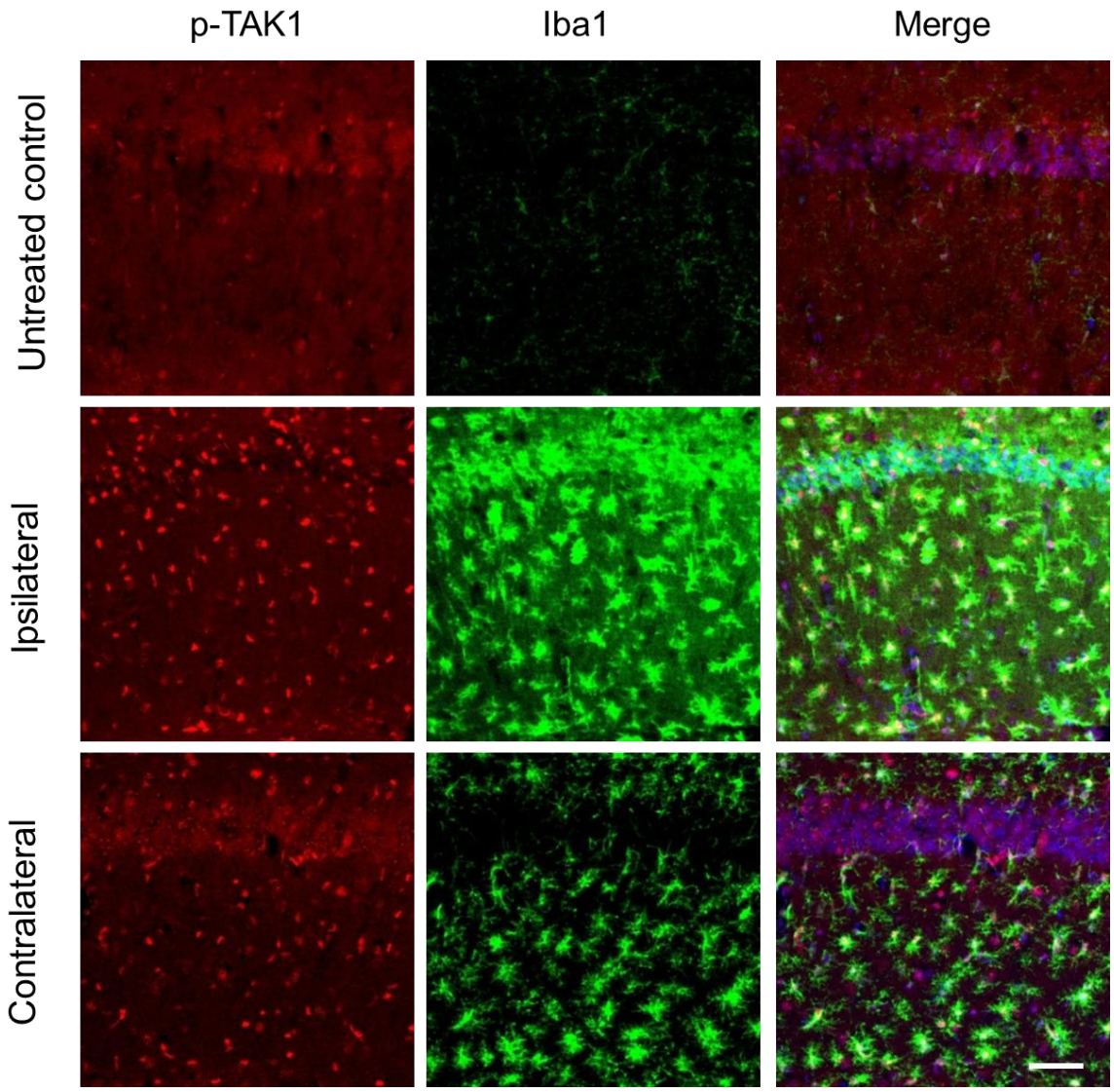

Figure 5.11 p-TAK1 / Iba1 / DRAQ5 triple-staining in the mouse hippocampus. Slices were prepared from brains of animals perfused 5 dpi after kainate induced *status epilepticus*. Activated TAK1 in microglia was detected by Iba1 (green) / p-TAK1 (red) / DRAQ5 (blue) triple staining. TAK1 was activated in Iba1-positive cells (microglia). Scale bar = 50 µm.

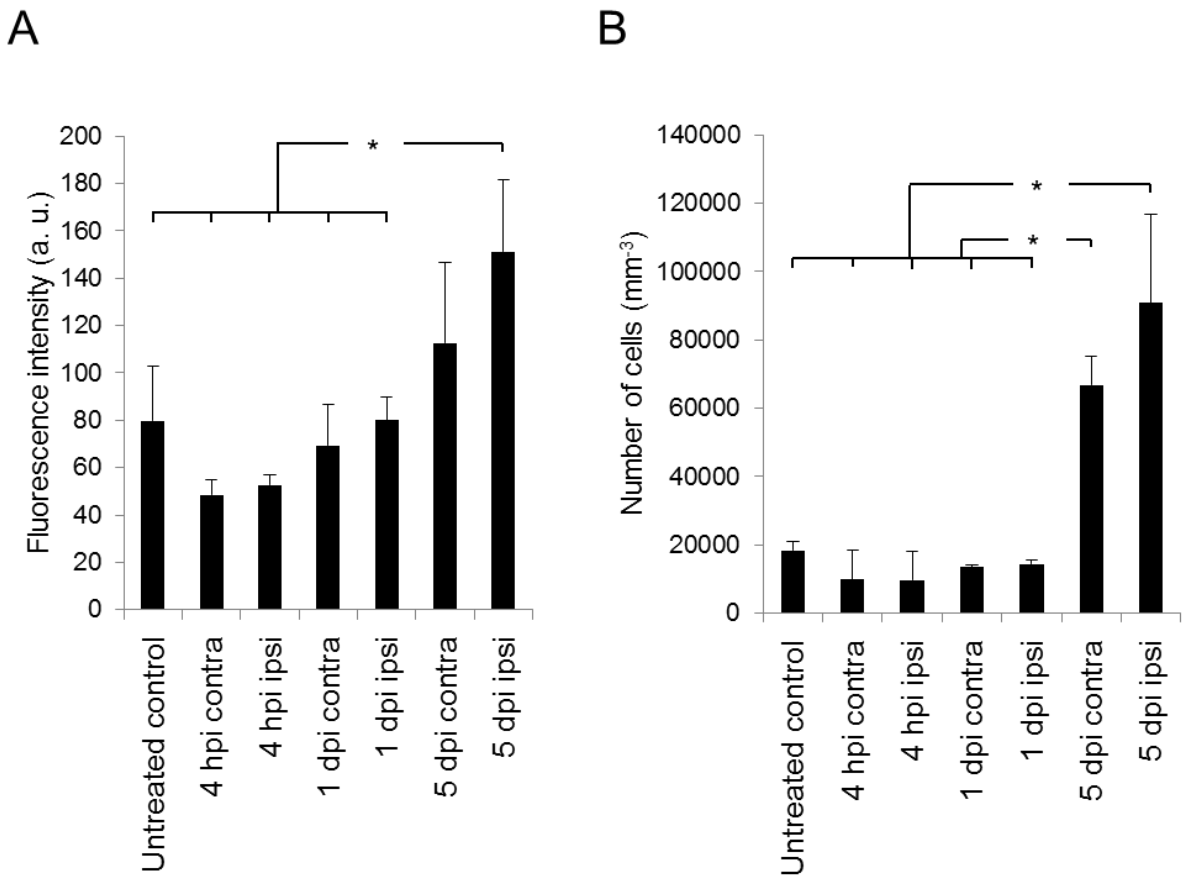

Figure 5.12 Quantification of TAK1 activation in microglial cells. TAK1 activation in microglia increased 5 dpi. A) Fluorescence intensity of p-TAK1 increased significantly on the ipsilateral side 5 dpi. B) The number of microglia cells showing activated Tak1 was significantly increased on ipsi as well as on contralateral sides 5 dpi. Quantification was performed in a volume of 150.39 x 150.39 x 19 µm^3 in the *stratum radiatum*. Asterisks indicate $p < 0.05$ (post hoc Tukey HSD).

5.2.3 Genotyping of the TAK1KO animals

To investigate the role of TAK1 in epileptogenesis, TAK1KO animals were used. For genotyping, animals were tested for the presence of the Tak1$^{fl/fl}$ allele (lower row) and the Cx3cr1^{CreER} transgene (upper row). Mouse number 1, 3, 4, 5, 6, 8 and 9 for instance, had a Tak1$^{fl/fl}$ as well as Cre-recombinase allele. In mice with this genotype TAK1 could be knocked out by TAM administration. Mouse number 2 and 7 had a Tak1$^{fl/fl}$ allele but lacked the Cre-recombinase and could therefore be used as a control.

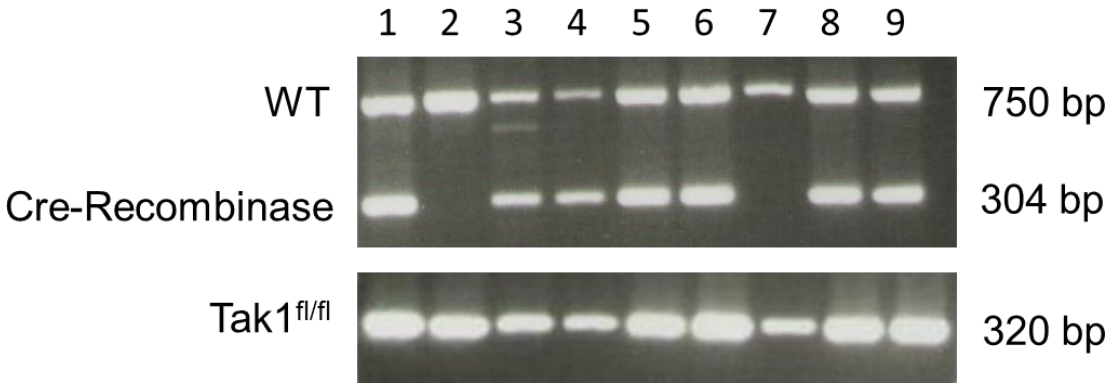

Figure 5.13 Genotyping PCR of the Cx3cr1^{CreER}:Tak1$^{fl/fl}$ mouse line. Deletion of the TAK1 gene was monitored by genotyping PCR. As heterozygous animals were crossed, all the animals showed a WT allele. Mouse number 1, 3, 4, 5, 6, 8 and 9 had alleles for Tak1$^{fl/fl}$ and Cre-recombinase. Mouse number 2 and 7 lacked the allele for Cre-recombinase.

5.2.4 Microglia activation in TAK1KO animals

Microglia activation was investigated after *status epilepticus* induced by unilateral intracortical kainate injection in TAK1KO and their Cre-negative (control) littermates. Five days after injection, animals were perfused and cryosections of the brains were stained with anti-Iba1 antibodies. Alterations in microglial morphology (hypertrophic cell bodies and processes) were much less in TAK1KO animals than in their control littermates (Fig. 5.14A). Also, Iba1 immunoreactivity was significantly less on the ipsilateral side of TAK1KO mice than on the ipsilateral and contralateral side of Cre-negative littermates 5 dpi (area occupied by Iba1: TAK1KO ipsi = 0.802 ± 0.313 %; TAK1KO contra = 1.2 ± 0.55 %; contr. ipsi = 3.089 ± 1.223 %; contr. contra = 3.076 ± 0.6 %, n = 9 slices from 3 animals for each condition, $p < 0.05$, post hoc Tukey HSD; Fig. 5.14B) as well as the number of Iba1-positive cells observed in a volume of 289 x 289 x 19 µm^3 was significantly lower in TAK1KO mice compared to Cre-negative littermates (number of Iba1-positive cells: TAK1KO ipsi = 50902 ± 4244; TAK1KO contra = 53703 ± 7397; contr. ipsi = 97604 ± 10258; contr. contra = 73868 ± 4679, n = 9 slices from 3 animals for each condition, $p < 0.05$, post hoc Tukey HSD; Fig. 5.14C).

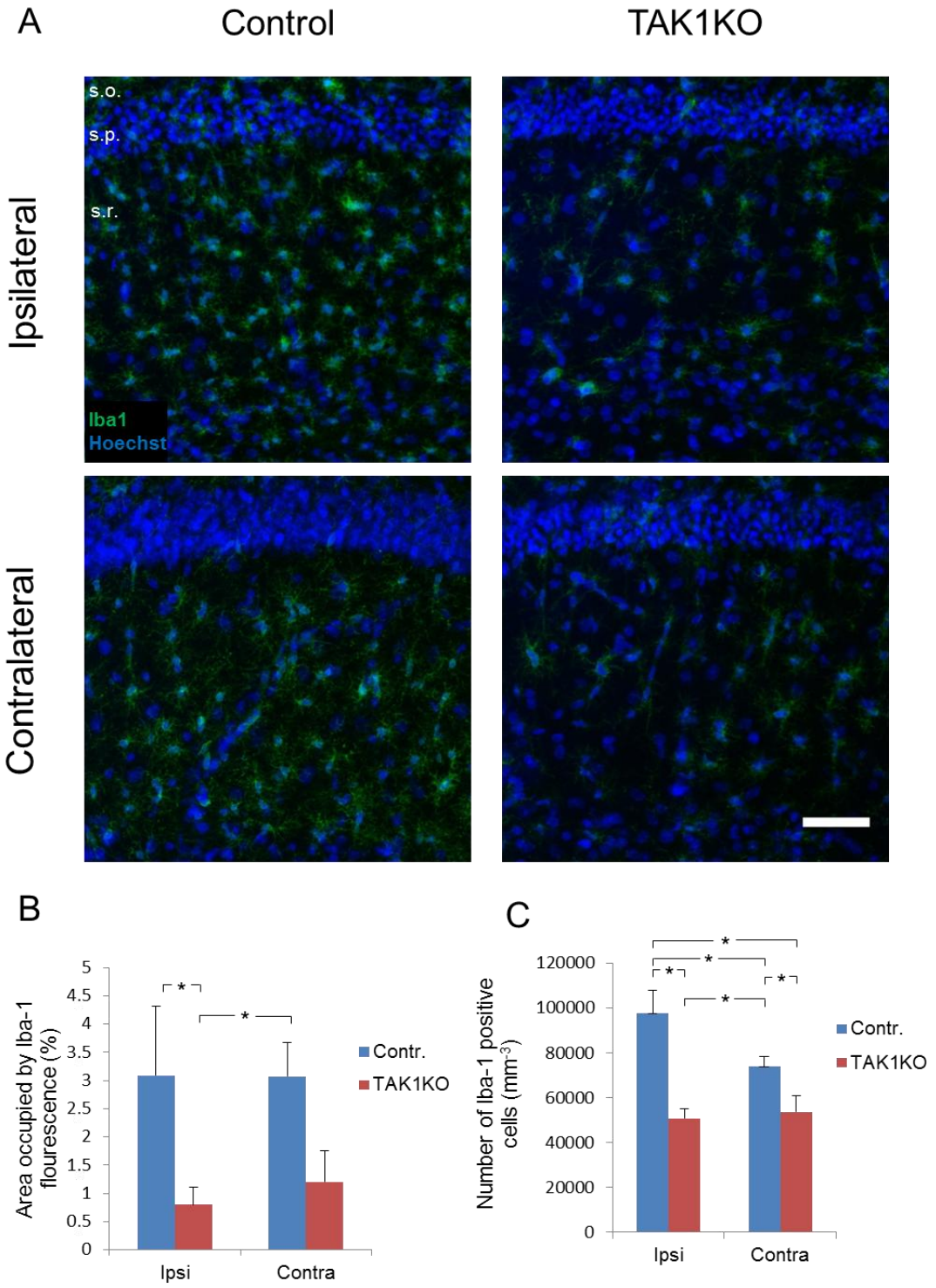

Figure 5.14 Microglia activation 5 dpi. Slices were prepared from brains of animals perfused 5 dpi. Microglia activation could be detected by Iba1 (green) / Hoechst (blue) double staining. A) Decreased microglia activation was observed in TAK1KO. B) The area occupied by Iba1-positive cells was significantly lower on ipsilateral side in TAK1KO mice and C) the number of Iba1-positive cells were significantly lower in

TAK1KO animals when compared to their control littermates. Scale bar = 50 µm. Asterisks indicate $p < 0.05$ (post hoc Tukey HSD). s.o. = stratum oriens; s.p. = stratum pyramidale; s.r. = stratum radiatum.

5.2.5 Kainate-induced seizure activity in TAK1KO animals

To investigate the seizure frequency in TAK1KO animals, EEG recordings with video monitoring were performed for one month after unilateral intracortical kainate injection in TAK1KO and control animals. Spontaneous seizure activity was assessed from 3 dpi, when the EEG recordings became stable, to 30 dpi. The seizure frequency was significantly lower in 4 out of 6 TAK1KO animals when compared with the controls (average seizures / d over a period of one month: TAK1KO = 1 ± 0.36 vs. contr. = 2.6 ± 0.7, n = 4 and 5 animals, respectively, $p < 0.05$, T-test; Fig. 5.15A). To identify the time point when TAK1KO and control animals start to show differences in seizure frequency, EEG data was analyzed in steps of 5 d duration over a period of a month. The seizure frequency for TAK1KO and control animals was averaged over five days. In the beginning there was no difference in seizure frequency between TAK1KO and controls but from day 11-15 the seizure frequency started decreasing for TAK1KO animals and increasing for control mice (Fig. 5.15B). The number of seizures / day was significantly lower in TAK1KO animals than in their Cre-negative littermates, averaged for the duration between 16-20 and 21-25 d (seizure / d averaged over a duration of 5 d: 3-5 d, TAK1KO = 1.25 ± 0.83 vs. contr. = 0.8 ± 0.5; 6-10 d, TAK1KO = 1.5 ± 0.52 vs. contr. = 1.28 ± 0.48; 11-15 d, TAK1KO = 1.18 ± 1.29 vs. contr. = 2.77 ± 0.87; 16-20 d, TAK1KO = 1.02 ± 0.51 vs. contr. = 3.35 ± 0.7; 21-25 d, TAK1KO = 0.75 ± 0.25 vs. contr. = 3.2 ± 1.32; 26-30 d, TAK1KO = 0.55 ± 0.3 vs. contr. = 3.74 ± 3.51; n = 4 and 5 animals, respectively, $p < 0.05$, T-test).

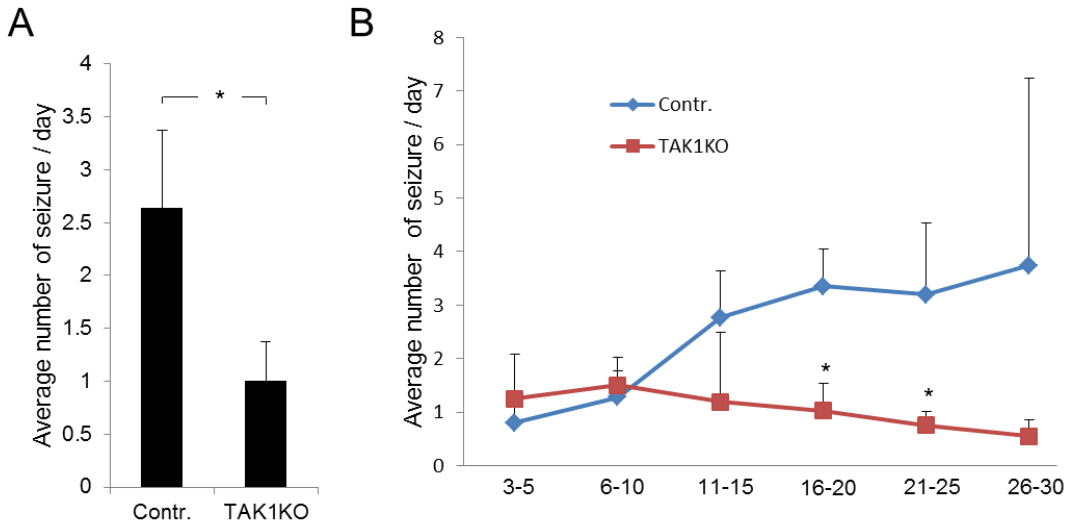

Figure 5.15 Seizure frequency after kainate-induced *status epilepticus* in control and TAK1KO mice. A) Generation of unprovoked spontaneous generalized seizures analyzed over a period of one month after kainate-induced *status epilepticus*. The seizure frequency was significantly reduced in TAK1KO mice compared to control littermates over a period of one month. B) Average number of seizures analyzed for durational steps of 5 d over a period of one month after kainate-induced *status epilepticus*. Number of seizures increased for control mice and decreased for TAK1KO littermates 10 days after *status epilepticus.* The difference in the number of seizures was significantly different at days 16-20 and 21-25. Asterisks indicate $p < 0.05$ (T-test).

6 Discussion

6.1 Consequences of EFSs on the hippocampal astrocytic network

6.1.1 EFSs generation

It has been reported that 20-60% of patients suffering from intractable epilepsy had a history of prolonged FSs during early childhood (Bender et al., 2004; McClelland et al., 2011). In Europe and the US, 2-4 % of all children experience at least one FS before the age of 5 years (Hauser, 1994). The occurrence of FSs varies in different geographical locations; in Japan 8 % (Hauser, 1994; Tsuboi, 1984) and in China 1 % (Hauser, 1994) of children experience seizures before the age of 5 years. In some follow-up studies it has been found that 2.4 % of the children having simple FSs and 6 to 8 % of the children experiencing complex FSs are at a higher risk for generation of unprovoked seizures and epilepsy development (Annegers et al., 1987; Hauser, 1994). It can be expected that FSs during early childhood cause some irreversible damage to the brain which in later age can lead to epilepsy. In rats generation of spontaneous seizures as a consequence of EFSs has been reported (Dube et al., 2006). To investigate the effects of FSs on brain during early childhood, EFSs were induced in immature mice. To study the effects of inflammation, age, genotype and duration of fever on FS generation, HT was induced under different conditions in young mice from two different genetic back-grounds summarized in Table 5.1 (section 5.1.1).

The duration of EFSs in our approach was 36 min and that corresponds to the duration of most of the FSs in children (Shinnar et al., 2008). In some cases, however, the FSs last longer than 36 min in children (Boggs and Waterhouse, 2001). Therefore in this study the duration of the HT-treatment was also increased to 60 min in some experiments while keeping all the other conditions the same. In all EFS experiments, HT-treatment did not cause dehydration, as the decrease in average body weight was less than 5 % (see Table 5.1). Mild, moderate and severe

dehydration in children is defined as a body weight loss greater than 5 %, 10 % and 15 % of total body weight, respectively (Portale et al., 2002).

The threshold temperature for EFSs in pups varied between 39.4 ± 0.2 °C and 40.7 ± 0.4 °C with no significant difference between different conditions (section 5.1.1 & Table 5.1), and it was slightly less than 40.8 °C as reported in rats (Dube et al., 2000) which can be due to differences in species and experimental setup. At the threshold temperature animals showed first sudden immobility, and it has been shown that first spikes on EEGs appear during this phase (Dube et al., 2000). During HT-treatment behavioral scoring of animals was recorded and scaled (Table 4.1; van Gassen et al., 2008). In all experiments, animals showed motor automatisms that involved movement of distal segments of hands, feet, mouth and tongue. These automatisms are typically observed in TLE but sometimes can also be found with frontal lobe seizures (Tufenkjian and Luders, 2012; Vendrame et al., 2011). During HT-treatment animals showed face automatisms involving chewing, swallowing and grooming. Clonic seizures were also observed in some mice and these clonic seizures are probably secondary generalized seizures, which originate also from the temporal lobe. These data suggest that in this study EFSs observed in animals originated mostly from the temporal lobe.

Under different conditions animals showed differences in frequency, intensity, duration and stage (Table 4.1) of EFSs, but no differences were observed in EFSs between two episodes of HT-treatment under the same conditions on consecutive days (section 5.1.1). LPS administration one day before HT-treatment increased frequency, intensity, duration and stage (Table 4.1) of EFSs (see section 5.1.1). It has been already reported that postnatal LPS administration increases susceptibility, intensity and frequency of seizures as observed in rats and mice (Auvin et al., 2010; Eun et al., 2015; Galic et al., 2008). Increasing the duration between LPS administration and HT-treatment even worsened EFSs, and EFSs continued to occur even after stopping the protocol after 36 min. It has been suggested that LPS decreases K^+ buffering via causing reduction in IGJC (Bedner et al., 2015) which can consequently increase the susceptibility to seizure generation. In addition, systemic

LPS administration induces peripheral inflammation that leads to neuroinflammation and can subsequently cause oxidative stress in the hippocampus which might increase the susceptibility to seizures (Ho et al., 2015). LPS administration triggers an inflammatory response which leads to the release of inflammatory cytokines like IL-1β and TNF-α (Bossu et al., 2012; Qin et al., 2007). Moreover, the damage produced by these inflammatory cytokines and oxidative stress might increase by increasing the duration between the two hits; therefore, it seems that the duration between LPS administration and HT-treatment can affect EFSs as observed in the present study. Altogether, it can be suggested that LPS-induced inflammation increases the susceptibility of mice to hyperthermic seizures.

The use of mice in the experiments (DH-III - DH-VI) at younger age while keeping all other conditions similar resulted in decreased hyperactive behavior, jumping and rearing. This might be due to the small body size of animals, as except hyperactivity, the younger animals showed seizures and / or behavior similar to the older animals during HT-treatment (section 5.1.1). After 36 min, hGFAP-eGFP animals started to show stage IV seizures (tonic-clonic convulsions), and the intensity of these seizures constantly increased toward the end of the protocol. Even after stopping the protocol and when back with the mother, stage IV seizures were observed. hGFAP-eGFP mice displayed stage IV seizures only in DH-IV experiments, in which the duration of HT-treatment was extended to 60 min. Here they showed continuous tonic clonic contractions of fore and hind limb with loss of consciousness. As differences in genotype can affect EFS onset and it has been shown that C57Bl6J mice are more sensitive to this type of seizures (van Gassen et al., 2008), C57Bl6J mice were used for EFSs generation. In these animals, there was an increase in intensity, frequency and duration of EFSs. These animals showed stage I-IV seizures during the experiment and stage IV seizures when back with the mother. C57Bl6J showed febrile *status epilepticus* of 8-10 min towards the end of the protocol in the experiments (DH-VI) in which HT was induced for 60 min (see section 5.1.1). In conclusion, intensity, duration or frequency of FSs seem to be dependent on the genotype and duration of HT-treatment and / or fever.

6.1.2 EFSs do not cause neuronal degeneration

Neuronal cell death as an effect of seizures has been revealed in animal models of epilepsy (Jiang et al., 1999; Pitkanen et al., 2002, Bedner et al., 2015). Similar to the situation in human TLE, pyramidal neurons in the CA1, CA3 and hilus were susceptible to neuronal cell death in the experimental models (Freund et al., 1992; Nadler, 1981). Previously, neuronal degeneration in the hippocamapal CA1 pyramidal layer has been shown to occur as early as 6 h post kainate injection in a mouse model of epilepsy (Bedner et al., 2015). However, in the present study no neuronal degeneration was observed at two different time points (6 h and 5 d) after EFSs (Fig. 5.1) (Khan et al., 2016). Also, there was no change in the density of pyramidal neurons in the CA1 region of stratum pyramidale 5 d after EFSs (Fig. 5.2B). Consistent with our findings it has been shown that EFSs induced by HT-treatment in rats resulted in enhanced hippocampal excitability in the absence of neuronal cell death (Bender et al., 2003; Dube et al., 2010). It is known from previous studies that the immature hippocampus is extraordinarily resistant to seizure-induced neuronal cell death (Haas et al., 2001) and prolonged *status epilepticus* is a prerequisite for neuronal degeneration (Sankar et al., 1998; Thompson et al., 1998). Further, it has been reported that fat-rich maternal milk can be protective against excitotoxicity (Sullivan et al., 2003). Because, the pups were placed with their mother after EFS generation and they were dependent on their mother's milk, it can be expected that the fat-rich maternal milk might have provided a protection from neuronal degeneration as a consequence of EFSs.

6.1.3 EFSs lead to microglia activation

Microglia are the resident macrophages of the brain. Under physiological conditions these cells continuously scan their surrounding tissue with their highly motile and ramified processes (Nimmerjahn et al., 2005). Due to this behavior these cells can rapidly respond to injury (Cherry et al., 2014; Rock et al., 2004) and become activated. The activated microglia become hypertrophic, retract their processes, extend filopodia, and increase their proliferation and migration. In addition to clearance of apoptotic cells and phagocytosis of cellular debris, activated microglia

release pro-inflammatory cytokines such as IL-1β, IL-6 and TNF-α (Smith et al., 2012; Vezzani et al., 2008).

Five days after EFSs, microglial cells with altered morphology (hypertrophic cell bodies and processes) were observed in the hippocampi of HT-treated mice as compared to room temperature-treated and untreated control littermate (Fig. 5.3A). Moreover, Iba1 immunoreactivity as well as the number of Iba1-positive cells was significantly increased in the hippocampi of HT-treated mice compared to the controls (see Fig. 5.3B, C) (Khan et al., 2016). In similar studies, microglia activation, increase in the expression and release of pro-inflammatory cytokines has been reported (Eun et al., 2015; Jung et al., 2011; Patterson et al., 2015). Furthermore, microglia activation has been observed as a result of *status epilepticus* induced by injection of chemoconvulsants (Avignone et al., 2008; Eyo et al., 2014, Bedner et al., 2015), and in patients suffering from intractable epilepsy (Beach et al., 1995). Also, increase in inflammatory cytokine release after FSs in children has been observed (Choi et al., 2011). In addition to PAMPs and DAMPs, it has been suggested that the release of ATP from hyperactive neurons can attract and activate microglia via purinergic signaling (Eyo et al., 2014; Haynes et al., 2006; Dissing-Olesen et al., 2014).

The present study confirms previous reports that EFSs induce CNS inflammation. Though astrocytes have been shown to contribute to the inflammatory response (Dube et al., 2010; Vezzani et al., 2008), activated microglia are the major source of inflammatory cytokines such as IL-1β, IL-6 and TNF-α (Smith et al., 2012; Vezzani et al., 2008). These inflammatory cytokines can modulate neuronal activity directly by affecting neuronal receptors and / or indirectly by altering glial function (Vezzani and Viviani, 2015). IL-1β and TNF-α were found to reduce IGJC in acute brain slices as well as in cultured astrocytes (Bedner et al., 2015; Meme et al., 2006). Also, IL-1β has been shown to reduce Kir4.1 expression in astrocytes (Zurolo et al., 2012). Reduction in IGJC and Kir4.1 dysfunction has been associated with epileptogenesis (Steinhäuser et al., 2012; Steinhäuser et al., 2016). These inflammatory cytokines also inhibit glutamate uptake by astrocyte (Hu et al., 2000; Zou and Crews, 2005)

and increase glutamate release from astrocyte and microglia (Bezzi et al., 2001; Takeuchi et al., 2006). This glutamate release activates slow inward currents, which might generate epileptiform activity through synchronization of pyramidal neurons of the hippocampus (Carmignoto and Fellin, 2006). IL-1β modulates NMDA receptor activity (Viviani et al., 2003; Yang et al., 2005), which results in neuronal hyperexcitability (Zhang et al., 2008; Zhang et al., 2010) and promotes seizure generation (Balosso et al., 2008). TNF-α increases hyperexcitability by exocytosis of AMPA receptors (Beattie et al., 2002; Stellwagen et al., 2005) and reduces inhibitory transmission through endocytosis of GABA-A receptors (Stellwagen et al., 2005). Activated microglia not only influence other cell types through release of cytokines but also through cell-cell interaction via gap junctions (Kielian, 2008).

6.1.4 Effect of EFSs on astrogliosis

In response to traumatic insults astrocytes undergo physiological, morphological and biochemical changes (Wilhelmsson et al., 2006), these changes are collectively termed as “reactive astrogliosis” (Sofroniew and Vinters, 2010). Reactive astrogliosis is a continuous progressive process, but for better understanding it was classified into three categories: mild to moderate reactive astrogliosis; severe diffuse reactive astrogliosis and severe reactive astrogliosis with compact glial scar formation (Sofroniew and Vinters, 2010). Mild reactive astrogliosis is characterized by GFAP up-regulation, hypertrophy of cell body and processes, little or no astrocyte proliferation, no overlap of processes of neighboring astrocytes and preservation of individual domains (Wilhelmsson et al., 2006). In sever diffuse reactive astrogliosis, there is dramatic up-regulation of GFAP expression, intense hypertrophy of cell body and processes, increased astrocyte proliferation resulting in overlap of processes of neighboring astrocytes and loss of individual domains. In severe reactive astrogliosis with compact glial scar formation the conditions associated with severe diffuse reactive astrogliosis are worsened along with dense, narrow and compact scar formation (Wanner et al., 2013). These scars formed around damaged tissue limit the infiltration of infectious agents, inflammatory cells and act as a neuroprotective barrier (Bush et al., 1999; Faulkner et al., 2004; Herrmann et al., 2008). Also,

astrocytes communicate profoundly with microglia, and can exert both inflammatory and anti-inflammatory effects on them (Min et al., 2006; Ovanesov et al., 2008).

In this study, five days after EFSs, there was no difference in the morphology of GFAP positive cells if compared to untreated control littermates (Fig. 5.4A). Also, no difference was observed in the area occupied by GFAP-positive cells between EFS-induced mice and untreated control littermates (Fig. 5.4B). In a similar study performed in rats, acute astrogliosis 24 h after EFSs has been observed but it returned to normal state after 96 h (Patterson et al., 2015). Dube et al. (2010) have shown that reactive astrocytes are more abundant 6 h after EFSs and are the source of IL-1β, but the morphology of astrocytes 24 h after EFSs was typical for their resting state. As in mild reactive astrogliosis, there is little or no reorganization of tissue architecture (Sofroniew and Vinters, 2010), and if the cause of reactive astrogliosis is resolved, the astrocytes return to their healthy state (Sofroniew and Vinters, 2010). Therefore, it is very likely that reactive astrogliosis observed early after EFSs (Dube et al., 2010) is of the mild reactive astrogliosis type and it explains the absence of reactive astrogliosis five days after EFSs as observed in the present study.

6.1.5 EFSs induce a reduction in IGJC

In the hippocampus astrocytes are connected with each other via gap junctions formed by Cx43 and Cx30 (Giaume and McCarthy, 1996; Gosejacob et al., 2011). These gap junctions serve as intercellular conduits between cells and directly connect the cytoplasm of different cells. As through these gap junctions ions, metabolites, glucose, and small molecules can pass from one cell to another, the astrocytic network plays a vital role in homeostatic regulation of extracellular pH, K^+, and glutamate levels (Kielian, 2008). Reduction in IGJC has been suggested to be associated with epileptogenesis (Steinhäuser et al., 2012; Steinhäuser et al., 2016).

To investigate the effects of FSs on the astroglial network, IGJC was studied five days after EFSs generation. More than 50 % reduction in the IGJC has been observed 5 d after EFSs (see section 5.1.5; Table 5.2; Fig. 5.5) (see Khan et al.,

2016). Previously, loss of IGJC has been shown in human sclerotic hippocampi from mTLE patients and in a mouse model of mTLE (Bedner et al., 2015). In addition to IL-1β and TNF-α, LPS (which causes the release of these inflammatory cytokines) has been shown to reduce IGJC in acute brain slices as well as in cultured astrocytes (Bedner et al., 2015; Liao et al., 2013; Meme et al., 2006). Increased levels of these cytokines have been reported in the hippocampus of EFS animals (Dube et al., 2010) and in CSF, plasma and serum of children with FSs (Choi et al., 2011; Haspolat et al., 2002; Tutuncuoglu et al., 2001; Virta et al., 2002b). LPS-induced inflammation in mice reduced the IGJC by 50 % (Bedner et al., 2015). In toll like receptor 4 knockout animals, kainate-induced *status epilepticus* did not cause reduction in IGJC (Bedner et al., 2015). These inflammatory cytokines are released from activated microglia and astrocytes (Wang et al., 2015). Also, reduced IGJC has been reported in the presence of activated microglia (Faustmann et al., 2003). In the present study microglia activation was observed 5 d after EFSs (section 5.1.3), at the same time point when reduction in IGJC was detected (section 5.1.5). The findings reported in the previous studies and the observations made in the present study suggest that EFS-induced reduction in IGJC is caused by pro-inflammatory cytokines released from activated microglia.

During hyperactivity, the extracellular level of K^+ increases to 10-12 mM from the resting level of 3 mM (Heinemann and Lux, 1977; Steinhäuser et al., 2012). The level of K^+ is balanced in the extracellular space via two distinct mechanisms: K^+ uptake and spatial K^+ buffering (Kofuji and Newman, 2004). K^+ is taken up by the astrocytes at the site of higher extracellular K^+ level and transferred via the astroglial syncytium to sites of lower K^+ concentration (Kofuji and Newman, 2004). Impairment in the clearance of extracellular K^+ can lead to neuronal depolarization and consequently to neuronal hyperexcitability (Steinhäuser et al., 2012). In a mouse model of mTLE, reduction in IGJC and impaired K^+ buffering has been observed before the appearance of neuronal degeneration, suggesting that reduction in IGJC is rather a cause than the consequence of epileptic seizures (Bedner et al., 2015). In conclusion, it is reasonable to assume that EFS-caused reduction in IGJC can trigger neuronal hyperexcitability due to insufficient clearance of extracellular K^+.

This glial dysfunction might represent an important factor in the course of epileptogenesis.

6.1.6 Protein expression of Cx43 and Cx30

Five days after EFSs, reduction in IGJC was observed (section 5.1.5). Dermietzel and colleagues have reported that in the hippocampus two Cx proteins, i.e. Cx43 and Cx30, are responsible for IGJC between astrocytes (Dermietzel et al., 2000). There are only a few studies performed to understand the regulation of Cx30, however, Cx43 has been investigated in detail. There are at least four possible ways, through which Cx43-mediated functional coupling can be regulated: expression of the Cx43 protein (John et al., 1999), its phosphorylation (Pahujaa et al., 2007; Solan and Lampe, 2009), cellular localization and internalization, and / or degradation of the Cx43 protein (Liao et al., 2013). Studies on myocytes and cultured astrocytes have provided evidence to support the assumption that Cx43 channels of a cell can be replaced within 1 to 3 h (Beardslee et al., 1998; Hertzberg et al., 2000; Laird et al., 1991) and post-translational modifications are usually rapid (Li et al., 1998; Nagy and Li, 2000).

WB analysis was performed to study the expression of Cx proteins and their phosphorylation status after EFS generation in the context of uncoupling. Expression of total Cx43 protein was significantly reduced in the hippocampus of EFSs mice compared to untreated control littermates, 5 d after EFSs (Fig. 5.6). It has been revealed that expression of Cx43 was significantly reduced in astrocytes in cocultures containing activated microglia compared with cocultures containing quiescent microglia (Faustmann et al., 2003). IL-1β triggers loss of Cx43 protein (Haghikia et al., 2008a; John et al., 1999; Meme et al., 2006) via down-regulation of Cx43 mRNA in cultured human fetal astrocytes (John et al., 1999). Reduced expression of Cx43 can be caused by two mechanisms: reduction in transcription and / or translation (John et al., 1999) or by increased degradation (Liao et al., 2013). It has been reported that inflammation can cause degradation of Cx43 via ubiquitination (Liao et al., 2013). Altogether, it can be suggested that activated

microglia and inflammatory cytokines released from activated microglia might be the cause of reduced Cx43 expression after EFS generation in the present study.

In addition to the decreased total Cx43 protein, altered phosphorylation of Cx43 has been observed (Fig. 5.6D). The fractional contribution for P1 and P2 phosphorylation state of Cx43 protein to total Cx43 protein was significantly increased 5 d after EFSs generation in EFSs animals than untreated control littermates (Fig. 5.6D), while the expression for P0 phosphorylation state of Cx43 remained unchanged (Fig. 5.6C). There was no change in the expression of total Cx30 5 d after EFSs generation (Fig. 5.7). These data suggest that the reduction in IGJC 5 d after EFSs generation might be the result of reduction in Cx43 protein and / or alteration in its phosphorylation status.

It is generally unclear whether changes in coupling and in expression of Cx43 have protective or harmful effects. There is experimental evidence that gap junction-mediated coupling contributes to a greater distribution of stress molecules and therefore can cause higher neuronal damage (de Pina-Benabou et al., 2005; Frantseva et al., 2002; Kielian, 2008). In addition, high neuronal activity, such as epileptic seizures, require an increased supply of energetic metabolites such as glucose and lactate. However, this is possible only with an intact astrocytic network (Rouach et al., 2008). These findings point to a pro-epileptic function of the astrocytic network. On the other hand, there are also contradictory studies which tend to favor an anti-epileptic function of the astrocytic network, as mice with reduced Cx43 expression experience greater damage after ischemia (Nakase et al., 2003). In cultured astrocytes it has been observed that gap junctional communication mediated by Cx43 provides resistance against cellular death from oxidative stress (Le et al., 2014). In acute brain sections it has been shown that reduced IGJC can cause a reduced K^+ buffering which leads to hyperexcitability of neurons and may result in further damage (Wallraff et al., 2006). Although these inconsistencies might be due to differences in methods and models, we raised in our group strong evidence that uncoupling plays an essential role in the early phase of epileptogenesis. This assumption is based on the results from our epilepsy model

that uses intracortical kainate injections (Bedner et al., 2015). In this study we found that uncoupling of astrocytes is one of the first events that occur very early after kainate administration (Bedner et al., 2015) and actually results in decreased K^+ buffering which can lead to hyperexcitability of the neurons and can generate epileptiform activity (Steinhäuser et al., 2016).

6.1.7 Generation of recurrent spontaneous generalized seizures after EFSs

Both retrospective and prospective studies have suggested a link between FSs and epilepsy (Bender et al., 2004; French et al., 1993; Shinnar, 2003). Also in animal models EFSs have been shown to increase susceptibility for seizures (Dube et al., 2000) and in some studies it has been revealed that EFSs in rats resulted in generation of unprovoked spontaneous seizures (Dube et al., 2006; Dube et al., 2010). Therefore, to investigate the effects of FSs in mice, EFSs were generated under different conditions (section 5.1.1; Table 5.1; Fig. 5.8). Previously, a former PhD student of our lab induced HT in four hGFAP-eGFP mice, out of which one animal showed unprovoked spontaneous seizures (Dupper, 2014). In previous studies, it has been reported that postnatal LPS administration increases susceptibility, intensity and frequency of seizures as observed in rats and mice (Auvin et al., 2010; Eun et al., 2015; Galic et al., 2008). Also, in the present study, LPS pre-treatment resulted in an increased intensity and duration of EFSs generated via HT-induction (see section 5.1.1). But it did not increase the incidence of epileptic animals. Recurrent spontaneous generalized seizures were observed in one out of 19 hGFAP-eGFP and one out of 9 C57Bl6J mice. It has been shown that the incidence of epilepsy development was 35-45 % in rats after experiencing EFSs (Dube et al., 2006; Dube et al., 2010). In the present study approximately 7 % of the mice developed epilepsy. The lower incidence of seizures may be explained by the differences between species (mouse vs. rat) and differences in the experimental approach. In addition, EEG recordings were made for a relative short duration (10-14 days), raising the possibility that in some epileptic animals the seizures were simply missed. The probability of developing epilepsy increases with increasing age (Hesdorffer et al., 2011), but in the present study EEG recordings were made after 2

months and it is, therefore, also possible that some of the animals had not developed epilepsy at this time point even when they were susceptible to epilepsy development. In this study EFSs were generated with two different HT durations: 36 min and 60 min. Two animals that became epileptic had experienced EFSs for 36 min. Prospective studies in humans have revealed that the risk for developing epilepsy increases with duration of FSs (Annegers et al., 1987). Similarly, in animal studies it has been shown that with increasing duration of EFSs the probability for epilepsy development increases (Dube et al., 2006; Dube et al., 2010). However, we did not observe increase in the incidence of epilepsy development with increased duration of EFSs and the more plausible explanation for this would be interspecies differences, which indeed may be the case as we observed difference in epileptiform activity even in two different strains of the mice. It has been suggested that the genetic background can play a role in epileptogenesis (van Gassen et al., 2008). In the present study, it has been observed that EFSs in two strains of mice affect the incidence of epilepsy development and the number of seizures observed in epileptic mice. Epileptic C57Bl6J mice had 6 times more seizures per day than hGFAP-eGFP mice (Fig. 5.8). In a similar study it has been reported that C57Bl6J are more susceptible to seizure generation (van Gassen et al., 2008). Furthermore, in prospective studies, it has been revealed that 2-10% of children with FSs experience develop epilepsy in later life (Shinnar, 2003), which seems to be near to the present study in which 7 % of mice showed unprovoked spontaneous seizures after EFSs. Altogether, it can be suggested that EFSs under different conditions can lead to unprovoked spontaneous seizure generation in mice, and the incidence of epileptic animals is similar to the risk factor in children.

6.2 Role of TAK1 in epilepsy

6.2.1 In astrocytes TAK1 is not activated

In the CNS inflammatory responses are elicited by astrocytes and microglia. Under pathological conditions astrocytes undergo physiological, morphological and biochemical changes (Wilhelmsson et al., 2006) and release inflammatory cytokines like IL-1β and TNF-α (Dube et al., 2010; Lau and Yu, 2001). Astrocytes express

TLRs (Bsibsi et al., 2002), through which they recognize PAMPs and DAMPs (Miller et al., 2005). Through TLRs TAK1 is activated in response to PAMPs and DAMPs (Irie et al., 2000; Sato et al., 2005), which in turn triggers activation and translocation of NF-κB to the nucleus (Sato et al., 2005; Shim et al., 2005), leading to the transcription and release of inflammatory cytokines (Hayden et al., 2006). TAK1 is a member of the MAPK family (Yamaguchi et al., 1995) and in addition to NF-κB it is an upstream modulator of MAPKs (Sato et al., 2005).

To investigate the role of TAK1 in epileptogenesis, TAK1 activation in astrocytes was assessed at different time points (4 hpi, 1 dpi and 5 dpi) after kainate-induced *status epilepticus*. Immunofluorescence staining showed that TAK1 was not activated in astrocytes (Fig. 5.10). Previously it has been shown that as a consequence of *status epilepticus* molecules like DAMPs, reactive oxygen species, ATP and glutamate are released from hyperactive and dying neurons (Meurs et al., 2008) which trigger inflammatory response in astrocytes (Liu et al., 2000). Furthermore, IL-1β and TNF-α can be released from microglia and these inflammatory cytokines are known trigger of inflammatory response in astrocytes (Sofroniew and Vinters, 2010). It has been suggested that NF-κB activation is needed for the release of inflammatory cytokines like IL-1β (Hayden et al., 2006) and it has been shown that seizure generation in rats results in the release of these inflammatory cytokine from astrocytes (Dube et al., 2010; Lau and Yu, 2001). In various studies it has been reported that NF-κB activation and translocation to the nucleus can take place via alternative pathways independent of TAK1 activation (Sun, 2011).

Altogether, this data shows that TAK1 is not activated in astrocytes, indicating that TAK1 activation is not involved in NF-κB activation and its translocation to the nucleus in astrocytes.

6.2.2 TAK1 is activated in microglia

TAK1 activation in microglia was investigated at different time points (4 hpi, 1 dpi and 5 dpi) after *status epilepticus* induced by unilateral intracortical kainate injection. Immunofluorescence staining revealed that TAK1 is activated in microglia 5 d after

kainate (Fig. 5.11). Furthermore, quantitative analysis showed that TAK1 activation in microglia and the number of microglia expressing phosphorylated TAK1 significantly increased 5 d after *status epilepticus* (Fig. 5.12A & 5.12B). It has been suggested that the release of ATP from hyperactive neurons can attract and activate microglia via purinergic signaling (Eyo et al., 2014; Haynes et al., 2006; Dissing-Olesen et al., 2014). As a result of *status epilepticus* hyperactive neurons release excessive glutamate. Microglia have been suggested to express receptors for neurotransmitters like glutamate which upon activation can trigger inflammatory responses in microglia (Domercq et al., 2013; Pocock and Kettenmann, 2007). Activated microglia release inflammatory cytokines (Smith et al., 2012) most of which are regulated by NF-κB activation (Hayden et al., 2006) and TAK1 is an upstream modulator of NF-κB (Sato et al., 2005; Shim et al., 2005). Furthermore, it has been revealed that *status epilepticus* results in oxidative stress (Folbergrova et al., 2016) and oxidative stress has been shown to activate TAK1 (Onodera et al., 2015). In addition it has been suggested that hippocampal depolarized neurons can release TNF-α (Renauld and Spengler, 2002) which again activates TAK1 (Takaesu et al., 2003). Previous studies confirm the findings of the present study and it can be concluded that TAK1 is activated in microglia after *status epilepticus*.

6.2.3 Microglia-specific TAK1KO mice

To further explore the role of TAK1 in epileptogenesis, microglia-specific TAK1KO mice were used. In these mice TAK1 is conditionally knocked out by Cre-recombinase fused to a mutant estrogen ligand-binding domain ($Cx3cr1^{CreER}$) (Yona et al., 2013) expressed under the promoter of CX3CR1. For Cre-recombinase activation, the presence of the estrogen antagonist TAM is required. PCR analysis was performed to confirm and differentiate $Cx3cr1^{CreER}$:$Tak1^{fl/fl}$ (TAK1KO) and $Tak1^{fl/fl}$ (Fig. 5.14). In $Cx3cr1^{CreER}$:$Tak1^{fl/fl}$ and $Tak1^{fl/fl}$ mice, TAM (1 mg / mouse) was injected two times a day for 5 consecutive days. As microglia are phagocytic descendants of the mesoderm, which migrate into the brain during embryonic development (Vilhardt, 2005), and because of their longevity and self-renewal, these cells persist throughout life of the organism without any input from peripheral immune cells. Therefore, three weeks after TAM administration TAK1 remained

knocked out only in CNS microglia (Goldmann et al., 2013), as peripheral immune cells in which TAK1 was knocked out due to TAM presence could be replaced by new cells after short time. After three weeks these mice were used for the experiment.

6.2.4 Inflammatory response is reduced in TAK1KO animals

It has already been revealed that in experimental autoimmune encephalomyelitis (EAE) microglia-specific TAK1KO mice showed strongly diminished CNS inflammatory responses including abolished activation of NF-κB, reduced expression and / or release of inflammatory cytokines like IL-1β, TNF-α and chemokines like CCL2 (Goldmann et al., 2013). Therefore, to investigate CNS inflammatory responses in microglia-specific TAK1KO mice in a mouse model of epilepsy, immunofluorescence staining for Iba1 was performed. The sections used for staining were obtained from animals perfused 5 d after *status epilepticus* induced by unilateral intracortical kainate injection. Immunofluorescence staining revealed reduced alteration in microglia morphology (hypertrophic cell bodies and processes) in microglia-specific TAK1KO mice as compared with their control littermates (Fig. 5.14A). Furthermore, the transgenic animals showed significantly reduced Iba1 immunoreactivity when compared to the Cre-negative controls (Fig. 5.14B). Moreover, the number of microglia was significantly lower in the hippocampi of microglia-specific TAK1KO mice compared to their controls (Fig. 5.14C). Microglia rapidly respond to noxious stimuli and are activated at a very early stage after an injury or infection (Cherry et al., 2014; Rock et al., 2004). In previous studies, activated microglia have been observed in animal models of epilepsy (Avignone et al., 2008; Eyo et al., 2014) as well as in brain tissue obtained from TLE patients (Beach et al., 1995; Najjar et al., 2011). Microglia activation is characterized by increased proliferation, morphological transformation and migration to the site of injury (Domercq et al., 2013). The significantly lower number of microglia in the conditional TAK1KO was presumably due to reduced proliferation and / or migration of the cells (Fig. 5.14C). In an EAE study, strongly diminished CNS inflammation and reduced tissue damage was found in microglia-specific TAK1KO mice (Goldmann et

al., 2013). Additionally, in the same study a significant reduction in NF-κB activation and inflammatory cytokines were observed in the transgenic animals (Goldmann et al., 2013). In an Experimental Subarachnoid Hemorrhage (SAH) study, TAK1 inhibition via its specific inhibitor 5Z-7-oxozeaenol (Ninomiya-Tsuji et al., 2003) resulted in diminished SAH-induced apoptosis, reduced NF-κB activation and translocation to the nucleus, and decreased phosphorylation of p38 and JNK (Zhang et al., 2015).

Altogether, it can be concluded that TAK1 deletion in microglia resulted in a reduced CNS inflammatory response.

6.2.5 TAK1 deletion in microglia can reduce chronic seizures

It has been suggested that inflammation promotes seizure generation based on the observations made in experimental animal models of epilepsy (Auvin et al., 2010; Balosso et al., 2008; Dube et al., 2010; Patterson et al., 2015) and outcomes of clinical studies (Choi et al., 2011; Haspolat et al., 2002; Tutuncuoglu et al., 2001; Virta et al., 2002b). In the present study, a reduced inflammatory response has been observed in microglia-specific TAK1KO mice 5 d after *status epilepticus* (section 5.2.4).

To investigate if the observed reduced inflammatory response in microglia-specific TAK1KO mice influences the seizure frequency in a mouse model of epilepsy, EEG recordings with video monitoring were made for one month after kainate-induced *status epilepticus* in TAK1KO and control mice. EEG recordings revealed that the average number of seizures / day was significantly lower in microglia-specific TAK1KO mice than in Cre-negative littermates (section 5.2.5; Fig. 5.15A). Furthermore, the average seizure frequency decreased in microglia-specific TAK1KO mice and increased in control littermates throughout the observed course of epileptogenesis (section 5.2.5; Fig. 5.15B). Inflammation and inflammatory cytokines have been suggested to promote epileptogenesis (Vezzani, 2014; Vezzani and Viviani, 2015). IL-1Ra, a member of the interleukin 1 cytokine family and a

natural inhibitor of the pro-inflammatory cytokine IL-1β, has been shown to exert potent anticonvulsant effects in various models of epilepsy (Auvin et al., 2010; Vezzani et al., 2002), and transgenic mice overexpressing IL-1Ra have been shown to be less sensitive to bicuculline-induced seizures (Vezzani et al., 2002). Moreover, VX-765, an inhibitor of IL-1β biosynthesis, was demonstrated to reduce chronic epileptic activity in a dose dependent manner after intrahipocampal injection of kainate (Maroso et al., 2011). Increased levels of IL-1β were observed in rats that developed epilepsy after EFSs (Dube et al., 2010). Furthermore, IL-1β administration has been shown to increase seizure susceptibility and seizure generation in animal models of epilepsy (Balosso et al., 2008; Dube et al., 2005). Moreover, polymorphism in the gene for IL-1β in humans has been linked to increased risk for FSs (Virta et al., 2002a). The bacterial endotoxin LPS was shown to cause CNS inflammation, microglia activation and release of inflammatory cytokines (Bossu et al., 2012; Qin et al., 2007). Administration of LPS has been shown to increase seizure susceptibility and proconvulsant activity (Auvin et al., 2010; Galic et al., 2008; Sayyah et al., 2003).

It has been revealed that IL-1β and TNF-α inhibit glutamate reuptake (Hu et al., 2000; Zou and Crews, 2005) and increase glial glutamate release (Bezzi et al., 2001), which can subsequently increase neuronal excitability (Vezzani and Granata, 2005). Moreover, glutamate release from glial cells activates slow inward currents, which might generate epileptiform activity through synchronization of pyramidal neurons of the hippocampus (Carmignoto and Fellin, 2006). Inflammatory cytokines also have been suggested to increase hyperexcitability and promote seizure generation by directly regulating neuronal activity (Vezzani and Viviani, 2015). IL1-β increases neuronal hyperexcitability (Zhang et al., 2008; Zhang et al., 2010) via mediating NMDA receptor activity (Viviani et al., 2003; Yang et al., 2005) through phosphorylation of the NMDA receptor subunit 2b (NR2B), which increases Ca^{2+} influx (Viviani et al., 2003). TNF-α promotes hyperexcitability by increasing trafficking of GluR2-lacking AMPA receptors, which enhances Ca^{2+} influx (Beattie et al., 2002; Stellwagen et al., 2005) and reduces inhibitory transmission through endocytosis of GABA-A receptors (Stellwagen et al., 2005). Furthermore, in response to IL-1β

astrocytes generate and release vasoactive substances like VEGF, which increase BBB permeability and promote leukocyte infiltration (Argaw et al., 2009; Argaw et al., 2012). As a result of inflammation, the BBB is disrupted resulting in hyperexcitability via reduction in glutamate uptake and K^+ buffering by astrocytes (Vezzani, 2014). In addition, a positive correlation between BBB leakage and frequency of spontaneous seizures has been reported (van Vliet et al., 2007).

Together, it can be concluded that TAK1 deletion in microglia can lead to reduced inflammatory responses, which might result in reduced chronic seizure generation.

7 Summary

Previous studies provided evidence that FSs in children increase the risk of epilepsy development. EFSs in animals confirmed this assumption. EFS generated with only hyperthermia induction caused astrocyte uncoupling, which was mediated by both reduced protein expression and alteration in the phosphorylation state of Cx43. These findings provide a mechanistic link between FSs and the development of epilepsy. EFS-induced inhibition of interastrocytic communication might be the consequence of inflammation via microglial activation. Astrocyte uncoupling occurs in the absence of neuronal death and astrogliosis, which suggests that these different aspects of astrocyte pathology are not mechanistically linked. EFSs generated with hyperthermia preceded by inflammation (DH experiments) did not increase the astrocyte uncoupling and did not influence the incidence of epilepsy.

There is increasing evidence suggesting that inflammation promotes epileptogenesis. TAK1 deletion and inhibition have been shown to reduce inflammation. TAK1 activation was investigated in astrocytes and microglia at different time points after *status epilepticus*. TAK1 was found to be activated in microglia, but not in astrocytes, in a time-dependent manner after *status epilepticus*. Therefore, in the second part of the study the role of inflammation in epileptogenesis was investigated via TAK1 deletion in microglia. TAK1 deletion in microglia resulted in reduced CNS inflammation. In microglia-specific TAK1KO animals the frequency of chronic seizures was significantly reduced. TAK1-dependent cytokine release from microglia, but not from astrocytes, might be involved in epileptogenesis.

8 Perspective

Epilepsy is a chronic brain disease and it affects two percent of the population. In the present study EFSs were investigated as a consequence of glial dysfunction which showed astrocytes and microglia respond to HT-treatment in different ways. To better understand FSs, it is needed to investigate the glial cell responses in the chronic phase. Moreover, to explore the activation of the NF-κB pathway followed by the production and release of inflammatory cytokines like IL-1β and TNF-α from specific glial cell types after EFSs, immunofluorescence staining should be made with cell specific markers. In addition to connexins, the activity of AQP4 and Kir1.4 channel should also be investigated after EFSs. As glutamine synthetase along with the glutamate transporters EAAT1 and EAAT2 have been implicated in epileptogenesis, the function of these molecules should be studied after EFSs. Furthermore, EEG recordings should be made for small durations at different time points after EFSs throughout the life time of animals to predict more accurate the incidence of epilepsy development.

Inflammation has been suggested to be involved in epileptogenesis. In the present study it has been shown that reducing inflammation via TAK1 deletion resulted in less chronic seizure generation. This finding should be confirmed by using TAK1 inhibition via its specific inhibitor 5Z-7-oxozeaenol. Moreover, it should be investigated which of the downstream targets of TAK1 are involved in epileptogenesis. NF-κB activation and release of inflammatory cytokines should be quantified after TAK1 deletion and inhibition. Also the number of animals should be increased to study chronic seizure generation via EEG recordings. In addition, neuronal degeneration and regeneration should be investigated in acute as well as chronic phases.

References

Agulhon C, Petravicz J, McMullen AB, Sweger EJ, Minton SK, Taves SR, Casper KB, Fiacco TA, McCarthy KD. 2008. What is the role of astrocyte calcium in neurophysiology? Neuron 59:932-946.

Ahlers KE, Karacay B, Fuller L, Bonthius DJ, Dailey ME. 2015. Transient activation of microglia following acute alcohol exposure in developing mouse neocortex is primarily driven by BAX-dependent neurodegeneration. Glia 63:1694-1713.

Allaman I, Belanger M, Magistretti PJ. 2011. Astrocyte-neuron metabolic relationships: for better and for worse. Trends Neurosci. 34:76-87.

Allen NJ, Barres BA. 2009. Neuroscience: Glia - more than just brain glue. Nature 457:675-677.

Amaral DG, Witter MP. 1989. The three-dimensional organization of the hippocampal formation: a review of anatomical data. Neuroscience 31:571-591.

Anderson M. 1993. Management of cerebral infection. J. Neurol. Neurosurg. Psychiatry 56:1243-1258.

Annegers JF, Hauser WA, Shirts SB, Kurland LT. 1987. Factors Prognostic of Unprovoked Seizures After Febrile Convulsions. New England Journal of Medicine 316:493-498.

Araque A. 2008. Astrocytes process synaptic information. Neuron Glia Biol. 4:3-10.

Araque A, Navarrete M. 2010. Glial cells in neuronal network function. Philos. Trans. R. Soc. Lond B Biol. Sci. 365:2375-2381.

Argaw AT, Asp L, Zhang J, Navrazhina K, Pham T, Mariani JN, Mahase S, Dutta DJ, Seto J, Kramer EG, Ferrara N, Sofroniew MV, John GR. 2012. Astrocyte-derived VEGF-A drives blood-brain barrier disruption in CNS inflammatory disease. J. Clin. Invest 122:2454-2468.

Argaw AT, Gurfein BT, Zhang Y, Zameer A, John GR. 2009. VEGF-mediated disruption of endothelial CLN-5 promotes blood-brain barrier breakdown. Proc. Natl. Acad. Sci. U. S. A 106:1977-1982.

Attwell D, Buchan AM, Charpak S, Lauritzen M, MacVicar BA, Newman EA. 2010. Glial and neuronal control of brain blood flow. Nature 468:232-243.

Auvin S, Shin D, Mazarati A, Sankar R. 2010. Inflammation induced by LPS enhances epileptogenesis in immature rat and may be partially reversed by IL1RA. Epilepsia 51 Suppl 3:34-38.

Avignone E, Ulmann L, Levavasseur F, Rassendren F, Audinat E. 2008. Status epilepticus induces a particular microglial activation state characterized by enhanced purinergic signaling. Journal of Neuroscience 28:9133-9144.

Balosso S, Maroso M, Sanchez-Alavez M, Ravizza T, Frasca A, Bartfai T, Vezzani A. 2008. A novel non-transcriptional pathway mediates the proconvulsive effects of interleukin-1 beta. Brain 131:3256-3265.

Banati RB, Gehrmann J, Schubert P, Kreutzberg GW. 1993. Cytotoxicity of microglia. Glia 7:111-118.

Bazargani N, Attwell D. 2016. Astrocyte calcium signaling: the third wave. Nat. Neurosci. 19:182-189.

Beach TG, Woodhurst WB, Macdonald DB, Jones MW. 1995. Reactive Microglia in Hippocampal Sclerosis Associated with Human Temporal-Lobe Epilepsy. Neuroscience Letters 191:27-30.

Beardslee MA, Laing JG, Beyer EC, Saffitz JE. 1998. Rapid turnover of connexin43 in the adult rat heart. Circ. Res. 83:629-635.

Beattie EC, Stellwagen D, Morishita W, Bresnahan JC, Ha BK, Von Zastrow M, Beattie MS, Malenka RC. 2002. Control of synaptic strength by glial TNF alpha. Science 295:2282-2285.

Bechade C, Cantaut-Belarif Y, Bessis A. 2013. Microglial control of neuronal activity. Front Cell Neurosci. 7:32.

Bedner P, Dupper A, Huttmann K, Muller J, Herde MK, Dublin P, Deshpande T, Schramm J, Haussler U, Haas CA, Henneberger C, Theis M, Steinhäuser C. 2015. Astrocyte uncoupling as a cause of human temporal lobe epilepsy. Brain 138:1208-1222.

Bender RA, Dube C, Baram TZ. 2004. Febrile seizures and mechanisms of epileptogenesis: Insights from an animal model. Recent Advances in Epilepsy Research 548:213-225.

Bender RA, Dube C, Gonzalez-Vega R, Mina EW, Baram TZ. 2003. Mossy fiber plasticity and enhanced hippocampal excitability, without hippocampal cell loss or altered neurogenesis, in an animal model of prolonged febrile seizures. Hippocampus 13:399-412.

Berg AT, Shinnar S. 1996. Unprovoked seizures in children with febrile seizures: short-term outcome. Neurology 47:562-568.

Berg AT, Shinnar S, Levy SR, Testa FM. 1999. Childhood-onset epilepsy with and without preceding febrile seizures. Neurology 53:1742-1748.

Bergles DE, Jabs R, Steinhäuser C. 2010. Neuron-glia synapses in the brain. Brain Res. Rev. 63:130-137.

Bergles DE, Roberts JD, Somogyi P, Jahr CE. 2000. Glutamatergic synapses on oligodendrocyte precursor cells in the hippocampus. Nature 405:187-191.

Berridge MJ, Bootman MD, Lipp P. 1998. Calcium--a life and death signal. Nature 395:645-648.

Bezzi P, Domercq M, Brambilla L, Galli R, Schols D, De Clercq E, Vescovi A, Bagetta G, Kollias G, Meldolesi J, Volterra A. 2001. CXCR4-activated astrocyte glutamate release via TNFa: amplification by microglia triggers neurotoxicity. Nature Neuroscience 4:702-710.

Blair RD. 2012. Temporal lobe epilepsy semiology. Epilepsy Res. Treat. 2012:751510.

Blomstrand F, Venance L, Siren AL, Ezan P, Hanse E, Glowinski J, Ehrenreich H, Giaume C. 2004. Endothelins regulate astrocyte gap junctions in rat hippocampal slices. Eur. J. Neurosci. 19:1005-1015.

Blumcke I. 2009. Neuropathology of focal epilepsies: a critical review. Epilepsy Behav. 15:34-39.

Boggs JG, Waterhouse EJ. 2001. Childhood Status Epilepticus. Epilepsy Curr. 1:25.

Bossu P, Cutuli D, Palladino I, Caporali P, Angelucci F, Laricchiuta D, Gelfo F, De BP, Caltagirone C, Petrosini L. 2012. A single intraperitoneal injection of endotoxin in rats induces long-lasting modifications in behavior and brain protein levels of TNF-alpha and IL-18. J. Neuroinflammation. 9:101.

Bourdiol F, Toulmond S, Serrano A, Benavides J, Scatton B. 1991. Increase in omega 3 (peripheral type benzodiazepine) binding sites in the rat cortex and striatum after local injection of interleukin-1, tumour necrosis factor-alpha and lipopolysaccharide. Brain Res. 543:194-200.

Bradl M, Lassmann H. 2010. Oligodendrocytes: biology and pathology. Acta Neuropathol. 119:37-53.

Brenner M, Kisseberth WC, Su Y, Besnard F, Messing A. 1994. GFAP promoter directs astrocyte-specific expression in transgenic mice. J. Neurosci. 14:1030-1037.

Bsibsi M, Ravid R, Gveric D, Van Noort JM. 2002. Broad expression of Toll-like receptors in the human central nervous system. J. Neuropathol. Exp. Neurol. 61:1013-1021.

Bush TG, Puvanachandra N, Horner CH, Polito A, Ostenfeld T, Svendsen CN, Mucke L, Johnson MH, Sofroniew MV. 1999. Leukocyte infiltration, neuronal degeneration, and neurite outgrowth after ablation of scar-forming, reactive astrocytes in adult transgenic mice. Neuron 23:297-308.

Bushong EA, Martone ME, Jones YZ, Ellisman MH. 2002. Protoplasmic astrocytes in CA1 stratum radiatum occupy separate anatomical domains. J. Neurosci. 22:183-192.

Carmignoto G, Fellin T. 2006. Glutamate release from astrocytes as a non-synaptic mechanism for neuronal synchronization in the hippocampus. Journal of Physiology-Paris 99:98-102.

Cendes F, Andermann F, Dubeau F, Gloor P, Evans A, Jonesgotman M, Olivier A, Andermann E, Robitaille Y, Lopescendes I, Peters T, Melanson D. 1993. Early-Childhood Prolonged Febrile Convulsions, Atrophy and Sclerosis of Mesial Structures, and Temporal-Lobe Epilepsy - An Mri Volumetric Study. Neurology 43:1083-1087.

Cherry JD, Olschowka JA, O'Banion MK. 2014. Neuroinflammation and M2 microglia: the good, the bad, and the inflamed. Journal of Neuroinflammation 11.

Chiu SS, Tse CYC, Lau YL, Peiris M. 2001. Influenza A infection is an important cause of febrile seizures. Pediatrics 108.

Choi J, Min HJ, Shin JS. 2011. Increased levels of HMGB1 and pro-inflammatory cytokines in children with febrile seizures. Journal of Neuroinflammation 8.

Chung IY, Benveniste EN. 1990. Tumor necrosis factor-alpha production by astrocytes. Induction by lipopolysaccharide, IFN-gamma, and IL-1 beta. J. Immunol. 144:2999-3007.

Chung WS, Allen NJ, Eroglu C. 2015. Astrocytes Control Synapse Formation, Function, and Elimination. Cold Spring Harbor Perspectives in Biology 7.

Clarke LE, Barres BA. 2013. Emerging roles of astrocytes in neural circuit development. Nat. Rev. Neurosci. 14:311-321.

Colangelo AM, Alberghina L, Papa M. 2014. Astrogliosis as a therapeutic target for neurodegenerative diseases. Neuroscience Letters 565:59-64.

Coulter DA, Eid T. 2012. Astrocytic regulation of glutamate homeostasis in epilepsy. Glia 60:1215-1226.

Crunelli V, Carmignoto G, Steinhäuser C. 2015. Novel astrocyte targets: new avenues for the therapeutic treatment of epilepsy. Neuroscientist. 21:62-83.

Danbolt NC. 2001. Glutamate uptake. Prog. Neurobiol. 65:1-105.

Dani JW, Chernjavsky A, Smith SJ. 1992. Neuronal activity triggers calcium waves in hippocampal astrocyte networks. Neuron 8:429-440.

Dani JW, Smith SJ. 1995. The triggering of astrocytic calcium waves by NMDA-induced neuronal activation. Ciba Found. Symp. 188:195-205.

Davalos D, Grutzendler J, Yang G, Kim JV, Zuo Y, Jung S, Littman DR, Dustin ML, Gan WB. 2005. ATP mediates rapid microglial response to local brain injury in vivo. Nat. Neurosci. 8:752-758.

de Pina-Benabou MH, Szostak V, Kyrozis A, Rempe D, Uziel D, Urban-Maldonado M, Benabou S, Spray DC, Federoff HJ, Stanton PK, Rozental R. 2005. Blockade of gap junctions in vivo provides neuroprotection after perinatal global ischemia. Stroke 36:2232-2237.

Dedek K, Schultz K, Pieper M, Dirks P, Maxeiner S, Willecke K, Weiler R, Janssen-Bienhold U. 2006. Localization of heterotypic gap junctions composed of connexin45 and connexin36 in the rod pathway of the mouse retina. Eur. J. Neurosci. 24:1675-1686.

Deng W, Aimone JB, Gage FH. 2010. New neurons and new memories: how does adult hippocampal neurogenesis affect learning and memory? Nat. Rev. Neurosci. 11:339-350.

Dermietzel R, Gao Y, Scemes E, Vieria D, Urban M, Kremer M, Bennett MVL, Spray DC. 2000. Connexin43 null mice reveal that astrocytes express multiple connexins. Brain Research Reviews 32:45-56.

Dibaj P, Nadrigny F, Steffens H, Scheller A, Hirrlinger J, Schomburg ED, Neusch C, Kirchhoff F. 2010. NO mediates microglial response to acute spinal cord injury under ATP control in vivo. Glia 58:1133-1144.

Domercq M, Vazquez-Villoldo N, Matute C. 2013. Neurotransmitter signaling in the pathophysiology of microglia. Front Cell Neurosci. 7:49.

Dube C, Chen K, Eghbal-Ahmadi M, Brunson K, Soltesz I, Baram TZ. 2000. Prolonged febrile seizures in the immature rat model enhance hippocampal excitability long term. Annals of Neurology 47:336-344.

Dube C, Richichi C, Bender RA, Chung G, Litt B, Baram TZ. 2006. Temporal lobe epilepsy after experimental prolonged febrile seizures: prospective analysis. Brain 129:911-922.

Dube C, Vezzani A, Behrens M, Bartfai T, Baram TZ. 2005. Interleukin-1 beta contributes to the generation of experimental febrile seizures. Annals of Neurology 57:152-155.

Dube CM, Brewster AL, Baram TZ. 2009. Febrile seizures: mechanisms and relationship to epilepsy. Brain Dev. 31:366-371.

Dube CM, Ravizza T, Hamamura M, Zha QQ, Keebaugh A, Fok K, Andres AL, Nalcioglu O, Obenaus A, Vezzani A, Baram TZ. 2010. Epileptogenesis Provoked by Prolonged Experimental Febrile Seizures: Mechanisms and Biomarkers. Journal of Neuroscience 30:7484-7494.

Duffy HS, John GR, Lee SC, Brosnan CF, Spray DC. 2000. Reciprocal regulation of the junctional proteins claudin-1 and connexin43 by interleukin-1beta in primary human fetal astrocytes. J. Neurosci. 20:RC114.

Dupper A. 2014. Entkopplung von Astrozyten als Ursache von Temporallappenepilepsie: Funktionelle Analysen im Tiermodell. PhD thesis. Bonn University.

Edwards FA, Konnerth A, Sakmann B, Takahashi T. 1989. A Thin Slice Preparation for Patch Clamp Recordings from Neurons of the Mammalian Central Nervous-System. Pflugers Archiv-European Journal of Physiology 414:600-612.

Eid T, Williamson A, Lee TS, Petroff OA, de Lanerolle NC. 2008. Glutamate and astrocytes--key players in human mesial temporal lobe epilepsy? Epilepsia 49 Suppl 2:42-52.

Elias LA, Wang DD, Kriegstein AR. 2007. Gap junction adhesion is necessary for radial migration in the neocortex. Nature 448:901-907.

Escartin C, Rouach N. 2013. Astroglial networking contributes to neurometabolic coupling. Front Neuroenergetics. 5:4.

Escayg A, MacDonald BT, Meisler MH, Baulac S, Huberfeld G, An-Gourfinkel I, Brice A, LeGuern E, Moulard B, Chaigne D, Buresi C, Malafosse A. 2000. Mutations of SCN1A, encoding a neuronal sodium channel, in two families with GEFS+2. Nat. Genet. 24:343-345.

Eun BL, Abraham J, Mlsna L, Kim MJ, Koh S. 2015. Lipopolysaccharide potentiates hyperthermia-induced seizures. Brain and Behavior 5.

Evans WH, De VE, Leybaert L. 2006. The gap junction cellular internet: connexin hemichannels enter the signalling limelight. Biochem. J. 397:1-14.

Eyo UB, Murugan M, Wu LJ. 2016. Microglia-Neuron Communication in Epilepsy. Glia.

Eyo UB, Peng JY, Swiatkowski P, Mukherjee A, Bispo A, Wu LJ. 2014. Neuronal Hyperactivity Recruits Microglial Processes via Neuronal NMDA Receptors and Microglial P2Y12 Receptors after Status Epilepticus. Journal of Neuroscience 34:10528-10540.

Eyo UB, Wu LJ. 2013. Bidirectional microglia-neuron communication in the healthy brain. Neural Plast. 2013:456857.

Falk MM, Kells RM, Berthoud VM. 2014. Degradation of connexins and gap junctions. FEBS Lett. 588:1221-1229.

Faulkner JR, Herrmann JE, Woo MJ, Tansey KE, Doan NB, Sofroniew MV. 2004. Reactive astrocytes protect tissue and preserve function after spinal cord injury. Journal of Neuroscience 24:2143-2155.

Faustmann PM, Haase CG, Romberg S, Hinkerohe D, Szlachta D, Smikalla D, Krause D, Dermietzel R. 2003. Microglia activation influences dye coupling and Cx43 expression of the astrocytic network. Glia 42:101-108.

Fernandez-Cobo M, Gingalewski C, Drujan D, De MA. 1999. Downregulation of connexin 43 gene expression in rat heart during inflammation. The role of tumour necrosis factor. Cytokine 11:216-224.

Fisher RS, Acevedo C, Arzimanoglou A, Bogacz A, Cross JH, Elger CE, Engel J, Jr., Forsgren L, French JA, Glynn M, Hesdorffer DC, Lee BI, Mathern GW, Moshe SL, Perucca E, Scheffer IE, Tomson T, Watanabe M, Wiebe S. 2014. ILAE official report: a practical clinical definition of epilepsy. Epilepsia 55:475-482.

Folbergrova J, Jesina P, Kubova H, Druga R, Otahal J. 2016. Status Epilepticus in Immature Rats Is Associated with Oxidative Stress and Mitochondrial Dysfunction. Front Cell Neurosci. 10:136.

Frantseva MV, Kokarovtseva L, Naus CG, Carlen PL, MacFabe D, Perez Velazquez JL. 2002. Specific gap junctions enhance the neuronal vulnerability to brain traumatic injury. J. Neurosci. 22:644-653.

French JA, Williamson PD, Thadani VM, Darcey TM, Mattson RH, Spencer SS, Spencer DD. 1993. Characteristics of Medial Temporal-Lobe Epilepsy - .1. Results of History and Physical-Examination. Annals of Neurology 34:774-780.

Freund TF, Ylinen A, Miettinen R, Pitkanen A, Lahtinen H, Baimbridge KG, Riekkinen PJ. 1992. Pattern of Neuronal Death in the Rat Hippocampus After Status Epilepticus - Relationship to Calcium-Binding Protein-Content and Ischemic Vulnerability. Brain Research Bulletin 28:27-38.

Gaietta G, Deerinck TJ, Adams SR, Bouwer J, Tour O, Laird DW, Sosinsky GE, Tsien RY, Ellisman MH. 2002. Multicolor and electron microscopic imaging of connexin trafficking. Science 296:503-507.

Galic MA, Riazi K, Heida JG, Mouihate A, Fournier NM, Spencer SJ, Kalynchuk LE, Teskey GC, Pittman QJ. 2008. Postnatal inflammation increases seizure susceptibility in adult rats. Journal of Neuroscience 28:6904-6913.

Giaume C, McCarthy KD. 1996. Control of gap-junctional communication in astrocytic networks. Trends Neurosci. 19:319-325.

Giepmans BN. 2004. Gap junctions and connexin-interacting proteins. Cardiovasc. Res. 62:233-245.

Goldmann T, Wieghofer P, Muller PF, Wolf Y, Varol D, Yona S, Brendecke SM, Kierdorf K, Staszewski O, Datta M, Luedde T, Heikenwalder M, Jung S, Prinz M. 2013. A new type of microglia gene targeting shows TAK1 to be pivotal in CNS autoimmune inflammation. Nat. Neurosci. 16:1618-1626.

Goodenough DA, Paul DL. 2009. Gap junctions. Cold Spring Harb. Perspect. Biol. 1:a002576.

Gosejacob D, Dublin P, Bedner P, Huttmann K, Zhang J, Tress O, Willecke K, Pfrieger F, Steinhäuser C, Theis M. 2011. Role of astroglial connexin30 in hippocampal gap junction coupling. Glia 59:511-519.

Griemsmann S, Höft SP, Bedner P, Zhang J, von Staden E, Beinhauer A, Degen J, Dublin P, Cope DW, Richter N, Crunelli V, Jabs R, Willecke K, Theis M, Seifert G, Kettenmann H, Steinhäuser C. 2015. Characterization of Panglial Gap Junction Networks in the Thalamus, Neocortex, and Hippocampus Reveals a Unique Population of Glial Cells. Cereb Cortex 25: 3420-3433.

Grosche A, Grosche J, Tackenberg M, Scheller D, Gerstner G, Gumprecht A, Pannicke T, Hirrlinger PG, Wilhelmsson U, Huttmann K, Hartig W, Steinhäuser C, Pekny M, Reichenbach A. 2013. Versatile and simple approach to determine astrocyte territories in mouse neocortex and hippocampus. PLoS. One. 8:e69143.

Haas KZ, Sperber EF, Opanashuk LA, Stanton PK, Moshe SL. 2001. Resistance of immature hippocampus to morphologic and physiologic alterations following status epilepticus or kindling. Hippocampus 11:615-625.

Haghikia A, Ladage K, Hinkerohe D, Vollmar P, Heupel K, Dermietzel R, Faustmann PM. 2008a. Implications of antiinflammatory properties of the anticonvulsant drug levetiracetam in astrocytes. J. Neurosci. Res. 86:1781-1788.

Haghikia A, Ladage K, Lafenetre P, Haghikia A, Hinkerohe D, Smikalla D, Haase CG, Dermietzel R, Faustmann PM. 2008b. Intracellular application of TNF-alpha impairs cell to cell communication via gap junctions in glioma cells. J. Neurooncol. 86:143-152.

Halassa MM, Fellin T, Takano H, Dong JH, Haydon PG. 2007. Synaptic islands defined by the territory of a single astrocyte. J. Neurosci. 27:6473-6477.

Hamati-Haddad A, bou-Khalil B. 1998. Epilepsy diagnosis and localization in patients with antecedent childhood febrile convulsions. Neurology 50:917-922.

Harada K, Kamiya T, Tsuboi T. 2015. Gliotransmitter Release from Astrocytes: Functional, Developmental, and Pathological Implications in the Brain. Front Neurosci. 9:499.

Harkin LA, Bowser DN, Dibbens LM, Singh R, Phillips F, Wallace RH, Richards MC, Williams DA, Mulley JC, Berkovic SF, Scheffer IE, Petrou S. 2002. Truncation

of the GABA(A)-receptor gamma2 subunit in a family with generalized epilepsy with febrile seizures plus. Am. J. Hum. Genet. 70:530-536.

Harris AL. 2007. Connexin channel permeability to cytoplasmic molecules. Prog. Biophys. Mol. Biol. 94:120-143.

Haspolat S, Mihci E, Coskun M, Gumuslu S, Ozben T, Yegin O. 2002. Interleukin-1beta, tumor necrosis factor-alpha, and nitrite levels in febrile seizures. J. Child Neurol. 17:749-751.

Hauser WA. 1994. The Prevalence and Incidence of Convulsive Disorders in Children. Epilepsia 35:S1-S6.

Hayden MS, West AP, Ghosh S. 2006. NF-kappaB and the immune response. Oncogene 25:6758-6780.

Haydon PG. 2001. GLIA: listening and talking to the synapse. Nat. Rev. Neurosci. 2:185-193.

Haydon PG, Carmignoto G. 2006. Astrocyte control of synaptic transmission and neurovascular coupling. Physiol Rev. 86:1009-1031.

Haynes SE, Hollopeter G, Yang G, Kurpius D, Dailey ME, Gan WB, Julius D. 2006. The P2Y(12) receptor regulates microglial activation by extracellular nucleotides. Nature Neuroscience 9:1512-1519.

He DS, Jiang JX, Taffet SM, Burt JM. 1999. Formation of heteromeric gap junction channels by connexins 40 and 43 in vascular smooth muscle cells. Proc. Natl. Acad. Sci. U. S. A 96:6495-6500.

Heida JG, Moshe SL, Pittman QJ. 2009. The role of interleukin-1beta in febrile seizures. Brain Dev. 31:388-393.

Heida JG, Pittman QJ. 2005. Causal links between brain cytokines and experimental febrile convulsions in the rat. Epilepsia 46:1906-1913.

Heinemann U, Lux HD. 1977. Ceiling of stimulus induced rises in extracellular potassium concentration in the cerebral cortex of cat. Brain Res. 120:231-249.

Heinrich C, Nitta N, Flubacher A, Muller M, Fahrner A, Kirsch M, Freiman T, Suzuki F, Depaulis A, Frotscher M, Haas CA. 2006. Reelin deficiency and displacement of mature neurons, but not neurogenesis, underlie the formation of granule cell dispersion in the epileptic hippocampus. J. Neurosci. 26:4701-4713.

Heneka MT, Kummer MP, Latz E. 2014. Innate immune activation in neurodegenerative disease. Nature Reviews Immunology 14:463-477.

Herculano-Houzel S, Mota B, Lent R. 2006. Cellular scaling rules for rodent brains. Proc. Natl. Acad. Sci. U. S. A 103:12138-12143.

Herman MA, Jahr CE. 2007. Extracellular glutamate concentration in hippocampal slice. J. Neurosci. 27:9736-9741.

Herrmann JE, Imura T, Song BB, Qi JW, Ao Y, Nguyen TK, Korsak RA, Takeda K, Akira S, Sofroniew MV. 2008. STAT3 is a critical regulator of astrogliosis and scar formation after spinal cord injury. Journal of Neuroscience 28:7231-7243.

Hertzberg EL, Saez JC, Corpina RA, Roy C, Kessler JA. 2000. Use of antibodies in the analysis of connexin 43 turnover and phosphorylation. Methods 20:129-139.

Hesdorffer DC, Logroscino G, Benn EK, Katri N, Cascino G, Hauser WA. 2011. Estimating risk for developing epilepsy: a population-based study in Rochester, Minnesota. Neurology 76:23-27.

Hibino H, Inanobe A, Furutani K, Murakami S, Findlay I, Kurachi Y. 2010. Inwardly rectifying potassium channels: their structure, function, and physiological roles. Physiol Rev. 90:291-366.

Ho YH, Lin YT, Wu CW, Chao YM, Chang AY, Chan JY. 2015. Peripheral inflammation increases seizure susceptibility via the induction of neuroinflammation and oxidative stress in the hippocampus. J. Biomed. Sci. 22:46.

Hu SX, Sheng WS, Ehrlich LC, Peterson PK, Chao SC. 2000. Cytokine effects on glutamate uptake by human astrocytes. Neuroimmunomodulation 7:153-159.

Huxley AF, STAMPFLI R. 1949. Evidence for saltatory conduction in peripheral myelinated nerve fibres. J. Physiol 108:315-339.

Iacobas DA, Iacobas S, Spray DC. 2007. Connexin43 and the brain transcriptome of newborn mice. Genomics 89:113-123.

Irie T, Muta T, Takeshige K. 2000. TAK1 mediates an activation signal from toll-like receptor(s) to nuclear factor-kappaB in lipopolysaccharide-stimulated macrophages. FEBS Lett. 467:160-164.

Jabaudon D, Shimamoto K, Yasuda-Kamatani Y, Scanziani M, Gahwiler BH, Gerber U. 1999. Inhibition of uptake unmasks rapid extracellular turnover of glutamate of nonvesicular origin. Proc. Natl. Acad. Sci. U. S. A 96:8733-8738.

Jacobs MP, Fischbach GD, Davis MR, Dichter MA, Dingledine R, Lowenstein DH, Morrell MJ, Noebels JL, Rogawski MA, Spencer SS, Theodore WH. 2001. Future directions for epilepsy research. Neurology 57:1536-1542.

Ji K, Akgul G, Wollmuth LP, Tsirka SE. 2013. Microglia actively regulate the number of functional synapses. PLoS. One. 8:e56293.

Jiang W, Duong TM, de Lanerolle NC. 1999. The neuropathology of hyperthermic seizures in the rat. Epilepsia 40:5-19.

Jinno S, Fleischer F, Eckel S, Schmidt V, Kosaka T. 2007. Spatial arrangement of microglia in the mouse hippocampus: a stereological study in comparison with astrocytes. Glia 55:1334-1347.

John GR, Scemes E, Suadicani SO, Liu JSH, Charles PC, Lee SC, Spray DC, Brosnan CF. 1999. IL-1 beta differentially regulates calcium wave propagation between primary human fetal astrocytes via pathways involving P2 receptors and gap junction channels. Proceedings of the National Academy of Sciences of the United States of America 96:11613-11618.

Jordan K, Chodock R, Hand AR, Laird DW. 2001. The origin of annular junctions: a mechanism of gap junction internalization. J. Cell Sci. 114:763-773.

Jung KH, Chu K, Lee ST, Park KI, Kim JH, Kang KM, Kim S, Jeon D, Kim M, Lee SK, Roh JK. 2011. Molecular alterations underlying epileptogenesis after prolonged febrile seizure and modulation by erythropoietin. Epilepsia 52:541-550.

Kettenmann H, Hanisch UK, Noda M, Verkhratsky A. 2011. Physiology of microglia. Physiol Rev. 91:461-553.

Kettenmann H, Ransom BR (1995) Neuroglia. Oxford University Press.

Khan D, Dupper A, Deshpande T, Graan PN, Steinhäuser C, Bedner P. 2016. Experimental febrile seizures impair interastrocytic gap junction coupling in juvenile mice. J Neurosci Res. 94(9):804-13

Kielian T. 2008. Glial connexins and gap junctions in CNS inflammation and disease. J. Neurochem. 106:1000-1016.

Kira R, Ishizaki Y, Torisu H, Sanefuji M, Takemoto M, Sakamoto K, Matsumoto S, Yamaguchi Y, Yukaya N, Sakai Y, Gondo K, Hara T. 2010. Genetic susceptibility to febrile seizures: case-control association studies. Brain Dev. 32:57-63.

Kitchens RL. 2000. Role of CD14 in cellular recognition of bacterial lipopolysaccharides. Chem. Immunol. 74:61-82.

Kobayashi E, Lopes-Cendes I, Guerreiro CA, Sousa SC, Guerreiro MM, Cendes F. 2001. Seizure outcome and hippocampal atrophy in familial mesial temporal lobe epilepsy. Neurology 56:166-172.

Kofuji P, Newman EA. 2004. Potassium buffering in the central nervous system. Neuroscience 129:1045-1056.

Kreutzberg GW. 1996. Microglia: a sensor for pathological events in the CNS. Trends Neurosci. 19:312-318.

Kunze A, Congreso MR, Hartmann C, Wallraff-Beck A, Huttmann K, Bedner P, Requardt R, Seifert G, Redecker C, Willecke K, Hofmann A, Pfeifer A, Theis

M, Steinhäuser C. 2009. Connexin expression by radial glia-like cells is required for neurogenesis in the adult dentate gyrus. Proc. Natl. Acad. Sci. U. S. A 106:11336-11341.

Laird DW. 2006. Life cycle of connexins in health and disease. Biochem. J. 394:527-543.

Laird DW, Puranam KL, Revel JP. 1991. Turnover and phosphorylation dynamics of connexin43 gap junction protein in cultured cardiac myocytes. Biochem. J. 273(Pt 1):67-72.

Lau LT, Yu AC. 2001. Astrocytes produce and release interleukin-1, interleukin-6, tumor necrosis factor alpha and interferon-gamma following traumatic and metabolic injury. J. Neurotrauma 18:351-359.

Lawson LJ, Perry VH, Dri P, Gordon S. 1990. Heterogeneity in the distribution and morphology of microglia in the normal adult mouse brain. Neuroscience 39:151-170.

Le HT, Sin WC, Lozinsky S, Bechberger J, Vega JL, Guo XQ, Saez JC, Naus CC. 2014. Gap junction intercellular communication mediated by connexin43 in astrocytes is essential for their resistance to oxidative stress. J. Biol. Chem. 289:1345-1354.

Ledeen RW, Chakraborty G. 1998. Cytokines, signal transduction, and inflammatory demyelination: review and hypothesis. Neurochem. Res. 23:277-289.

Li WE, Ochalski PA, Hertzberg EL, Nagy JI. 1998. Immunorecognition, ultrastructure and phosphorylation status of astrocytic gap junctions and connexin43 in rat brain after cerebral focal ischaemia. Eur. J. Neurosci. 10:2444-2463.

Liang SL, Carlson GC, Coulter DA. 2006. Dynamic regulation of synaptic GABA release by the glutamate-glutamine cycle in hippocampal area CA1. J. Neurosci. 26:8537-8548.

Liao CK, Jeng CJ, Wang HS, Wang SH, Wu JC. 2013. Lipopolysaccharide induces degradation of connexin43 in rat astrocytes via the ubiquitin-proteasome proteolytic pathway. PLoS. One. 8:e79350.

Liu JS, John GR, Sikora A, Lee SC, Brosnan CF. 2000. Modulation of interleukin-1beta and tumor necrosis factor alpha signaling by P2 purinergic receptors in human fetal astrocytes. J. Neurosci. 20:5292-5299.

Love S. 2006. Demyelinating diseases. J. Clin. Pathol. 59:1151-1159.

MacDonald BK, Johnson AL, Sander JWAS, Shorvon SD. 1999. Febrile convulsions in 220 children - Neurological sequelae at 12 years follow-up. European Neurology 41:179-186.

Maroso M, Balosso S, Ravizza T, Iori V, Wright CI, French J, Vezzani A. 2011. Interleukin-1beta biosynthesis inhibition reduces acute seizures and drug resistant chronic epileptic activity in mice. Neurotherapeutics. 8:304-315.

Martin DL. 1992. Synthesis and release of neuroactive substances by glial cells. Glia 5:81-94.

Martin SJ, Morris RG. 2002. New life in an old idea: the synaptic plasticity and memory hypothesis revisited. Hippocampus 12:609-636.

Matthias K, Kirchhoff F, Seifert G, Hüttmann K, Matyash M, Kettenmann H, Steinhäuser C. 2003. Segregated expression of AMPA-type glutamate receptors and glutamate transporters defines distinct astrocyte populations in the mouse hippocampus. J. Neurosci 23:1750-1758.

McClelland S, Dube CM, Yang J, Baram TZ. 2011. Epileptogenesis after prolonged febrile seizures: Mechanisms, biomarkers and therapeutic opportunities. Neuroscience Letters 497:155-162.

Meme W, Calvo CF, Froger N, Ezan P, Amigou E, Koulakoff A, Giaume C. 2006. Proinflammatory cytokines released from microglia inhibit gap junctions in astrocytes: potentiation by beta-amyloid. FASEB J. 20:494-496.

Meme W, Ezan P, Venance L, Glowinski J, Giaume C. 2004. ATP-induced inhibition of gap junctional communication is enhanced by interleukin-1 beta treatment in cultured astrocytes. Neuroscience 126:95-104.

Mese G, Richard G, White TW. 2007. Gap junctions: basic structure and function. J. Invest Dermatol. 127:2516-2524.

Meurs A, Clinckers R, Ebinger G, Michotte Y, Smolders I. 2008. Seizure activity and changes in hippocampal extracellular glutamate, GABA, dopamine and serotonin. Epilepsy Res. 78:50-59.

Miller SI, Ernst RK, Bader MW. 2005. LPS, TLR4 and infectious disease diversity. Nat. Rev. Microbiol. 3:36-46.

Min KJ, Yang MS, Kim SU, Jou I, Joe EH. 2006. Astrocytes induce hemeoxygenase-1 expression in microglia: A feasible mechanism for preventing excessive brain inflammation. Journal of Neuroscience 26:1880-1887.

Musil LS, Goodenough DA. 1993. Multisubunit assembly of an integral plasma membrane channel protein, gap junction connexin43, occurs after exit from the ER. Cell 74:1065-1077.

Nadler JV. 1981. Kainic Acid As A Tool for the Study of Temporal-Lobe Epilepsy. Life Sciences 29:2031-2042.

Nagelhus EA, Mathiisen TM, Ottersen OP. 2004. Aquaporin-4 in the central nervous system: cellular and subcellular distribution and coexpression with KIR4.1. Neuroscience 129:905-913.

Nagy JI, Li WE. 2000. A brain slice model for in vitro analyses of astrocytic gap junction and connexin43 regulation: actions of ischemia, glutamate and elevated potassium. Eur. J. Neurosci. 12:4567-4572.

Najjar S, Pearlman D, Miller DC, Devinsky O. 2011. Refractory epilepsy associated with microglial activation. Neurologist. 17:249-254.

Nakase T, Fushiki S, Naus CC. 2003. Astrocytic gap junctions composed of connexin 43 reduce apoptotic neuronal damage in cerebral ischemia. Stroke 34:1987-1993.

Nave KA. 2010. Myelination and support of axonal integrity by glia. Nature 468:244-252.

Nedergaard M, Ransom B, Goldman SA. 2003. New roles for astrocytes: redefining the functional architecture of the brain. Trends Neurosci. 26:523-530.

Nedergaard M, Verkhratsky A. 2012. Artifact versus reality--how astrocytes contribute to synaptic events. Glia 60:1013-1023.

Neher E, Sakmann B. 1976. Single-Channel Currents Recorded from Membrane of Denervated Frog Muscle-Fibers. Nature 260:799-802.

Nelson KB, Ellenberg JH. 1976. Predictors of Epilepsy in Children Who Have Experienced Febrile Seizures. New England Journal of Medicine 295:1029-1033.

Newton K, Dixit VM. 2012. Signaling in innate immunity and inflammation. Cold Spring Harb. Perspect. Biol. 4.

Nimmerjahn A, Kirchhoff F, Helmchen F. 2005. Resting microglial cells are highly dynamic surveillants of brain parenchyma in vivo. Science 308:1314-1318.

Ninomiya-Tsuji J, Kajino T, Ono K, Ohtomo T, Matsumoto M, Shiina M, Mihara M, Tsuchiya M, Matsumoto K. 2003. A resorcylic acid lactone, 5Z-7-oxozeaenol, prevents inflammation by inhibiting the catalytic activity of TAK1 MAPK kinase kinase. Journal of Biological Chemistry 278:18485-18490.

Ninomiya-Tsuji J, Kishimoto K, Hiyama A, Inoue J, Cao Z, Matsumoto K. 1999. The kinase TAK1 can activate the NIK-I kappaB as well as the MAP kinase cascade in the IL-1 signalling pathway. Nature 398:252-256.

Nishiyama A, Komitova M, Suzuki R, Zhu X. 2009. Polydendrocytes (NG2 cells): multifunctional cells with lineage plasticity. Nat. Rev. Neurosci. 10:9-22.

Nolte C, Matyash M, Pivneva T, Schipke CG, Ohlemeyer C, Hanisch UK, Kirchhoff F, Kettenmann H. 2001. GFAP promoter-controlled EGFP-expressing transgenic mice: A tool to visualize astrocytes and astrogliosis in living brain tissue. Glia 33:72-86.

Norenberg MD. 1979. Distribution of glutamine synthetase in the rat central nervous system. J. Histochem. Cytochem. 27:756-762.

O'Keefe GM, Nguyen VT, Ping Tang LL, Benveniste EN. 2001. IFN-gamma regulation of class II transactivator promoter IV in macrophages and microglia: involvement of the suppressors of cytokine signaling-1 protein. J. Immunol. 166:2260-2269.

O'Neill LA, Bowie AG. 2007. The family of five: TIR-domain-containing adaptors in Toll-like receptor signalling. Nat. Rev. Immunol. 7:353-364.

Oberheim NA, Takano T, Han X, He W, Lin JH, Wang F, Xu Q, Wyatt JD, Pilcher W, Ojemann JG, Ransom BR, Goldman SA, Nedergaard M. 2009. Uniquely hominid features of adult human astrocytes. J. Neurosci. 29:3276-3287.

Oberheim NA, Wang X, Goldman S, Nedergaard M. 2006. Astrocytic complexity distinguishes the human brain. Trends Neurosci. 29:547-553.

Ogata K, Kosaka T. 2002. Structural and quantitative analysis of astrocytes in the mouse hippocampus. Neuroscience 113:221-233.

Onodera Y, Teramura T, Takehara T, Shigi K, Fukuda K. 2015. Reactive oxygen species induce Cox-2 expression via TAK1 activation in synovial fibroblast cells. FEBS Open. Bio 5:492-501.

Ovanesov MV, Ayhan Y, Wolbert C, Moldovan K, Sauder C, Pletnikov MV. 2008. Astrocytes play a key role in activation of microglia by persistent Borna disease virus infection. Journal of Neuroinflammation 5.

Pahujaa M, Anikin M, Goldberg GS. 2007. Phosphorylation of connexin43 induced by Src: Regulation of gap junctional communication between transformed cells. Experimental Cell Research 313:4083-4090.

Pannasch U, Rouach N. 2013. Emerging role for astroglial networks in information processing: from synapse to behavior. Trends Neurosci. 36:405-417.

Pathak S, Borodkin VS, Albarbarawi O, Campbell DG, Ibrahim A, van Aalten DM. 2012. O-GlcNAcylation of TAB1 modulates TAK1-mediated cytokine release. EMBO J. 31:1394-1404.

Patterson KP, Brennan GP, Curran M, Kinney-Lang E, Dube C, Rashid F, Ly C, Obenaus A, Baram TZ. 2015. Rapid, Coordinate Inflammatory Responses after Experimental Febrile Status Epilepticus: Implications for Epileptogenesis. eNeuro. 2.

Pavlidou E, Panteliadis C. 2013. Prognostic factors for subsequent epilepsy in children with febrile seizures. Epilepsia 54:2101-2107.

Pitkanen A, Nissinen J, Nairismagi J, Lukasiuk K, Grohn OHJ, Miettinen R, Kauppinen R. 2002. Progression of neuronal damage after status epilepticus and during spontaneous seizures in a rat model of temporal lobe epilepsy. Do Seizures Damage the Brain 135:67-83.

Pocock JM, Kettenmann H. 2007. Neurotransmitter receptors on microglia. Trends Neurosci. 30:527-535.

Polito A, Reynolds R. 2005. NG2-expressing cells as oligodendrocyte progenitors in the normal and demyelinated adult central nervous system. J. Anat. 207:707-716.

Pomeroy SL, Holmes SJ, Dodge PR, Feigin RD. 1990. Seizures and other neurologic sequelae of bacterial meningitis in children. N. Engl. J. Med. 323:1651-1657.

Portale AA, Mathias RS, Potter DE, Rozansky DR. 2002. Kidneys and electrolytes. In: Rudolph AM, Kamei RK, Overby KJ, editors. Rudolph's Fundamentals Pediatrics. New york: McGraw-Hill; pp. 593–645.

Prochnow N, Dermietzel R. 2008. Connexons and cell adhesion: a romantic phase. Histochem. Cell Biol. 130:71-77.

Qin L, Wu X, Block ML, Liu Y, Breese GR, Hong JS, Knapp DJ, Crews FT. 2007. Systemic LPS causes chronic neuroinflammation and progressive neurodegeneration. Glia 55:453-462.

Ransohoff RM, Perry VH. 2009. Microglial physiology: unique stimuli, specialized responses. Annu. Rev. Immunol. 27:119-145.

Reimann F, Ashcroft FM. 1999. Inwardly rectifying potassium channels. Curr. Opin. Cell Biol. 11:503-508.

Renauld AE, Spengler RN. 2002. Tumor necrosis factor expressed by primary hippocampal neurons and SH-SY5Y cells is regulated by alpha(2)-adrenergic receptor activation. J. Neurosci. Res. 67:264-274.

Retamal MA, Froger N, Palacios-Prado N, Ezan P, Saez PJ, Saez JC, Giaume C. 2007. Cx43 hemichannels and gap junction channels in astrocytes are regulated oppositely by proinflammatory cytokines released from activated microglia. J. Neurosci. 27:13781-13792.

Rietschel ET, Brade H, Holst O, Brade L, Muller-Loennies S, Mamat U, Zahringer U, Beckmann F, Seydel U, Brandenburg K, Ulmer AJ, Mattern T, Heine H, Schletter J, Loppnow H, Schonbeck U, Flad HD, Hauschildt S, Schade UF, Di PF, Kusumoto S, Schumann RR. 1996. Bacterial endotoxin: Chemical

constitution, biological recognition, host response, and immunological detoxification. Curr. Top. Microbiol. Immunol. 216:39-81.

Robel S, Sontheimer H. 2016. Glia as drivers of abnormal neuronal activity. Nat. Neurosci. 19:28-33.

Rock RB, Gekker G, Hu S, Sheng WS, Cheeran M, Lokensgard JR, Peterson PK. 2004. Role of microglia in central nervous system infections. Clin. Microbiol. Rev. 17:942-64, table.

Rouach N, Avignone E, Meme W, Koulakoff A, Venance L, Blomstrand F, Giaume C. 2002a. Gap junctions and connexin expression in the normal and pathological central nervous system. Biol. Cell 94:457-475.

Rouach N, Calvo CF, Glowinski J, Giaume C. 2002b. Brain macrophages inhibit gap junctional communication and downregulate connexin 43 expression in cultured astrocytes. Eur. J. Neurosci. 15:403-407.

Rouach N, Koulakoff A, Abudara V, Willecke K, Giaume C. 2008. Astroglial metabolic networks sustain hippocampal synaptic transmission. Science 322:1551-1555.

Sagar HJ, Oxbury JM. 1987. Hippocampal neuron loss in temporal lobe epilepsy: correlation with early childhood convulsions. Ann. Neurol. 22:334-340.

Sah P, Hestrin S, Nicoll RA. 1989. Tonic activation of NMDA receptors by ambient glutamate enhances excitability of neurons. Science 246:815-818.

Sankar R, Shin DH, Liu HT, Mazarati A, de Vasconcelos AP, Wasterlain CG. 1998. Patterns of status epilepticus-induced neuronal injury during development and long-term consequences. Journal of Neuroscience 18:8382-8393.

Sato S, Sanjo H, Takeda K, Ninomiya-Tsuji J, Yamamoto M, Kawai T, Matsumoto K, Takeuchi O, Akira S. 2005. Essential function for the kinase TAK1 in innate and adaptive immune responses. Nat. Immunol. 6:1087-1095.

Sayyah M, Javad-Pour M, Ghazi-Khansari M. 2003. The bacterial endotoxin lipopolysaccharide enhances seizure susceptibility in mice: involvement of proinflammatory factors: nitric oxide and prostaglandins. Neuroscience 122:1073-1080.

Scemes E. 2008. Modulation of astrocyte P2Y1 receptors by the carboxyl terminal domain of the gap junction protein Cx43. Glia 56:145-153.

Scemes E, Dermietzel R, Spray DC. 1998. Calcium waves between astrocytes from Cx43 knockout mice. Glia 24:65-73.

Schools GP, Zhou M, Kimelberg HK. 2006. Development of gap junctions in hippocampal astrocytes: evidence that whole cell electrophysiological

phenotype is an intrinsic property of the individual cell. J. Neurophysiol. 96:1383-1392.

Schumann RR, Pfeil D, Freyer D, Buerger W, Lamping N, Kirschning CJ, Goebel UB, Weber JR. 1998. Lipopolysaccharide and pneumococcal cell wall components activate the mitogen activated protein kinases (MAPK) erk-1, erk-2, and p38 in astrocytes. Glia 22:295-305.

Seifert G, Carmignoto G, Steinhäuser C. 2010. Astrocyte dysfunction in epilepsy. Brain Res. Rev. 63:212-221.

Seifert G, Schilling K, Steinhäuser C. 2006. Astrocyte dysfunction in neurological disorders: a molecular perspective. Nat. Rev. Neurosci. 7:194-206.

Seiffert E, Dreier JP, Ivens S, Bechmann I, Tomkins O, Heinemann U, Friedman A. 2004. Lasting blood-brain barrier disruption induces epileptic focus in the rat somatosensory cortex. J. Neurosci. 24:7829-7836.

Seri B, Garcia-Verdugo JM, McEwen BS, varez-Buylla A. 2001. Astrocytes give rise to new neurons in the adult mammalian hippocampus. J. Neurosci. 21:7153-7160.

Shim JH, Xiao C, Paschal AE, Bailey ST, Rao P, Hayden MS, Lee KY, Bussey C, Steckel M, Tanaka N, Yamada G, Akira S, Matsumoto K, Ghosh S. 2005. TAK1, but not TAB1 or TAB2, plays an essential role in multiple signaling pathways in vivo. Genes Dev. 19:2668-2681.

Shinnar S. 2003. Febrile Seizures and Mesial Temporal Sclerosis. Epilepsy Curr. 3:115-118.

Shinnar S, Glauser TA. 2002. Febrile seizures. Journal of Child Neurology 17:S44-S52.

Shinnar S, Hesdorffer DC, Nordli DR, Pellock JM, O'Dell C, Lewis DV, Frank LM, Moshe SL, Epstein LG, Marmarou A, Bagiella E. 2008. Phenomenology of prolonged febrile seizures - Results of the FEBSTAT study. Neurology 71:170-176.

Sierra A, Abiega O, Shahraz A, Neumann H. 2013. Janus-faced microglia: beneficial and detrimental consequences of microglial phagocytosis. Front Cell Neurosci. 7:6.

Simard M, Nedergaard M. 2004. The neurobiology of glia in the context of water and ion homeostasis. Neuroscience 129:877-896.

Simpson I, Rose B, Loewenstein WR. 1977. Size limit of molecules permeating the junctional membrane channels. Science 195:294-296.

Smith JA, Das A, Ray SK, Banik NL. 2012. Role of pro-inflammatory cytokines released from microglia in neurodegenerative diseases. Brain Research Bulletin 87:10-20.

Sofroniew MV. 2009. Molecular dissection of reactive astrogliosis and glial scar formation. Trends Neurosci. 32:638-647.

Sofroniew MV. 2015. Astrocyte barriers to neurotoxic inflammation. Nature Reviews Neuroscience 16:249-263.

Sofroniew MV, Vinters HV. 2010. Astrocytes: biology and pathology. Acta Neuropathologica 119:7-35.

Sohl G, Maxeiner S, Willecke K. 2005. Expression and functions of neuronal gap junctions. Nat. Rev. Neurosci. 6:191-200.

Sohl G, Willecke K. 2004. Gap junctions and the connexin protein family. Cardiovasc. Res. 62:228-232.

Solan JL, Lampe PD. 2009. Connexin43 phosphorylation: structural changes and biological effects. Biochemical Journal 419:261-272.

Spray DC, Iacobas DA. 2007. Organizational principles of the connexin-related brain transcriptome. J. Membr. Biol. 218:39-47.

Dissing-Olesen L, Ledue JM, Rungta RL, Hefendehl JK, Choi HB, MacVicar BA. 2014. Activation of Neuronal NMDA Receptors Triggers Transient ATP-Mediated Microglial Process Outgrowth. Journal of Neuroscience 34:10511-10527.

Stanhope JM, Brody JA, Brink E, Morris CE. 1972. Convulsions among the Chamorro people of Guam, Mariana islands. II. Febrile convulsions. Am. J. Epidemiol. 95:299-304.

Steinhäuser C, Grunnet M, Carmignoto G. 2016. Crucial role of astrocytes in temporal lobe epilepsy. Neuroscience 323:157-169.

Steinhäuser C, Seifert G. 2012. Astrocyte dysfunction in epilepsy.

Steinhäuser C, Seifert G, Bedner P. 2012. Astrocyte dysfunction in temporal lobe epilepsy: K+ channels and gap junction coupling. Glia 60:1192-1202.

Stellwagen D, Beattie EC, Seo JY, Malenka RC. 2005. Differential regulation of AMPA receptor and GABA receptor trafficking by tumor necrosis factor-alpha. Journal of Neuroscience 25:3219-3228.

Stiles J, Jernigan TL. 2010. The basics of brain development. Neuropsychol. Rev. 20:327-348.

Strohschein S, Huttmann K, Gabriel S, Binder DK, Heinemann U, Steinhäuser C. 2011. Impact of aquaporin-4 channels on K+ buffering and gap junction coupling in the hippocampus. Glia 59:973-980.

Sullivan PG, Dube C, Dorenbos K, Steward O, Baram TZ. 2003. Mitochondrial uncoupling protein-2 protects the immature brain from excitotoxic neuronal death. Annals of Neurology 53:711-717.

Sun SC. 2011. Non-canonical NF-kappaB signaling pathway. Cell Res. 21:71-85.

Szczepanik AM, Fishkin RJ, Rush DK, Wilmot CA. 1996. Effects of chronic intrahippocampal infusion of lipopolysaccharide in the rat. Neuroscience 70:57-65.

Takaesu G, Surabhi RM, Park KJ, Ninomiya-Tsuji J, Matsumoto K, Gaynor RB. 2003. TAK1 is critical for IkappaB kinase-mediated activation of the NF-kappaB pathway. J. Mol. Biol. 326:105-115.

Takano T, Tian GF, Peng W, Lou N, Libionka W, Han X, Nedergaard M. 2006. Astrocyte-mediated control of cerebral blood flow. Nat. Neurosci. 9:260-267.

Takeuchi H, Jin SJ, Wang JY, Zhang GQ, Kawanokuchi J, Kuno R, Sonobe Y, Mizuno T, Suzumura A. 2006. Tumor necrosis factor-alpha induces neurotoxicity via glutamate release from hemichannels of activated microglia in an autocrine manner. Journal of Biological Chemistry 281:21362-21368.

Thompson K, Holm AM, Schousboe A, Popper P, Micevych P, Wasterlain C. 1998. Hippocampal stimulation produces neuronal death in the immature brain. Neuroscience 82:337-348.

Town T, Nikolic V, Tan J. 2005. The microglial "activation" continuum: from innate to adaptive responses. Journal of Neuroinflammation 2.

Tremblay ME, Lowery RL, Majewska AK. 2010. Microglial interactions with synapses are modulated by visual experience. PLoS. Biol. 8:e1000527.

Tremblay ME, Stevens B, Sierra A, Wake H, Bessis A, Nimmerjahn A. 2011. The Role of Microglia in the Healthy Brain. Journal of Neuroscience 31:16064-16069.

Tsuboi T. 1984. Epidemiology of Febrile and Afebrile Convulsions in Children in Japan. Neurology 34:175-181.

Tsuboi T, Okada S. 1984. Seasonal variation of febrile convulsion in Japan. Acta Neurol. Scand. 69:285-292.

Tufenkjian K, Luders HO. 2012. Seizure Semiology: Its Value and Limitations in Localizing the Epileptogenic Zone. Journal of Clinical Neurology 8:243-250.

Tutuncuoglu S, Kutukculer N, Kepe L, Coker C, Berdeli A, Tekgul H. 2001. Proinflammatory cytokines, prostaglandins and zinc in febrile convulsions. Pediatr. Int. 43:235-239.

van der Hel WS, Notenboom RG, Bos IW, van Rijen PC, van Veelen CW, de Graan PN. 2005. Reduced glutamine synthetase in hippocampal areas with neuron loss in temporal lobe epilepsy. Neurology 64:326-333.

van Gassen KLI, Hessel EVS, Ramakers GMJ, Notenboom RGE, Wolterink-Donselaar IG, Brakkee JH, Godschalk TC, Qiao X, Spruijt BM, van Nieuwenhuizen O, de Graan PNE. 2008. Characterization of febrile seizures and febrile seizure susceptibility in mouse inbred strains. Genes Brain and Behavior 7:578-586.

van Vliet EA, da Costa AS, Redeker S, van SR, Aronica E, Gorter JA. 2007. Blood-brain barrier leakage may lead to progression of temporal lobe epilepsy. Brain 130:521-534.

Vendrame M, Zarowski M, Alexopoulos AV, Wyllie E, Kothare SV, Loddenkemper T. 2011. Localization of pediatric seizure semiology. Clinical Neurophysiology 122:1924-1928.

Verity CM, Butler NR, Golding J. 1985. Febrile convulsions in a national cohort followed up from birth. II--Medical history and intellectual ability at 5 years of age. Br. Med. J. (Clin. Res. Ed) 290:1311-1315.

Verity CM, Greenwood R, Golding J. 1998. Long-term intellectual and behavioral outcomes of children with febrile convulsions. N. Engl. J. Med. 338:1723-1728.

Verkhratsky A, Orkand RK, Kettenmann H. 1998. Glial calcium: homeostasis and signaling function. Physiol Rev. 78:99-141.

Vestergaard M, Pedersen CB, Sidenius P, Olsen J, Christensen J. 2007. The long-term risk of epilepsy after febrile seizures in susceptible subgroups. American Journal of Epidemiology 165:911-918.

Vezzani A. 2014. Epilepsy and inflammation in the brain: overview and pathophysiology. Epilepsy Curr. 14:3-7.

Vezzani A, Granata T. 2005. Brain inflammation in epilepsy: experimental and clinical evidence. Epilepsia 46:1724-1743.

Vezzani A, Moneta D, Richichi C, Aliprandi M, Burrows SJ, Ravizza T, Perego C, De Simoni MG. 2002. Functional role of inflammatory cytokines and antiinflammatory molecules in seizures and epileptogenesis. Epilepsia 43 Suppl 5:30-35.

Vezzani A, Ravizza T, Balosso S, Aronica E. 2008. Glia as a source of cytokines: Implications for neuronal excitability and survival. Epilepsia 49:24-32.

Vezzani A, Viviani B. 2015. Neuromodulatory properties of inflammatory cytokines and their impact on neuronal excitability. Neuropharmacology 96:70-82.

Vilhardt F. 2005. Microglia: phagocyte and glia cell. Int. J. Biochem. Cell Biol. 37:17-21.

Virta M, Hurme M, Helminen M. 2002a. Increased frequency of interleukin-1beta (-511) allele 2 in febrile seizures. Pediatr. Neurol. 26:192-195.

Virta M, Hurme M, Helminen M. 2002b. Increased plasma levels of pro- and anti-inflammatory cytokines in patients with febrile seizures. Epilepsia 43:920-923.

Viviani B, Bartesaghi S, Gardoni F, Vezzani A, Behrens MM, Bartfai T, Binaglia M, Corsini E, Di Luca M, Galli CL, Marinovich M. 2003. Interleukin-1 beta enhances NMDA receptor-mediated intracellular calcium increase through activation of the Src family of kinases. Journal of Neuroscience 23:8692-8700.

Volterra A, Meldolesi J. 2005. Astrocytes, from brain glue to communication elements: The revolution continues. Nature Reviews Neuroscience 6:626-640.

Wahab A, Albus K, Gabriel S, Heinemann U. 2010. In search of models of pharmacoresistant epilepsy. Epilepsia 51 Suppl 3:154-159.

Wallace RH, Wang DW, Singh R, Scheffer IE, George AL, Jr., Phillips HA, Saar K, Reis A, Johnson EW, Sutherland GR, Berkovic SF, Mulley JC. 1998. Febrile seizures and generalized epilepsy associated with a mutation in the Na+-channel beta1 subunit gene SCN1B. Nat. Genet. 19:366-370.

Wallraff A, Kohling R, Heinemann U, Theis M, Willecke K, Steinhäuser C. 2006. The impact of astrocytic gap junctional coupling on potassium buffering in the hippocampus. J. Neurosci. 26:5438-5447.

Wallraff A, Odermatt B, Willecke K, Steinhäuser C. 2004. Distinct types of astroglial cells in the hippocampus differ in gap junction coupling. Glia 48:36-43.

Wang C, Deng L, Hong M, Akkaraju GR, Inoue J, Chen ZJ. 2001. TAK1 is a ubiquitin-dependent kinase of MKK and IKK. Nature 412:346-351.

Wang DD, Bordey A. 2008. The astrocyte odyssey. Prog. Neurobiol. 86:342-367.

Wang WY, Tan MS, Yu JT, Tan L. 2015. Role of pro-inflammatory cytokines released from microglia in Alzheimer's disease. Ann. Transl. Med. 3:136.

Wanner IB, Anderson MA, Song B, Levine J, Fernandez A, Gray-Thompson Z, Ao Y, Sofroniew MV. 2013. Glial Scar Borders Are Formed by Newly Proliferated, Elongated Astrocytes That Interact to Corral Inflammatory and Fibrotic Cells via STAT3-Dependent Mechanisms after Spinal Cord Injury. Journal of Neuroscience 33:12870-12886.

Wiencken-Barger AE, Djukic B, Casper KB, McCarthy KD. 2007. A role for Connexin43 during neurodevelopment. Glia 55:675-686.

Wilhelmsson U, Bushongt EA, Price DL, Smarr BL, Phung V, Terada M, Ellisman MH, Pekny M. 2006. Redefining the concept of reactive astrocytes as cells that remain within their unique domains upon reaction to injury. Proceedings of the National Academy of Sciences of the United States of America 103:17513-17518.

Wilkins A, Majed H, Layfield R, Compston A, Chandran S. 2003. Oligodendrocytes promote neuronal survival and axonal length by distinct intracellular mechanisms: a novel role for oligodendrocyte-derived glial cell line-derived neurotrophic factor. J. Neurosci. 23:4967-4974.

Yamaguchi K, Shirakabe K, Shibuya H, Irie K, Oishi I, Ueno N, Taniguchi T, Nishida E, Matsumoto K. 1995. Identification of a member of the MAPKKK family as a potential mediator of TGF-beta signal transduction. Science 270:2008-2011.

Yang S, Liu ZW, Wen L, Qiao HF, Zhou WX, Zhang YX. 2005. Interleukin-1 beta enhances NMDA receptor-mediated current but inhibits excitatory synaptic transmission. Brain Research 1034:172-179.

Yona S, Kim KW, Wolf Y, Mildner A, Varol D, Breker M, Strauss-Ayali D, Viukov S, Guilliams M, Misharin A, Hume DA, Perlman H, Malissen B, Zelzer E, Jung S. 2013. Fate mapping reveals origins and dynamics of monocytes and tissue macrophages under homeostasis. Immunity. 38:79-91.

Yu HM, Liu WH, He XH, Peng BW. 2012. IL-1beta: an important cytokine associated with febrile seizures? Neurosci. Bull. 28:301-308.

Zenz R, Eferl R, Scheinecker C, Redlich K, Smolen J, Schonthaler HB, Kenner L, Tschachler E, Wagner EF. 2008. Activator protein 1 (Fos/Jun) functions in inflammatory bone and skin disease. Arthritis Res. Ther. 10:201.

Zhang D, Yan H, Li H, Hao S, Zhuang Z, Liu M, Sun Q, Yang Y, Zhou M, Li K, Hang C. 2015. TGFbeta-activated Kinase 1 (TAK1) Inhibition by 5Z-7-Oxozeaenol Attenuates Early Brain Injury after Experimental Subarachnoid Hemorrhage. J. Biol. Chem. 290:19900-19909.

Zhang R, Yamada J, Hayashi Y, Wu Z, Koyama S, Nakanishi H. 2008. Inhibition of NMDA-induced outward currents by interleukin-1 beta in hippocampal neurons. Biochemical and Biophysical Research Communications 372:816-820.

Zhang RY, Sun L, Hayashi Y, Liu X, Koyama S, Wu Z, Nakanishi H. 2010. Acute p38-mediated inhibition of NMDA-induced outward currents in hippocampal CA1 neurons by interleukin-1 beta. Neurobiology of Disease 38:68-77.

Zhu X, Hill RA, Dietrich D, Komitova M, Suzuki R, Nishiyama A. 2011. Age-dependent fate and lineage restriction of single NG2 cells. Development 138:745-753.

Zurolo E, Groot M, Iyer A, Anink J, Vliet EA, Heimans JJ, Reijneveld JC, Gorter JA, Aronica E. 2012. Regulation of Kir4.1 expression in astrocytes and astrocytic tumors: a role for interleukin-1 β. J. Neuroinflammation 9: 280.

Zou JY, Crews FT. 2005. TNF alpha potentiates glutamate neurotoxicity by inhibiting glutamate uptake in organotypic brain slice cultures: neuroprotection by NF kappa B inhibition. Brain Research 1034:11-24.

List of figures

List of tables

Erklärung

Hiermit versichere ich, dass diese Dissertation von mir selbst und ohne unerlaubte Hilfe angefertigt worden ist. Es wurden keine anderen als die angegebenen Hilfsmittel verwendet. Ferner erkläre ich, dass die vorliegende Arbeit an keiner anderen Hochschule als Dissertation eingereicht worden ist.

Bonn, den 06.02.2017

Dilaware Khan

Publications

Khan D, Dupper A, Deshpande T, Graan PN, Steinhäuser C, Bedner P (2016). Experimental febrile seizures impair interastrocytic gap junction coupling in juvenile mice. J Neurosci Res; 94(9):804-13. doi: 10.1002/jnr.23726.

Lobastova L, Kraus D, Glassmann A, **Khan D**, Steinhäuser C, Wolff C, Veit N, Winter J, Probstmeier R (2016). Collective cell migration of thyroid carcinoma cells: A beneficial ability to override unfavourable substrates. Cellular oncology; 40(1):63-76. doi: 10.1007/s13402-016-0305-5. Epub 2016 Nov 8.

Zhang Y, **Khan D**, Delling J, Tobiasch E (2012). Mechanisms Underlying the Osteo- and Adipo-Differentiation of Human Mesenchymal Stem Cells. TheScientificWorldJOURNAL; 2012: 793823. Published online 2012 Mar 12. doi: 10.1100/2012/793823.

Khan D, Kleinfeld C, Winter M, Tobiasch E (2012). Oral Tissues as Source for Bone Regeneration in Dental Implantology. Jamie Davies (Ed.), Tissue Regeneration, Intech-Open Access Publisher. ISBN 978-953-307-876-2.